29th Symposium on Naval Hydrodynamics
Gothenburg, Sweden, 26-31 August 2012

Computational Ship Hydrodynamics: Nowadays and Way Forward

Frederick Stern, Jianming Yang, Zhaoyuan Wang,
Hamid Sadat-Hosseini, Maysam Mousaviraad, Shanti Bhushan[1], Tao Xing[2]
(IIHR-Hydroscience & Engineering, University of Iowa,
Iowa City, IA 52242, USA)

ABSTRACT

Computational fluid dynamics for ship hydrodynamics has made monumental progress over the last ten years, which is reaching the milestone of providing first-generation simulation-based design tools with vast capabilities for model- and full-scale simulations and optimization. This is due to the enabling technologies such as free surface tracking/capturing, turbulence modeling, 6DOF motion prediction, dynamic overset grids, local/adaptive grid refinement, high performance computing, environmental modeling, and optimization methods. Herein, various modeling, numerical methods, and high performance computing approaches for computational ship hydrodynamics are evaluated thereby providing a vision for the development of the next-generation high-fidelity simulation tools. Verification and validation procedures and their applications, including resistance and propulsion, seakeeping, maneuvering, and stability and capsize, are reviewed. Issues, opportunities, and challenges for advancements in higher-fidelity two-phase flow are addressed. Fundamental studies for two-phase flows are also discussed. Conclusions and future directions are also provided.

1 INTRODUCTION

In just over 30 years computational fluid dynamics (CFD) for ship hydrodynamics has surpassed all expectations in reaching astronomical progress, capabilities and milestone of providing the first-generation simulation-based design (SBD) tools for model- and full-scale simulations and optimization enabling innovative cost-saving designs to meet the challenges of the 21st century, especially with regard to safety, energy and economy. CFD is changing the face of ship hydrodynamics as the SBD approach is replacing the now old-fashioned build-and-test approach such that model testing is only required at the final design stage; however, towing tank and wave basin facilities are needed additionally for model development and CFD validation, which requires even more advanced measurement systems for global and local flow variables and more stringent requirements on experimental uncertainty analysis as it plays an important role in validation procedures.

In the following, the development of computational ship hydrodynamics over the past 30 years is briefed using example references idiosyncratic to the authors and their colleagues. In the early 1980s integral methods still predominated, which worked well for two-dimensions but had great difficulty in extensions to three-dimensions due to inability to model cross-flow velocity profiles (von Kerczek et al., 1984). Thus three-dimensional boundary layer finite difference methods were soon developed, which worked well for thin boundary layers but had great difficulty for thick boundary layers and flow separation (Stern, 1986). Quickly partially parabolic approaches were developed (Stern et al., 1988a) followed by full RANS solvers with viscous-inviscid interaction approaches for nonzero Froude number (Tahara et al., 1992). Soon thereafter large domain RANS methods using free surface tracking methods (Tahara et al., 1996) along with extensions for improved turbulence and propulsor modeling, multi-block, overset grids and parallel computing were developed (Paterson et al., 2003) allowing full/appended/model captive simulations for resistance and propulsion. Next enabling technologies of level-set free surface capturing, inertial reference frames, and dynamic overset grids allowed wave breaking and ship motions (Carrica et al. 2007) and of anisotropic URANS and DES turbulence modeling allowed better resolved turbulence (Xing et al., 2007; 2012). Extensions soon followed for semi-coupled air-water flows (Huang et al., 2008), 6DOF simulations using controllers for calm-water maneuvering (Carrica et al., 2012b) and capsize predictions (Sadat-Hosseini et al., 2011b) including rotating propellers (Carrica et al., 2012a), exhaust plumes (Huang et al., 2012), wall functions for full-scale DES simulations (Bhushan et al., 2012c), damaged stability including motions

[1] Current affiliation: Center for Advanced Vehicular Systems, Mississippi State University, Starkville, MS 39759

[2] Current affiliation: Mechanical Engineering Department, University of Idaho, Moscow, ID 83844

(Sadat-Hosseini et al., 2012c), and high performance computing (HPC) (Bhushan et al., 2011a). Innovative procedures not possible in towing tanks were also developed for both resistance and propulsion (Xing et al., 2008) and seakeeping (Mousaviraad et al., 2010) and CFD with system identification has shown ability for improvement in system-based mathematical models for maneuvering in calm water and waves (Araki et al., 2012a, b).

The next-generation high-fidelity SBD tools are already under development for milestone achievement in increased capability focusing on orders of magnitude improvements in accuracy, robustness, and exascale HPC capability for fully resolved, fully coupled, sharp-interface, multi-scale, multi-phase, turbulent ship flow utilizing billions of grid points. Current capabilities are for Cartesian grids with immersed boundary methods (Yang and Stern, 2009; Wang et al., 2009a, b), for orthogonal curvilinear grids (Wang et al., 2012a, b), for overset Cartesian/orthogonal curvilinear grids (Bhushan et al., 2011b), and extensions in progress for non-orthogonal curvilinear grids. High-fidelity large eddy simulation (LES) simulations for plunging breaking waves and surface-piercing wedges and cylinders have resolved for the first time and identified physics of the plunging wave breaking process (Koo et al., 2012), spray formation (Wang et al., 2010b) and wake spreading (Suh et al., 2011). Realization non-orthogonal curvilinear grids (Yang et al., 2012) will enable similarly resolved simulations for practical geometries and conditions with increased physical understanding thereby revolutionizing ship design; however, considerable research is still needed, as high-fidelity general purpose solvers with the aforementioned functionality do not yet exist.

Quantitative verification and validation (V&V) procedures and an adequate number of well-trained expert users are also essential ingredients for the successful implementation of SBD. Here again, computational ship hydrodynamics has played leadership role in V&V (Stern et al., 2006a; Xing and Stern, 2010) and development of CFD educational interface for teaching expert users at both introductory and intermediate levels (Stern et al., 2006b; 2012). V&V research is still needed especially for single-grid methods and LES turbulence models. General-purpose CFD educational interfaces for teaching CFD are not yet available.

The research paradigm of integrated code development, experiments, and uncertainty analysis along with step-by-step building block approach and international collaborations for synergistic research magnifying individual institute capabilities as exemplified by IIHR (Stern et al., 2003) has been foundational in the unprecedented achievements of computational ship hydrodynamics.

Progress in CFD for ship hydrodynamics has been well benchmarked in CFD workshops for resistance and propulsion and seakeeping (most recently, Larsson et al., 2011) and calm water maneuvering (Stern et al., 2011a) along with the Proceedings of the ITTC both for applications and CFD itself. Optimization capabilities for ship hydrodynamics were recently reviewed by Campana et al. (2009). Sanada et al. (2012) provides an overview of the past captive towing tank and current free running wave basin experimental ship hydrodynamics for CFD validation as background for description of the new IIHR wave basin and trajectories and local flow field measurements around the ONR tumblehome in maneuvering motion in calm water and head and following waves.

Computational ship hydrodynamics current functionality, initiation of the development of the next generation high-fidelity SBD tools, contributions to V&V and CFD education, research paradigm and international collaborations, CFD workshops and ITTC Proceedings and optimization capabilities as demonstrated by the example references given above arguably equals if not surpasses other external flow industrial applications such as aerospace, automotive and rolling stock capabilities such that ship hydrodynamics in spite of its relatively small size community is at the forefront in computational science and technology and research and development.

Herein computational ship hydrodynamics is reviewed with a different perspective and special focus on the critical assessment of modeling, numerical methods and HPC both nowadays and prognosis for way forward. Quantitative V&V procedures and their application for evaluation of captive and free running simulation capabilities along with fundamental studies for two-phase flows are also reviewed with the latest results obtained at IIHR as selected examples. Conclusions and future directions are also provided.

2 COMPUTATIONAL SHIP HYDRODYNAMICS

Application areas are at the core of computational method requirements as they guide the choice of modeling, which in return guide the grid and accuracy requirements of the simulation. The grid requirements along with HPC determine the efforts required for grid generation, problem setup, solution turnaround time and post processing efforts. Computational methods for ship hydrodynamics include modeling, numerical methods and HPC capability as summarized in Fig. 1. Models required for naval applications are hydrodynamics, air flow and two-phase flow solvers, turbulence models, interface models, motion solvers,

propulsion models, sea condition or wave models, etc. The numerical methods encompass the grids and discretization schemes for the governing equations. High performance computing encompasses the ability to use larger grids, more parallel processors and speedup solution turnaround time.

ITTC 2011 Specialist Committee on Computational Fluid dynamics report (ITTC, 2011) provides a detailed review of numerical methods commonly used for ship hydrodynamics. Most of them are also discussed here, and readers are referred to ITTC (2011) for the complete picture of CFD in ship hydrodynamics from a different angle. The discussions herein focus on the advantages and limitations of the computational methods currently used in ship hydrodynamics, and recommendation are made for the most appropriate methods for a given application area. The following two sections also review upcoming computational methods focusing on the multiscale issues, which may provide hints of new development directions of high fidelity solvers for ship hydrodynamics. The upcoming numerical methods include higher-order discretization schemes and novel interface tracking schemes, and HPC challenges of exascale computing.

3 MATHEMATICAL MODELING

3.1 Ship flows

The fluids involved in ship hydrodynamics are water and air (vapor phase in cavitation can be treated as a gas phase as the air in the solvers). In general, they can be considered as Newtonian fluids. The flow phenomena can also be considered as incompressible due to usually very low Mach numbers. Therefore, the governing equations for ship flows are the incompressible Navier-Stokes equations. Solvers for ship flows are categorized based on the solution methods for the two different fluids involved in as: (a) free-surface flow; (b) air flow; and (c) two-phase flow solvers.

3.1.1 Free-surface hydrodynamics

In free-surface flow solvers, only the water phase is solved using atmospheric pressure boundary condition at the free-surface. Many ship hydrodynamics solvers have adopted mathematical models for free-surface models, for example, CFDShip-Iowa versions 3 (Tahara et al., 1996) and 4 (Carrica et al., 2007) from IIHR, χship (Di Mascio et al., 2007) from INSEAN, SURF (Hino et al., 2010) from NMRI, PARNASSOS (Hoekstra, 1999) from MARIN, ICARE (Ferrant et al., 2008) from ECN/HOE, WISDAM (Orihara & Miyata, 2003) from the University of Tokyo, among others. These solvers are applicable in a wide range of applications, since the water phase accounts for most resistance. However, most of these solvers are not capable of solving problems with wave breaking and air entrainment, which have become more and more important in ship hydrodynamics due to the development of non-conventional hull shapes and studies of bubbly wake, among others.

3.1.2 Air Flows

For many problems in ship hydrodynamics, the effects of air flow on the water flow are negligible but the air flow around the ship is still of interest. This includes analysis of environmental conditions and air wakes around a ship in motion with complex superstructures, maneuverability and seakeeping under strong winds, capsizing, exhaust plumes (Huang et al., 2012a), etc. Most CFD research of ship aero-hydrodynamics simplified the problem by neglecting the free surface deformation and velocities, which restricted the range of problems that could be considered. A semi-coupled approach was developed by Huang et al. (2008) where the water flow is solved first and the air flow is solved with the unsteady free-surface water flow as boundary conditions. The limitation of the semi-coupled approach is its inabilities to deal with air entrainment, wind-driven wave generation, cavitation, etc., as the water flow is only affected by the air flow through ship motion driven by air flow load.

3.1.3 Two-phase flows

In the two-phase solvers, both the air and water phase are solved in a coupled manner, which requires treatment of the density and viscosity jump at the interface (Huang et al., 2007; Yang et al., 2009). The two-phase solvers are more common in commercial codes such as FLUENT, CFX, STAR-CCM+ (COMET) and open-source CFD solver OpenFOAM, as they are more general tools for a wide range of applications. However, air flows including air entrainment were seldom shown in ship flow applications performed with these solvers, due to high total grid resolution requirements for resolving the air flow besides the water flow. On the other hand, two-phase models are slowly being implemented in upcoming ship hydrodynamics research codes such as CFDShip-Iowa version 6 (Yang et al., 2009) from IIHR, ISIS-CFD (Queutey & Visonneau, 2007) from ECN/CNRS, FreSCo+ (Rung et al., 2009) from HAS/TUHH, and WAVIS (Park & Chun, 1999) from MOERI. Two-phase flow simulations are of interest in many applications, in particular, wind generated waves, breaking waves, air entrainment, and bubbly wakes, among others. Theoretically, it is possible to solve each phase

separately and couple the solutions at the interface. However, this approach is only feasible for cases with mild, non-breaking waves or a very limited number of non-breaking bubbles/droplets. Most solvers for practical applications adopt a one-field formulation in which a single set of governing equations is used for the description of fluid motion of both phases. In a one-field formulation, it is necessary to identify each phase using a marker or indicator function; also, surface tension at the interface becomes a singular field force in the flow field instead of a boundary condition in the phase-separated approaches. These issues are discussed in the following air-water interface modeling section.

3.2 Air-water interface modelling

3.2.1 Interface conditions

Air-water interface modeling must satisfy kinematic and dynamic constraints. The kinematic constraint imposes that the particles on the interface remain on the interface, whereas the dynamic conditions impose continuous stress across the interface. The stresses on the interface are due to viscous stresses and surface tension. The latter is usually neglected for many ship hydrodynamics applications.

3.2.2 Interface representation

One fundamental question for interface modeling is the indication and description of the interface. Smoothed particle hydrodynamics (SPH) method uses particles of specified physical properties to identify phase information without the need of tracking the interface explicitly (e.g., Oger et al., 2006). The particle density can be used as an indicator function to give the interface position for specifying surface tension. Of course, Lagrangian interface tracking methods such as front tracking or marker point tracking can give accurate interface position for adding surface tension. However, it is still required to obtain a field function to identify the phase information at each location within the flow field. Eulerian methods such as volume-of-fluid, level set, and phase field methods directly give the indicator functions at each point, but the interface position is embedded in the Eulerian field and is not explicitly specified. Another important issue of air-water interface modeling is the treatment of the air-water interface, i.e., is it a transition zone with a finite thickness or a sharp interface with zero thickness? Different answers determine different mathematical formulations and the numerical methods to the solution. In general, this concerns the variations of physical properties such as density and viscosity across the interface. On the other hand, surface tension can also be treated in both sharp and diffusive interface manners, even though the specific treatments are not directly tied to the mathematical approximation of jumps in the fluid physical properties. Detailed discussion of interface tracking is given in the numerical method section.

3.2.3 Sea conditions and wave models

Wave models are required to simulate flow fields with incident waves or sea environments. Wave generation can be achieved by imposing proper boundary conditions on the inlet boundaries. The boundary conditions can be imposed by emulating the wave makers used in actual wave tanks or by imposing velocity and wave height following the theories of ocean waves. Ambient waves for the reproduction of actual sea environments can be achieved by imposing waves with a given spectrum (Mousaviraad, 2010). For deep water calculations, waves are considered as a Gaussian random process and are modeled by linear superposition of an arbitrary number of elementary waves. The initial and boundary conditions (free surface elevations, velocity components and pressure) are defined from the superposition of exact potential solutions of the wave components. Sea spectra for ordinary storms such as Pierson Moskowitz, Bretschneider, and JONSWAP, or for hurricane-generated seas with special directional spreading may be implemented. Linear superposition of waves can also be used to create deterministic wave groups for special purposes. Examples include especially designed wave groups for single-run RAOs (Mousaviraad et al., 2010) and ship in three sisters rogue waves simulations (Mousaviraad, 2010). Figure 2 shows the exact potential solution for a linear wave component and generated random waves inside the computational domain as well as snapshots of the ship in three sisters simulations. For shallow water calculations, where the nonlinearities are significant, regular nonlinear waves may be generated using for example the Stokes second-order perturbation theory. Numerical issues associated with application of such conditions include achieving progression of waves without damping and the non-reflecting outflow boundary conditions.

3.3 Motions

3.3.1 Prescribed and predicted ship motions

As evident from G2010 test cases, most ship motion computations are for up to 3 degree of freedom (DoF): roll decay; sinkage and trim or pitch and heave in waves; maneuvering trajectories constrained from pitch, heave and roll; and PMM predicting pitch, heave

and roll. There are limited computations for 6DoF motions under varied seakeeping and maneuvering conditions. The motions are computed by solving the rigid body dynamics equations due to the forces and moments acting on the ship (Fossen, 1994). The forces and moments are generally obtained by integrating the contribution of pressure and viscous forces on the hull. This approach is accurate, but its implementation may be complicated for immersed boundary and overset methods. An alternative approach is to balance linear and angular momentum over a large control volume containing the body. This approach is easier to implement, but is prone to inaccuracies associated with numerical errors.

The influence of motion on the fluid flow governing equations can be either accounted as body forces in the ship system (Sato et al. 1999) or the governing equations can be solved in the inertial coordinates for which the grids move following the body (Carrica et al. 2007). For the first approach, the grids do not need to be deformed or moved during the computation but important features such as the free surface may shift to poor quality grid region. The second approach, although more expensive than the former, is more appropriate as it allows not only proper grid resolution during the simulation but also allows multi-body simulation. In the second approach, deformable, regenerated or overset grids should be used to move the objects. Grid deformation and regeneration methods are used mostly for finite volume solvers, and their application is limited to small amplitude motions. The dynamic overset grids provide huge flexibility in capturing motions and have been successfully applied for wide range of problems such as broaching, parametric roll, ship-ship interaction to name a few (Sadat-Hosseini et al., 2011b).

3.3.2 One-field formulations for motion prediction

The body domain can be included in the computational domain and the whole system can be represented as a gas-liquid-solid three-phase system, and solved using a one-field formulation. Although the structural deformation can be considered by including the structural constitutive models, rigid body motions are usually adequate for many applications. There is a large body of research for incorporated structural motion prediction in the flow solvers. Recently, several studies discussed monolithic fluid structure interaction on Cartesian grids (Robinson-Mosher et al, 2011; Gibou and Min, 2012). These methods require the modifications of the linear systems for consideration of solid motion coupled with fluid motion in a single step. On the other hand, partitioned approaches allow the solutions of solid motion and fluid flow using most suitable algorithms for each phase. Yang & Stern (2012) developed a simple and efficient approach for strongly coupled fluid-structure interactions using an immersed boundary method developed by Yang and Balaras (2006) with great simplification. The fluid-structure coupling scheme of Yang et al. (2008a) was also significantly expedited by moving the fluid solver out of the predictor-corrector iterative loop without altering the strong coupling property. This approach can be extended to gas-liquid-solid system similarly to the method in Yang & Stern (2009) for strongly coupled simulations of wave-structure interactions.

3.4 Propulsor modelling

Fully discretized rotating propellers have the ability to provide a complete description of the interaction between a ship hull and its propeller(s), but the approach is generally too computationally expensive (Lübke, 2005). Simplification such as use of single blade with periodic boundary conditions in the circumferential direction (Tahara, et al., 2005) can help ease the computational expense, but are still expensive for general purpose applications. Discretized propellers along with periodic conditions to define the interaction between the blades are mostly used for open water propeller simulations.

3.4.1 Body force and fully discretized propellers

Most commonly used propulsor model is the body force method. This approach does not require discretization of the propeller, but body forces are applied on propeller location grid points. The body forces are defined so that they integrate numerically to the thrust and torque of the propulsor. One of the most common techniques is to prescribe an analytic or polynomial distribution of the body forces. The distributions range from a constant distribution to complex functions defining transient, radially and circumferentially varying distribution. Stern et al. (1988b) derived axisymmetric body force with axial and tangential components. The radial distribution of forces was based the Hough and Ordway circulation distribution (Hough and Ordway, 1965) which has zero loading at the root and tip. More sophisticated methods can use a propeller performance code in an interactive fashion with the RANS solver to capture propeller-hull interaction and to distribute the body force according to the actual blade loading. Stern et al. (1994) presented a viscous-flow method for the computation of propeller-hull interaction in which the RANS method was coupled with a propeller-performance program in an interactive and iterative manner to predict the ship wake flow including the propeller effects. The strength of the body forces were computed using unsteady program PUF-2 (Kerwin et al., 1978) and field point

velocity. The unsteady wake field input to PUF-2 was computed by subtracting estimates of the propeller-induced velocities from the total velocities calculated by the RANS code. The estimates of induced velocities were confirmed by field point velocity calculations done using the circulation from PUF-2. Simonsen and Stern (2005) used simplified potential theory-based infinite-bladed propeller model (Yamazaki, 1968) coupled with the RANS code to give a model that interactively determines propeller-hull-rudder interaction without requiring detailed modeling of the propeller geometry. Fully discretized CFD computations of propellers in the presence of the ship hull have been performed in several studies. Abdel-Abdel-Maksoud et al. (1998) used multi-block technique to simulate the rotating propeller blades and shaft behind the ship for propeller-hull interaction investigation. Zhang (2010) simulated the rotating propeller using sliding mesh technique for the propeller behind a tanker. Carrica et al. (2010a, 2012b) included the actual propellers in the simulations by using dynamic overset grid. Muscari et al. (2010) also simulated the real propeller geometry using dynamic overlapping grids approach.

3.4.2 Waterjet propulsion

There is a growing interest in waterjet propulsion because it has benefits over conventional screw propellers such as for shallow draft design, smooth engine load, less vibration, lower water borne noise, no appendage drag, better efficiency at high speeds and good maneuverability. The waterjet systems can be modeled in CFD by applying axial and vertical reaction forces and pitching reaction moment, and by representing the waterjet/hull interaction using a vertical stern force (Kandasamy et al., 2010). Real waterjet flow computations are carried out including optimization for the waterjet inlet by detailed simulation of the duct flow (Kandasamy et al., 2011). Figure 3 shows the waterjet flow computation results for the two waterjet propelled high-speed ships studied, i.e. JHSS and Delft catamaran.

3.4.3 Propulsor modelling on Cartesian grids

Simulations with discretized propellers are increasingly becoming common practice in ship hydrodynamics. Immersed boundary methods can be used for greatly simplified grid generation in this type of applications. Posa et al. (2011) performed LES of mixed-flow pumps using a direct forcing immersed boundary method and obtained good agreement with experimental data. The Reynolds number is 1.5×10^5, based on the average inflow velocity and the external radius of the rotor, and the total number of grid points is 28 million. It is expected to see more applications of this type of simple approaches in propulsor modeling.

3.5 Turbulence modelling

The grid requirements for direct numerical simulation (DNS) of the Navier-Stokes equation for turbulent flows increases with Reynolds number, i.e, $O(Re^{9/4})$ (Piomelli and Balaras, 2002). Model scale $Re \sim 10^6$ and full scale 10^9 ship calculations would require 10^{13} and 10^{20} grid points, respectively. However, the current high performance computing capability allows $\sim 10^9$ grid points (Wang et al., 2012d). The alternative is to use turbulence modeling, which has been an important research topic over the last decades. A large number of models have been proposed, tested and applied, but no 'universal' model has been developed. In turbulence modeling, the turbulent velocity field is decomposed into resolved ($\widehat{\mathbf{u}}$) and fluctuating ($\mathbf{u}'$) scales of motion using a suitable filter function (Pope, 2000), which results in an additional turbulent stress term ($\boldsymbol{\tau}$), which can be expressed using a generalized central moment λ as:

$$\tau_{ij} = \lambda\left(\hat{u}_i, \hat{u}_j\right) = \widehat{u_i u_j} - \hat{u}_i \hat{u}_j. \qquad (1)$$

The main contribution of the above stresses is to transfer energy between the resolved and turbulent scales. The physics associated with the transfer depends on the choice of filter function, thus different turbulence modeling approaches focus on different aspects.

The most commonly used turbulence model is the Unsteady Reynolds Averaged Navier-Stokes (URANS) approach. In this approach only the large scales of motion are resolved and the entire turbulence scale is modeled. An emerging approach is Large Eddy Simulations (LES) (Hanjalic, 2005; Fureby, 2008). In LES the solution relies less on modeling and more on numerical methods, and provides more detailed description of the turbulent flow than URANS. The grid requirements for LES are still large especially in the near-wall region, and cannot be applied for next couple of decades (Spalart, 2009). Hybrid RANS-LES (HRL) models combines the best of both approaches, where URANS is used in the boundary layer and LES in the free-shear layer region (Spalart, 2009; Bhushan and Walters, 2012). Full scale simulations require extremely fine grid resolution near the wall, which leads to both numerical as well as grid resolution issues. Wall-functions are commonly used for full scale to alleviate these limitations, and they also allow the modeling of surface roughness (Bhushan et al., 2009).

3.5.1 URANS

In URANS the filter function represents an ensemble average, which is typically interpreted as an infinite-time average in stationary flows, a phase-average in periodic unsteady flows, and/or averaging along a dimension of statistical homogeneity if one is available. For such averaging, the entire turbulence spectrum is modeled and the resolved scales are assumed above the inertial subrange. URANS models should account for: (a) appropriate amount of turbulent dissipation; and (b) momentum and energy transfer by turbulent diffusion, which affects flow separation and vortex generation (Gatski and Jongen, 2000).

The most theoretically accurate approach for URANS is the differential Reynolds stress modeling. However, solutions of at least seven additional equations are expensive. The Reynolds stress equations also tend to be numerically stiff and often suffer from lack of robustness.

At the other extreme lie the linear eddy-viscosity models based on Boussinesq hypothesis, which are calibrated to produce an appropriate amount of dissipation. These do not account for the stress anisotropy as the three-dimensionality of the turbulent diffusion terms is not retained. The linear equation models have evolved from zero-equation, where eddy viscosity is computed from the mean flow, to most successful two equation models, where two additional equations are solved to compute the eddy viscosity. The k-ε model performs quite well in the boundary layer region, and k-ω in the free-shear regions. Menter (1994) introduces blended k-ε/ k-ω (BKW) model to take advantage of both these models. This is the most commonly used model for ship hydrodynamics community. The one equation SA (Spalart, 2009) model solves for only one additional equation of the eddy viscosity. This model is more common in the aerospace community, probably due to the availability of a transition option.

An intermediate class of models is the non-linear eddy viscosity or algebraic stress models (ASM). The algebraic models are derived by applying weak-equilibrium assumptions to the stress transport equations, which provides a simplified but implicit anisotropic stress equation. The solution of the equations can be obtained by inserting a general form of the anisotropy which results in a system of linear equations for the anisotropy term coefficients. These models have similar computational cost as the linear models, but provide higher level of physical description by retaining many of the features of the Reynolds stress transport equations. Several notable models in this category have been presented (Wallin and Johansson, 2002). It must be noted that algebraic models are more difficult to implement and often less robust than the conventional eddy-viscosity models. For this reason they are far less common than linear models, despite potential for increased accuracy. In G2010, there were limited submissions using such models, and they reproduced the measured structure of the turbulence better than linear models (Visonneau, Chapter 3 - G2010 proceedings). Stern et al. (Chapter 7 - G2010 proceedings) performed calculations for straight ahead 5415 using CFDShip-Iowa V4 on up to 50M grids using k-ω based anisotropic (ARS) and linear model (BKW). ARS showed significantly better velocity, turbulent kinetic energy and stress profiles at the nominal wake plane than the linear model, as shown in Fig. 4. However, the turbulent kinetic energy and normal stresses were over predicted by 60% even on 50M grid. Further, the ARS model does not show good predictions for the stress anisotropy.

URANS simulations with anisotropic models on 10s to 100s million grids are desirable to obtain benchmark URANS predictions. But improved mean vortical and turbulent structure predictions require further improvements in the models, such as ability to account for rotation/curvature effects or structure-based non-linear effects (Kassinos, 2006).

3.5.2 LES

In LES, the filtering scale is assumed to lie within the inertial subrange, such that the organized coherent turbulent structures are resolved and small-scale quasi-isotropic turbulent fluctuations are modeled. Key aspects for LES modeling include: (a) resolution of energy transfers between the coherent and fluctuating turbulent scales, which involves both forward and backscatter of energy; and (b) the requirement of initial background fluctuation energy to instigate coherent turbulence fluctuations via the production term (Batten et al., 2004).

The most commonly used LES models are the eddy-viscosity type model. These models are similar to the linear URANS models, except that the length scale is defined explicitly as the grid size. These models can only account for the forward transfer of energy, unless dynamic coefficients are used to allow backscatter in an averaged sense (Lilly, 1992). Backscatter of energy is identified to be a very important aspect for atmospheric flows, which involves both 2D and 3D turbulence (Kraichnan, 1976). Studies in this community have incorporated backscatter explicitly via an additional stochastic forcing term (Schumann, 1995). The second most common class of LES models are the variants of the scale-similarity model (Bardina et al., 1983), which are developed based on the assumption that the flow in the subgrid scale copy the turbulence

scales an octave above. These models have been found to be under dissipative, and are often combined with the eddy viscosity model to obtain nonlinear mixed models (Meneveau and Katz, 2000). These models have also been extended to include dynamic model coefficient evaluation to account for backscatter in an averaged sense (Horiuti, 1997). Another class of model which has gained popularity for applications is the Implicit LES (ILES) models, where the numerical dissipation from the 2nd or 3rd order upwind schemes is of the same order as the subgrid-scale dissipation (Boris et al, 1992).

One of the major issues with the use of LES is the extremely fine grid requirements in the boundary layer, i.e., the grids have to be almost cubical, whereas URANS can accommodate high aspect ratio grids. Piomelli and Balaras (2002) estimate that grid resolution required resolving inner boundary layer (or 10% of the boundary layer thickness) requires ~ $Re^{1.8}$ points which gives, 10^{11} and 10^{16} points for model and full scale, respectively.

Fureby (2008) reviewed the status of LES models for ship hydrodynamics, and concluded that the increases in computational power in the past decade are making possible LES of ships, submarines and marine propulsors. However, the LES resolution of the inner part of the hull boundary layer won't be possible for another one- or two-decades. To meet the current demand of the accurate predictions of turbulent and vortical structures, modeling efforts should focus on development/assessment of wall-modeled LES or hybrid RANS-LES models.

3.5.3 Hybrid RANS-LES

From a broad perspective the only theoretical difference between the URANS and LES formulations is the definition of the filter function. HRL models can be viewed as operating in different "modes" (LES or URANS) in different regions of the flow-field, with either an interface or transition zone in between. HRL models are judged based on their ability to: (a) blend URANS and LES regions and (b) maintain accuracy in either mode and in the transition zone (or interface).

The HRL models available in the literature can be divided into either zonal or non-zonal approaches. In the zonal approach, a suitable grid interface is specified to separate the URANS and LES solution regions, where typically the former is applied in the near wall region and the latter away from the wall (Piomelli et al., 2003). This approach provides flexibility in the choice of URANS and LES models, enabling accurate predictions in either mode (Temmerman et al., 2005). However, there are unresolved issues with regard to the specification of the interface location and the coupling of the two modes. For example, smaller scale fluctuations required as inlet conditions for LES region are not predicted by the URANS solution. Several approaches have been published to artificially introduce small-scale forcing, either by a backscatter term, isotropic turbulence, or an unsteady coefficient to blend the total stress or turbulent viscosity across the interface (Batten et al., 2004).

Non-zonal approaches can be loosely classified as adopting either a grid-based or physics-based approach to define the transition region. The most common grid-based approach is detached eddy simulation (DES). In DES, a single grid system is used and the model transitions from URANS to LES and vice versa, based on the ratio of URANS to grid length scale (Spalart and Allmaras, 1992). This approach provides transition in a simpler manner than the zonal approach, and the need for artificial boundary conditions at the interface is avoided. The DES approach assumes that: the adjustment of the dissipation allows development of the coherent turbulent scales in the LES mode; and that the LES regions have sufficient resolved turbulence to maintain the same level of turbulence production across the transition region. However, these criteria are seldom satisfied and errors manifest as grid/numerical sensitivity issues, e.g., LES convergence to an under dissipated URANS result due to insufficient resolved fluctuations, modeled stress depletion in the boundary layer, or delayed separated shear layer breakdown (Xing et al., 2010a). Delayed DES (DDES) models and other variants have been introduced to avoid the stress depletion issue in the boundary layer (Shur et al., 2008). But these modifications do not address the inherent limitations of the method, which is identification of the transition region primarily based on grid scale.

Several studies have introduced transition region identification based on flow physics (Menter and Egorov, 2010). Girimaji (2006) introduced partially averaged Navier-Stokes (PANS) modeling approach based on the hypothesis that a model should approach URANS for large scales and DNS for smaller scales. These models have been applied for various applications with varying levels of success, but have not undergone the same level of validation as LES models. Hence their predictive capability in pure LES mode cannot be accurately ascertained (Sagaut and Deck, 2009). Ideally, a hybrid RANS-LES model should readily incorporate advances made in URANS and LES community, rather than representing an entirely new class of model.

Recently, Bhushan and Walters (2012) introduced a dynamic hybrid RANS-LES framework (DHRL), wherein the URANS and LES stresses are blended as below:

$$\tau_{ij} = (1-\alpha)\tau_{ij}^{LES} + \alpha\tau_{ij}^{URANS} \quad (2)$$

The blending function α is solved to blend the turbulent kinetic energy (TKE) production in the URANS and LES regions as below:

$$\Longrightarrow \alpha = 1 - \frac{\overline{u_i'' u_j''}\,\bar{S}_{ij}}{\max(\tau_{ij}^{URANS}\bar{S}_{ij} - \overline{\tau_{ij}^{LES}}\,\bar{S}_{ij}, 10^{-20})} \quad (3)$$

The model to operate in a pure LES mode only if the resolved scale production is equal to or greater than the predicted URANS production, otherwise the model behaves in a transitional mode where an additional URANS stress compensates for the reduced LES content. Likewise, in regions of the flow with no resolved fluctuations (zero LES content), the SGS stress is zero and the model operates in a pure URANS mode. The advantage of the DHRL model includes: (a) it provides the flexibility of merging completely different URANS and LES formulations; and (b) allows a seamless coupling between URANS and LES zones by imposing smooth variation of turbulence production, instead of defining the interface based on predefined grid scale.

Non-zonal DES approach has been used to study the vortical and turbulent structures and associated instability for flows of ship hydrodynamics interest on up to large 300M grids using CFDShip-Iowa V4. Simulations have been performed for surface-piercing NACA 0024 airfoil (Xing et al., 2007), Wigley hull at β = 45° and 60° (Heredero et al., 2010), wetted transom flow for model and full-scale bare hull and appended Athena (Bhushan et al., 2012c), wet and dry transom-model (Drazen et al., 2010), 5415 at straight ahead conditions, 5415 with bilge keels at β = 20° (Bhushan et al., 2011a), and KVLCC2 at β=0, 12° and 30° (Xing et al., 2012).

Surface-piercing NACA 0024 airfoil simulations help study the effect of free-surface on flow separation and turbulence structures in the separation region. Wetted transom bare hull and appended Athena and transom-model simulations help identify the transom free-surface unsteadiness due to the transom vortex shedding as shown in Fig. 5. The straight ahead 5415 simulation provided a detailed resolution of the evolution and interaction of the vortical structures, and provided a plausible description of the sparse experimental data as shown in Figs. 4 and 6. The static drift simulations were performed to analyze the flow features and guide the ongoing experiments. The vortical structures predicted for KVLCC2 at β = 30° are shown in Fig. 7, and those for 5415 with bilge keels at β = 20° including preliminary comparison with experiments in Fig. 8. Studies have shown Karman-like, horseshoe vortex, shear layer, flapping and helical vortex instabilities as summarized in Table 1.

The Karman-like instabilities were observed for wave induced separation for surface piercing NACA 0024 airfoil, for transom vortex shedding for wetted transom Athena and transom model flows, due to the interaction of hull and tip vortices in Wigley hull, due to the interaction of bow vortices for KVLCC2, and interaction of vortices on the leeward sonar dome. These instabilities are caused by the interaction of two opposite vortices initiated by shear layer instability, and are scaled using half wake width H and shear layer velocity (U_S). Sigurdson (1995) reported a universal Strouhal number $St_H = fH/U_S$ range of 0.07 – 0.09. For surface-piercing NACA 0024 simulation, St_H ~ 0.067, and it was found that free-surface reduces both the strength and frequency of the vortex shedding resulting in lower St_H. The ship geometries show averaged St_H ~ 0.088, which is towards the higher end of the expected range.

Horseshoe vortices were predicted for the appended Athena simulations at rudder-hull, strut-hull and strut-propeller-shaft interactions. Simpson (2001) reviewed horseshoe vortex separations, and identified that they occur at junction flows when a boundary layer encounters an obstacle. These instabilities are associated with two vortex system, or dual peak in frequency. The secondary peak amplitude decreases with the increase in the angle of attack and sweep angle. These structures are scaled using the thickness of the obstacle T and largest dominant frequency, and show $St_T = fT/U_0$ = 0.17 - 0.28. Athena simulations predicted St_T = 0.146±3.9% at rudder-hull intersection and St_T = 0.053±2% at strut-hull interaction.

Shear layer instabilities, which are associated with the boundary layer separation, were predicted for free-surface separation and inside the separation bubble for surface piercing NACA 0024 studies; boundary layer separation close to the appendages for appended Athena; on the leeward side for the static drift cases, in particular at hull bow and keel for Wigley hull, at the bow for KVLCC2, and sonar dome separation bubble for 5415. Such instability is scaled using boundary layer at separation (θ) and U_S and shows St_θ = 0.0056±2% for airfoil boundary layer separation (Ripley and Pauley, 1993). For surface-piercing NACA 0024, St_θ = 0.00384±0.5% for free-surface separation, and varied inversely with the non-dimensional adverse pressure gradient at separation. The boundary layer separation for appended Athena showed St_θ = 0.0067±3%, and for leeward side flow separation for static cases St_θ ~ 0.001 ~ 0.003, and in some cases even lower.

Flapping instability was predicted for the free-surface separation bubble in surface-piercing NACA 0024 simulations, and transom wake for bare hull

Athena simulations. Such instability occurs when a recirculation region exhibits a periodic enlargement and shrinkage, and is scaled using the reattachment length X_R and free stream velocity U_0. For canonical cases, $St_R = fX_R/U_0 \sim 0.073 - 0.12$ (Kandasamy et al., 2009). The surface-piercing NACA 0024 and Athena simulations showed $St_R = 0.28$ and 0.144, respectively.

Static drift simulations show helical vortices. For the Wigley hull at $\beta = 60°$ and KVLCC2 at $\beta = 30°$ such vortices were generated on the leeward side, and for 5415 at $\beta = 20°$ from the bilge keel tip and fore-body keel. For both KVLCC2 and 5415, the vortex core frequency decreased downstream such that the St_X based on the distance from the separation point remains constant, similar to the tip vortices formed over a delta wing. Overall, for most of the vortices $St_X \sim 0.095 - 1.45$ compares well with the Delta wing tip vortex range of 0.75 – 1.35. However further analysis is required to confirm the identity of these instability mechanisms, including comparison with slender fuselage vortices.

The transom flow pattern for dry transom-model flow shows shoulder waves emanating from the transom edge, which moves towards the center-plane, overturns and breaks. A similar breaking wave pattern was also predicted for bare hull Athena URANS simulation (Wilson, 2005). This instability causes unsteady wave elevation pattern in the rooster tail region. Instability mechanism associated with such unsteadiness has not been identified.

Fully appended Athena wetted transom flow shows unsteady pitch and heave motion, whereas the dry transom simulations show steady motions. The motion unsteadiness were attributed to the Karman-like transom vortex shedding, as both show the same dominant frequency. This instability was called "vortex-induced-motion" and scaled using ship length L and U_0 which resulted in $St_L = 2.19$.

Studies have shown good predictions for the resolved turbulence levels around 80% to 95% for NACA 0024, bare hull and appended Athena, and static drift cases, when the flow separation was dictated by the geometry. However, for the straight ahead 5415 case the resolved turbulence was not triggered, which resulted in stronger, under dissipated vortices. Stern et al. (Chapter 7 - G2010 proceedings) identified that the under resolved turbulence is due to the limitations of DES model in triggering resolved turbulence, and not due to numerical dissipation issues. For the KVLCC2 simulations on 305M grid, Xing et al. (2011) observed that the model over-predicted the velocity near the symmetry plane, Reynolds stresses at the propeller plane and showed grid induced separation and modeled-stress depletion in the boundary layer. The delayed DES (DDES) version of the model was able to resolve the induced separation issue, but not the modeled stress depletion. Recently, Bhushan et al. (2012b) applied DHRL and DES models for straight ahead 5415 in single phase using commercial software Fluent. The DHRL model was able to trigger resolved turbulence, whereas DES failed to do so.

Hybrid RANS-LES simulations on 100s millions to billions of grid points for model-scale are required to enable resolution of small-scale physics, improve understanding of turbulence and vortical structures, two-phase flow and air entrainment. Such simulations will help in explaining the observation in sparse experimental data and guide experiments, and provide benchmark datasets to develop better URANS models. However, the existing Hybrid RANS-LES models have not been previously applied for similar simulations, hence detailed verification and validation needs to be performed. Further, the available grid verification methodologies were developed for URANS (Stern et al, 2006a; Xing and Stern, 2010), and cannot be applied straightforwardly to hybrid RANS-LES due to the coupling of modeling and numerical errors. Thus, new verification methods need to be developed.

3.5.4 Wall-functions

The boundary layer thickness decreases with the Reynolds number, thus near wall grid resolution ($y^+ \sim 1$) for full-scale ship computations require very high grid density. A rough estimate suggests that the number of grids required in the wall normal direction to resolve the inner boundary layer is $\sim Re^{0.6}$ points, i.e., around 250K grid points in the wall normal direction (Piomelli and Balaras, 2002). The extremely fine grid spacing may also lead to numerical issues, such as increases the errors of computing mass and momentum fluxes in high aspect ratio cells. The use of "wall-functions" avoids the numerical limitations of the near-wall turbulence model and significantly reduces the computational cost. In wall-function approach the solution in the inner boundary-layer is circumvented using flat-plate boundary layer assumptions, i.e., the flow is governed by the pressure gradients outside the boundary layer and the velocity profile follows the universal sub- and log-layer. The boundary conditions are applied at the first grid point away from the wall, called matching point. The accuracy of such models depends on their ability to: (a) account for the variation of the grid resolution y^+ on the hull, (b) prediction of the flow separation point, and (b) robustness of the implementation.

The most commonly used wall-function is the standard wall-function. This approach is based on the stringent criteria that the matching point lies in the log-layer (one-layer only). However, variation of the boundary layer thickness along the ship hull makes it

difficult to always place the matching point in the log-layer. This deficiency has been addressed by introducing multi-layer models, where the boundary conditions for the velocity and turbulent quantities switch smoothly between the sub- and log-layer profiles depending upon the local y+ value (Bhushan et al., 2009). Some studies have implemented pressure gradient effect in wall-function formulation to improve predictions for separated flows (Kim and Chaudhury, 1995). But often the pressure gradient magnitude needs to be clipped to avoid numerical instability. Thus the benefit of including pressure gradient effect is questionable (Kalitzin et al., 2005).

Implementation of wall-function models requires evaluation of the friction velocity to provide boundary conditions for velocity and turbulence variables. A one-point approach proposed by Kim and Chaudhary (1995) uses the flow variables at the wall neighboring cells only, and allows solutions of the momentum equations up to the matching point. This approach can be implemented easily for finite-volume schemes, but introduces additional challenges for finite-difference schemes. An alternative two-point approach (Tahara et al., 2002) uses the velocity magnitude and direction at the second grid point away from the wall to obtain the boundary conditions at the matching point. Implementation of this approach is straightforward for finite-difference scheme. However, the one-point approach is expected to be more accurate than the two-point approach, as the former does not restrict the flow streamline at the matching point.

Effect of surface roughness is more important for full-scale computations than for model-scale. The most commonly used model for surface roughness is based on downshift of the log-layer profile (Patel, 1998). Several studies have validated the existence of downshift of log-law in the transitional roughness regime, this provides some confidence in such modeling (Jimenez, 2004). However, the amount of shift based on roughness length is still an area of active research.

Applicability of wall-function for ship flows has been demonstrated by several researches for both model scale and full scale (Oh and Kang 1992). Bhushan et al. (2009) implemented multi-layer wall function using with wall roughness and pressure gradient effects using two-point approach in CFDShip-Iowa V4 and performed verification and validation for smooth and rough wall Athena resistance, propulsion and seakeeping, and 5415 maneuvering simulations. The results (selected results shown in Fig. 9) were compared with model scale predictions and with limited full scale data, for which the predictions were encouraging.

Wall-functions are a viable option for full-scale ship simulations and implementation of wall roughness effects. The obvious limitations of the wall-functions are in accurately predicting separated flows and 3-D boundary layers with significant cross-flow. Nevertheless, near-wall turbulence models also suffer from the same deficiency as the model constants are derived under similar turbulent boundary layer assumptions (So and Lai, 1988). Multi-layer models have performed well for ship flows including resistance, propulsion, seakeeping, and maneuvering. However, further research is required to develop improved pressure gradient models for accurate flow separation predictions, and better relation of the downshift of log-law with roughness length.

3.5.5 Two-phase turbulence modeling

In ship hydrodynamics, the wall boundary and the air-water interface are the two major sources of difficulties of resolving turbulence at high Reynolds numbers. The former has been the sole theme of many research topics for many years; the investigations of the latter have been limited to DNS and highly-resolved LES, and modeling means like RANS turbulence models for the former, which are more or less mature, though imperfect, are not reached yet. Droplet/bubble-laden turbulent flows are even less understood, especially, when interacting with the boundary layer near a solid wall. Due to the extremely high computational cost, DNS is limited to low Re number turbulent flows. Some large-eddy simulation (LES) studies (Sreedhar and Stern, 1998a, b; Broglia et al., 2003) have been conducted at very low *Fr* numbers with the air effect neglected. For two-phase interfacial flows, the eddy viscosity is often over-predicted if the single phase based LES and RANS models are used (Liovic and Lakehal, 2007). Liu et al. (2009) investigated the coupled air-water turbulent boundary layers using direct numerical simulations. In Toutant et al. (2009a), the two-phase LES concept was developed at a given level of description that the filter is much smaller than the bubbles/drops. Away from the two-phase mixture region, the single-phase LES concept still applies. In general, turbulence modeling of two-phase interfacial flows is in its early stage. High-resolution DNS studies and detailed experimental measurements are required for the development, improvement, and validation of two-phase turbulence modeling techniques. It is expected the new models are built on top of the corresponding single phase models.

4 NUMERICAL METHODS

4.1 Reference frames

The governing equations for ship hydrodynamics are the incompressible Navier-Stokes equations which are solved in an absolute inertial earth-fixed reference frame for resistance, pitch, heave and roll simulation, or a relative inertial reference frame for an arbitrary non-deforming control volume involving surge, yaw and sway motions (Xing et al., 2008). It is common practice to have a ship-fixed non-inertial reference frame for solving the ship motions.

4.2 Interface tracking/capturing

In pure Lagrangian, meshless flow solvers, such as SPH (Oger et al., 2006) and MPS (Moving Particle Semi-implicit, Shibata et al., 2009), different fluids are represented by particles of different densities. As a result, there is no need to track the interface between different phases. On the other hand, Lagrangian particles can also be used for interface tracking in Eulerian grid-based flow solvers. In this type of methods, such as front tracking or point set methods, connected or unconnected marker particles are placed on the interface and moved to new positions according to the local fluid velocity. In theory, they are the most straightforward methods that can provide high accuracy. However, rapid topological changes of the interface may make the operations on the marker particles very tedious and difficult. Mass conservation during the interface evolution is not explicitly enforced and an indicator function is required to be obtained from the geometric information of the interface for phase identification.

Many free-surface flow solvers adopted surface-fitting methods, in which the grids, structured or unstructured, were iteratively updated to conform with the free surfaces (e.g., Tahara et al., 1996; Starke et al. 2010). However, the approach has limitations for large free surface deformations, such as for steep or breaking waves; may have singular solution at the transom corner for wet-dry transition Fr range (Li and Matusiak, 2001); and grid deformation is numerically expensive. Therefore, these methods are more suitable for steady flow computations with mild waves. Wackers et al. (2011) described three ship flow solvers with different interface tracking/capturing schemes, i.e., surface fitting, level set, and volume of fluid (VOF) methods.

The level set function can be treated as a general scalar and its advection equation can be solved using temporal and spatial discretization schemes similar to those of the fluid flow. Geometrical information such as interface normal and curvature is easily derived from the level set function. These advantages have greatly increased its applications in many CFD fields including ship hydrodynamics (e.g., Carrica et al., 2007; Yang & Stern, 2009). However, there is no volume constraint in the course of level set evolution through the level set advection equation, which makes the mass conservation a serious issue in level set methods. For example, in CFDShip-Iowa version 5 (Huang et al., 2007), two-phase ship flows were solved on multi-block structured grids with the level set method for interface capturing. A major issue to extend this solver to dynamic overset grids was the discontinuous interface (i.e., the level set function) across the overlapping grids due to different rates of mass loss on grids of different resolution. In Huang et al. (2012b) a geometry-based approach was proposed to fix this issue for overset grids, in which the level set advection and reinitialization equations were discretized along the upwind streamline and level set gradient directions, respectively. It was essentially an unstructured approach disregarding the resolution differences between overset grids, although the discretization was implemented in a finite differences approach.

Many schemes have been developed for possible improvements, such as the particle level set methods (Enright et al., 2002; Wang et al., 2009a), coupled level set and volume of fluid methods (Sussman & Puckett, 2000; Wang et al., 2009b). Recently, Sussman's group developed a level set method with volume constraint (Wang et al., 2012). Some studies chose different definitions of the level set function, for instance in Olsson & Kreiss (2005) a smoothed heaviside function was used with value 0~1 across the interface at iso-level 0.5, instead of a signed distance function. Although they were called level set methods since a reinitializtion step was still involved, in some sense they are closer to other methods such as phase field, constrained interpolated propagation (CIP, Hu and Kashiwagi, 2010), and color function methods that define a smoothed transition band between different phases.

There is a large body of studies on interface capturing schemes using the volume fraction as a conservatively advected scalar. Usually their schemes were also named volume of fluid (VOF) methods, the focus of research was on the design of compressive advection scheme to reduce the numerical diffusion and restrict the interface represented by the volume fraction within a narrow band. The algebraic VOF schemes implemented in OpenFOAM are particular representative examples. In Wackers et al. (2011) such a VOF scheme was discussed for unstructured grids. A major problem of these schemes is the blurred interface, which requires very high resolution for capturing small-scale interfacial phenomena such as droplets and bubbles.

On the other hand, in the geometrical VOF methods, the phase marker function is directly advected and a special interface reconstruction step is required due to the sharp jump in the marker function across the interface. The evaluation of geometric information such as interface normal and curvature is not easy due to the discontinuous marker function. Therefore, VOF methods combined with a level set function can be quite useful for this purpose. Wang et al. (2012a) developed a new VOF method on general structured grids with a distance function constructed from the VOF function, which greatly expands the applicability of the VOF method. Further improvements on VOF methods have been investigated through tracking additional information such as the material centroids in the moment of fluid method (Ahn & Shashkov, 2009). Recently Sussman's group coupled the level set method with the moment of fluid method (Jemison et al., 2012). It is also possible to couple front tracking methods with the VOF methods such as in Aulisa et al. (2004). Of course, their methods are usually more complicated compared with the level set and algebraic VOF methods, but their minimized interface position errors and optimized mass conservation properties are highly desirable in high-fidelity simulations of ship hydrodynamics studies with small-scale interfacial phenomena.

4.3 Velocity-pressure coupling

The incompressible Navier-Stokes equations have a mixed parabolic-elliptic character. For steady flows, the equations are of elliptic type and this property can be used in the solution strategies. That is, the continuity and momentum equations can be solved in a fully coupled form, as implemented in CFX and PARNASSOS (Hoekestra, 1999), among others. Such methods are expected to be robust; however, the fully coupled manner results in very large systems of linear equations that are quite expensive to solve. They are usually called pressure-based methods. In a density-based method, e.g., the artificial compressibility method, the continuity equation is cast into a form akin to one that is widely used for compressible flows by adding a first-order time-derivative of pressure. Addition of this term leads to a hyperbolic system of continuity and momentum equations, which can be solved in a coupled manner (Rosenfeld et al., 1991). SURF (Hino et al., 2010) and Tenasi (Briley et al., 2006) ship hydrodynamics solvers use this method. It is usually required to adjust an artificial compressibility parameter in these methods for achieving good performance of convergence.

Most solvers have adopted a different approach, i.e., the projection method, in which the continuity equation is satisfied through a Poisson equation for pressure (correction). For steady flow problems, the SIMPLE-family (SIMPLE, SIMPLER, SIMPLEC) algorithms are predominant in commercial solvers and ship hydrodynamics solvers. For unsteady problems, these algorithms can also be used, but the SIMPLE-based PISO method is more suitable. In all these methods, the solutions are advanced in multiple iterations or time-steps. The momentum equations are first solved without pressure or with pressure from the previous iteration or time-step. Next, the Poisson equation for pressure (correction) is solved. Finally, the velocity field is corrected using the new pressure (correction). This segregation or decoupling of the originally coupled equations often makes the projection method-based solutions converge more slowly than the fully-coupled solvers discussed above. Nonetheless, the majority of contributing CFD codes at the Gothenburg 2010 workshop adopted the projection method (Larsson et al., 2010).

Fully coupled and SIMPLE-family methods discussed above were developed mainly for solving steady flows. Although techniques such as dual-stepping and PISO can be used for unsteady problems, these schemes are inherently limited in the choices of different numerical schemes for temporal and spatial discretization. On the other hand, fractional-step methods, also one type of projection methods, are in general more suitable for time-dependent simulations and widely used in high-fidelity simulation methodologies such as DNS and LES. There are two types of fractional-step methods, depending on the collocation of velocity components. The staggered arrangement (MAC grid) is usually called exact projection as the velocity-pressure coupling is tight and the discrete divergence is exactly zero (in practice a small value depending on the solution of the pressure Poisson equation). However, the staggered variable arrangement makes it inconvenient for general grids and coordinate systems. With approximate projection methods the exact discrete divergence free condition is relaxed and cell-centered variable arrangement is usually used. On the other hand, Dong & Shen (2010) developed an unconditionally stable rotational velocity-correction scheme for incompressible flows, which can be categorized as an approximate projection method. They further developed their method in (Dong & Shen, 2012) by proposing a time-stepping scheme involving constant coefficient matrices for phase-field simulations of two-phase incompressible flows with large density ratios.

4.4 Semi-coupled air-water flows

For implementing the semi-coupled approach, a proper treatment is required for the boundary and initial conditions for air over water (Mousaviraad, 2010). A

potential solution is obtained for air over water waves which have a discontinuity since the tangential velocity changes sign across the surface. Then a blending function is introduced to treat the discontinuity in the potential solution and roughly represent the thin viscous layer above the water waves. For irregular waves, the same potential solution and blending function is used to define each elementary wave component in the superposition.

The semi-coupled approach in CFDShip-Iowa V4.5 is used to study the effects of head winds on ship forces, moments, motions, and airwake flows for calm water straight ahead, static drift, and dynamic PMM maneuvers of the ONR tumblehome with validations against wind towing tank experiments (Mousaviraad et al., 2012). Figure 10 shows examples of the air flow field results for static conditions. Computations are also carried out for pitch and heave in regular head waves and 6DOF motions in irregular waves simulating hurricane CAMILLE (Mousaviraad et al., 2008). Thermal and concentration transport models are implemented in CFDShip-Iowa version 4.5 (Huang et al., 2010) to investigate the exhaust plume around ship superstructures. Figure 11 shows exhaust plume of the ONR Tumblehome in an extreme motions condition. Complicated vortical structures are observed in air including a pair of counter-rotating vortices downstream of the stack for cross-flow, and bended bird-plume shape in the symmetry plane and varying arc-shape in axial sections both for temperature and NOx concentration fields.

4.5 Spatial discretization

The discretization of the governing equations are performed either using finite-volume (FV) or finite-difference (FD) approach. A survey of the G2010 submissions shows that the FV approach is more common in ship hydrodynamics community than FD approached (Larsson et al., 2010). This is because FV approach can be applied for arbitrary polyhedral grid volumes which are easier to generate than curvilinear structured grids required for FD. However, FV methods are not suited for implementation of higher order schemes and mostly use second-order schemes. On the other hand, FD approach allows implementation of 3rd-order and 5th-order schemes with ease (Yang & Stern, 2009). The diffusion terms are mostly discretized using central-differencing, whereas upwind-biased schemes are used for convective terms. Higher-order schemes provide better accuracy, yet often at the expense of additional numerical cost and solution instability. Numerical methods often include flux-limiter or slope-limiter designed to suppress unphysical oscillations in solutions (Ismail et al., 2010).

4.6 Temporal discretization

The majority of CFD solvers use implicit time-marching schemes. Implicit time-marching schemes allow one to use much larger time-step size than explicit time-marching schemes, speeding up numerical solutions for flows with large characteristic time scales. Implicit time-marching, however, requires solutions of system of coupled non-linear equations, which incur computational cost. Explicit time-marching, which forces much smaller time-step size, is rarely used for RANS computations. Time step discretization is achieved by using first-order backward Euler scheme for steady-state cases, and second-order schemes such as Crank-Nicolson and three-level backward schemes for time-accurate solutions (Larsson et al., 2010). Limited studies have used 4th-order Runge-Kutta schemes. Studies often use solution relaxation to improve stability of the solution.

4.7 Semi-Lagrangian advection schemes

In general, high Reynolds number turbulent flows are advection dominated. Therefore, the advection schemes used for the momentum equation are critical for the accuracy of simulations. Higher-order advection schemes are difficult to be made implicit in time. Thus treatments like deferred corrections are quite popular in engineering CFD solvers, because explicit Eulerian advection schemes are subject to the CFL number for time step restriction. When the flow velocity is high and/or the grid spacing is small, the CFL restriction due to the time step from the explicit advection schemes can be prohibitive. Semi-Lagrangian advection schemes have been enjoyed for a long time in the numerical weather prediction community. With these unconditionally stable schemes, higher-order spatial/temporal accuracy can be retained and significantly increased maximum allowable time steps with CFL numbers up to 4~5 can be safely used. In Xiu & Karniadakis (2001), a high-order semi-Lagrangian spectral element method was developed for incompressible flows. Recently, Wang et al. (2012b) developed a semi-Lagrangian advection scheme for the VOF method, which are more accurate than the corresponding Eulerian scheme and much improved with regard to mass conservation. With the increased popularity of adaptive mesh refinement techniques, more and more studies of semi-Lagrangian schemes have been conducted. Min and Gibou (2006) developed a second-order projection method using a semi-Lagrangian advection scheme for incompressible flows on adaptive Cartesian grids. They also reported a second-order semi-Lagrangian level set method on adaptive grids later (Min and Gibou, 2007). Most recent studies have been focused on conservative semi-

Lagrangian advection schemes, such as Lentine et al. (2011) and Qiu & Shu (2011).

4.8 Grid generation

Numerical grids are categorized into Cartesian, structured and unstructured. Most solvers in ship hydrodynamics community including both research and application solvers use unstructured grids wherein the fluid region is sub-divided into tetrahedral cells in the boundary layer and polyhedral cells elsewhere (Marcum, 1995). Octree subdivision, Delaunay point insertion, and advancing front techniques are used to create the tetrahedral cells near the wall. These grids are relatively easy to make for complex geometry, but it is difficult to control the grid quality (Baker et al., 1989). Structured grids use body fitted hexahedral cells, and are quite complicated to generate for complex geometries (Thompson et al., 1985). Elliptical smoothing algorithms are often used to improve the quality of the grids. These structured grids are used along with multi-block overset grid techniques to ease the grid generation complexity. Multi-block techniques use topological inter-connections to connect the faces of the blocks. This can be done using overset or overlapping techniques, where the interpolation is applied across local cell volumes and faces. These interpolation schemes can be applied dynamically to form transient moving and sliding grids to account for the relative motions of the ship hull and the rotation of the propulsion system and appendages (Noack, 2006; Wang and Parthasarthy, 2000). The Cartesian grid methods and upcoming technology are discussed separately.

4.9 Solution adaptation

Solution adaptation in CFD is the process in which the computational approaches are modified during the solution process of a given problem, in order to obtain a more accurate description of the fluid flow or maintain a similar order of accuracy but with reduced computational cost. There are four types of solution adaptation strategies: i) m-adaption, in which different mathematical models are used within different portions of the computational domain, for example, the coupling of a potential solver and a viscous solver for ship flows, the coupling of an Euler solver and a Navier-Stokes solver for aerodynamic flows, also, the coupling of RANS models within the boundary layer and LES in the bulk flow in a hybrid RANS/LES simulation; ii) p-adaption, in which discretization schemes of different orders are used in different portions of the computational domain, for instance, in finite element methods the p-adaptive strategy is frequently used with different shape functions represented by different orders of polynomials in each element; iii) r-adaption, in which the grid points are allowed to move, but without changing the grid connectivity, in the solution process to give better resolution to an interested area; and iv) h-adaption, in which grids points are added or deleted by changing the grid connectivity. The h-adaption is the most popular approach as there are no coupling issues between different mathematical models and discretization schemes and it is not limited by the initial number of grid points and the difficulty of grid quality control as in the r-adaption. Overset grid techniques can be used to obtain h-adaption, but usually the refinement regions such as the free surface and wake are determined beforehand instead of adaptively during the computations due to the extra computational overhead of grid oversetting procedure (Carrica et al., 2007). A directional adaptive mesh refinement method was developed in Wackers et al. (2012) in ISIS-CFD using unstructured hexahedral finite volume meshes.

The solution adaptation processes require the evaluation of adaptation metric to identify the regions of interest. The choice of adaptation metric depends on the application. The simplest techniques define the solution adaptation region based on the experience and knowledge of the user, for example wake planes or wave surfaces. Vorticity is often used for improved vortex-core resolution. Other methods include feature-detection where the feature of interest is associated with a flow regime or specific characteristic or property. For example, in turbulent flows the following metrics have been used: Q-criterion, $\lambda 2$, λci, and $\lambda +$ (Hunt et al., 1988; Jeong and Hussain, 1995; Horiuti, 2003). The Q-criterion uses the rotation rate tensor to refine the mesh around areas of high rotation. The $\lambda 2$ metric seeks to capture pressure minima. λci metric refines the mesh based on the velocity gradient tensor. Finally, the $\lambda +$ metric works by calculating the strainrate-vorticity correlation. Both h- and r-adaption methods as well as hybrid approaches have been used successfully for improved flow feature detection, local reduction in discretization error, and convergence to an optimal grid.

4.10 Cartesian grid methods

Several Cartesian grid methods were presented for ship wave problems in the literature. Miyata et al. (1985b) developed a modified Marker and Cell method (TUMMAC) for the finite difference solution of non-linear wave generation in the near field of ships. A Cartesian grid approach was presented in (Sussman and Dommermuth, 2000) with a coupled level-set/volume-of-fluid method for interface capturing and an embedded boundary method for the immersed geometry. They also reported another approach (NFA) using immersed-body and volume-of-fluid methods and its

recent development was given in Dommermuth et al. (2007) for ship wave simulations. Brucker et al (2010) gave some recent applications of NFA and another Cartesian grid solver BDIM developed at MIT. Hu et al. (2010) developed a CIP based Cartesian grid method for numerical simulation of strongly nonlinear wave-ship interaction. Yang & Stern (2009) developed a coupled immersed-boundary/level-set method for wave-body interactions. A second-order sharp interface immersed boundary method was used for two-phase flows with multiple moving bodies on fixed Cartesian grids. A ghost-fluid method is used without smearing the density across the fluid-fluid interface. This method was applied in the study of ship model DTMB 5512 at Fr=0.41 in Yang et al. (2008b). The instantaneous air-water interface colored by the elevation is shown in Fig. 12. The breaking bow waves and scars induced by them are evident. Figure 13 shows the instantaneous vortical structures colored by streamwise vorticity in the air flow. There are many Cartesian grid methods for other areas of applications, the reader is referred to Yang & Stern (2009) for related discussions and references therein.

On the other hand, the application of Cartesian grid methods can become practically prohibitive for high Reynolds number flows due to the demanding resolution requirement near the wall boundary, since most of Cartesian grid methods approximate the velocity field near the wall boundary by a linear distribution, which is only correct in the viscous sublayer. For example, in order to resolve the viscous sublayer for a turbulent flow case at $Re = 10^6$, the near-wall grid spacing has to be in the range of $10^{-5}L$ (L is the reference length), and the total number of grid points will be more than a few billions. Therefore, some forms of wall-layer models have to be included such that the effects of boundary layer can be taken into account properly.

4.11 High-fidelity curvilinear grid solvers

Cartesian grids have some desirable properties not available in other types of grids, especially, triangles (2D) and tetrahedra (3D). For example, the errors introduced in the discretization of diffusion terms can be cancelled out completely at two opposite cell faces; higher order schemes can be implemented much easier; also, automatic generation of Cartesian grids with local refinement is much simpler than that of triangles or tetrahedral. Therefore, it is preferred to use Cartesian grids wherever possible and use other types of grids elsewhere. For instance, Karman & Wilson (2008) developed an automatic grid generation algorithm based on octree refinement Cartesian grid with general cutting allowing viscous boundary layer grid generation. Their development was implemented in Tenasi, a general purpose unstructured grid solver for a wide range of applications.

On the other hand, usually it is not necessary to pursue such level of universality, e.g., using unstructured grids with all types of grid elements, for ship hydrodynamics applications, since the geometries are more or less confined to hull forms, appendages, and propellers of a limited range of variations. Once the surface topology of a geometrical object is determined, a nearly-optimized surface decomposition can be obtained and the corresponding surface quadrilateral grid can be generated with usually good orthogonality, not to mention that most shapes have been given as parameterized solid modeling surfaces which are readily dividable in u - v coordinates during the design process. This also explains why structured grids are still predominately used in computational ship hydrodynamics.

In addition, high-order schemes can be easily implemented in structured grids. For example, in Suh et al. (2011) and Wang et al. (2012c), the Cartesian grid solver CFDShip-Iowa V6.1 was extended into an orthogonal curvilinear solver (V6.2) with similar accuracy and efficiency, where turbulent boundary layers and small droplets/bubbles are resolved at once. Numerical methods and HPC components in V6.2 are about the same as in V6.1. It uses a recently developed novel volume-of-fluid method for general structured grids with a constructed level set function (Wang et al., 2012a), thus it can be used for detailed simulations of interfacial phenomena such as wave breaking and wave-body interactions with simple geometries like cylinder, sphere, wedge, foil, etc. The orthogonal curvilinear grid solver has been used for studying the high Reynolds number, high Froude number turbulent flow past an interface-piercing circular cylinder and a wedge-shaped bow. In addition, an overset grid solver, CFDShip-Iowa V6.2.5, was presented in Bhushan et al. (2011b), which couples the Cartesain grid solver and the orthogonal curvilinear grid solver via overset grid package SUGGAR (Noack, 2006). Based on the Cartesian grid solver and the orthogonal curvilinear grid solver, a general multi-block structured grid solver (V6.3) is currently being developed (Yang et al., 2012). It maintains and extends the higher-order advection and volume conservative interface tracking schemes, and enhanced capabilities of handling complex geometries in ship hydrodynamics.

One additional complication besides the air-water interface and high-Re boundary layer that has to be considered is the motions of a ship and its control surfaces and propellers (when discretized propellers instead of models are used). Multi-blocked structured grids, even with moving grid and/or sliding interface capabilities, are usually considered to be too restricted for large displacement/angle motions, especially, when

ship-ship interactions are to be addressed. Theoretically, unstructured grids with grid deformation and regeneration capabilities can be applicable, but the computational cost of grid operation could be high, especially, for running on tens/hundreds or thousands processes, and the grid quality and algorithm robustness are concerns too. The overset grid techniques have been very successful in ship flow computations (e.g., Carrica et al., 2007); it is expected to continue playing an important role in future high fidelity ship hydrodynamics solvers due to its capability and flexibility.

Therefore, it is envisioned that the next-generation, high-fidelity ship hydrodynamics solvers will be based on Cartesian grids with local/adaptive refinement capabilities for the bulk flow and immersed boundary wall modeling techniques or body-fitted multi-block structured grids for the high-Re boundary layers. For the latter, overset grid techniques with improved conservation properties will facilitate grid connection and movement.

5 HIGH-PERFORMANCE COMPUTING

5.1 HPC advances

Advances in HPC capability, i.e., as the computational capability doubles every two years as per Moore's law, are enabling the use of larger grids and more processors. However, as the grid size and number of processors increase, so does the communication time. Further, HPC hardware architecture is undergoing fundamental changes. Today's systems are hybrid clusters of multicore processors that have shared and distributed memory inside and across the nodes, respectively. Thus a parallel algorithm should effectively utilize the memory of such systems to achieve better performance (Shalf, 2009). Most ship codes use message passing interface (MPI) parallelization, which has limitations on the hybrid networks as the processes running on different nodes dictate the communication time (Rabenseifner and Wellein, 2003). Hybrid parallelization is well suited for hybrid networks, such as the MPI for the internode parallelization and open multi-processing (OpenMP) for the intranode parallellization. However, the OpenMP implementation overhead often outweighs the reduction of communication time, but may be beneficial for codes with substantial collective communication on high-latency inter-node connection (Kaushik et al., 2009). Upcoming graphics processing units (GPUs) can achieve up to 10 times better performance than the central processing units (CPUs) and are being applied for CFD (Cohen and Molemaker, 2009). However, they are not yet ready for production level applications, as multi-GPU and double precision calculations are still in the developmental stage.

5.2 HPC in computational ship hydrodynamics

Ship hydrodynamics community mostly uses MPI based domain decomposition, and the HPC efforts are geared to either run production jobs faster (strong scalability) or to improve the capability of running larger jobs that can resolve more physics with less reliance on modeling (weak scalability). Scalability studies of free surface CFD codes are scarce and are dependent on hardware, thus conclusions are difficult to reach. Overall, incompressible flow codes show limited strong scalability, i.e., speed up is typically 60 to 80% of the ideal scalability for 1000 processors (Kremenetsky 2008, Bhushan et al. 2011a). On the other hand, compressible solvers show linear scalability for up to 10's thousands of processors (Gicquel et al. 2008). The poor scalability of the incompressible solvers is due to the solution of pressure Poisson equation. Weak scalability is usually more easily achieved and has been the focus of most recent developments in ship hydrodynamics community.

Static ship computations of hundreds of millions of grid points have been reported for curvilinear and Cartesian grid solvers (Bhushan et al. 2011a), while dynamic moving computations up to 70 million grid points were performed (Carrica et al. 2010). These computations enable a degree of detail in the flow physics that cannot be achieved with coarser grids, allowing the use of more accurate turbulence models like hybrid RANS-LES and LES. Computations including ship motions are harder and limited by the need of re-gridding or computation of overset connectivity. Computations with motions are routine for grids ranging between 5 and 25 million grid points. New promising numerical techniques and hardware technologies are rapidly changing the landscape of high-performance computing. Super-scalable Cartesian grid solvers are breaking the 1 billion grid point limit with distributed memory platforms (Wang et al. 2012d), and soon 10 and 100 billion grid points will be possible. The HPC challenges of such solvers are discussed below.

5.3 HPC challenges

In general, system memory, interconnection, and I/O are the major bottlenecks in high-fidelity flow simulations. The current norm for system memory is about 2GB/core with around 10% reserved for system usage. This imposes a hard limit with regard to the degrees of freedom one core can effectively handle and thus the minimum number of cores required for a problem of a given size. In many solvers, some data proportional to the global size of the problem are used in some stages of the solution procedure, which further exacerbates

the limit. For instance, many solvers use the root process to read some initial data such as input information and grid data, and then distribute them to other processes. These data may be of large size and not containable within the memory capacity of one computer node. Current computer nodes are usually equipped with tens of processor cores, ranging from 8 to 64. It is expected that a transition from multi-core to many-core will be seen in more and more HPC platforms. The oncoming exascale systems may be equipped with nodes containing hundreds or even thousands of cores. It is unlikely the system memory available to each core will be increased in a scalable way, and actually the decrease of memory size per core is more likely to happen due to cost consideration. Therefore, it is critical to minimize memory usage in high-fidelity solvers for being able to run them on tomorrow's HPC platforms. For this point of view, Cartesian grid solvers have some particular advantages. In contrast to curvilinear structured grids or unstructured grids, only one-dimensional arrays are required for grid coordinates and Jacobian matrix information. Also, discretization stencils are far smaller if the same order-of-accuracy is sought. For example, second-order finite difference discretization of the Lapacian operation gives a seven-point stencil on Cartesian grids, but nineteen-point stencil on general curvilinear grids. On the other hand, pre-processing steps such as grid generation could become a major constraint to solvers for solving billions of degrees of freedom using curvilinear grids or unstructured grids. With the current mainstream grid generation techniques, usually done on a workstation with interactive human input, it is very difficult to produce billion-point grids. Recently Wang et al. (2012d) performed high-fidelity simulations of plunging breaking waves behind a bump using 2.2 billion grid points. It was possible to generate a 2D grid using a commercial grid generator and the 3D grid was obtained through translational extrusion, thanks to the simple geometry.

Interconnection performance between computer nodes is constrained by network bandwidth and communication latency. Because high-fidelity simulations may involve millions of parallel tasks, collective and synchronization operations, which are usually unavoidable in many solvers, can become the determining factor for the overall algorithm scalability. It is necessary to develop algorithms that can greatly reduce communication. Currently, there is a clear trend to change from pure MPI programming mode to hybrid MPI/OpenMP programming due to the transition of multi-core CPU toward many-core CPU. Within one node, the OpenMP mode can avoid MPI communication latency, reduce request of network bandwidth, and reduce system memory usage involved in storing additional ghost cells in pure MPI mode. On the other hand, implicit schemes usually require many synchronization operations. Semi-Lagrangian advection schemes could be much advantageous in this regard because they usually only involve localized operations.

Parallel I/O is another major bottleneck of high-fidelity simulations. For simulations with billions of degrees of freedom, it is impossible to use old-fashioned modes that one or a few nodes read/write all the files. Similarly, with thousands of nodes, or millions of cores, the approach in which each node/core reads/writes its own data files is not manageable. Even the current MPI I/O is severely limited in many systems, a major I/O operation such as writing solution and restart data files using hundreds/thousands of cores may cost the amount of CPU time for running tens or even hundreds of time steps. For high-fidelity simulations requiring frequent data output this could be a major scalability problem, which could be worse on larger systems as the network and I/O bandwidths become more congested. Related data post-processing for high-fidelity simulations also poses major difficulties. Data visualization and analysis has to be done on-site or on-the-fly. Data analysis and reduction within the solvers will become essential components for mitigating network and I/O bandwidth requirement of the solvers. Again, compared with solvers mainly using curvilinear and unstructured grids, Cartesian grid methods or solvers using mostly Cartesian grids have some advantages in terms of I/O when there are changes in grids such as movement, deformation, and adaption.

6 V&V PROCEDURES

6.1 Background

In spite of the ever-increasing need and importance for standards for CFD uncertainty analysis/accuracy estimation and code certification for industrial applications, there are currently many viewpoints covering all aspects from basic concepts and definitions to detailed methodology and procedures. Verification and validation are processes to estimate the numerical and modeling errors, respectively. Although the definition of validation is fairly widely accepted (ASME Performance Test Codes Committee PTC 61, 2009), many opinions on verification are controversial. Herein, we focus on quantitative verification and validation (V&V) methodology and procedures (Stern et al., 2006a), which are essential ingredients for the successful implementation of SBD. Different verification methodologies will be reviewed and their shortcomings and criticisms will be discussed.

6.2 Overview of V&V

The approximation used in numerical simulations will result in error δ_S, which is the difference between a simulation value S and the truth T. However, the true values of simulation quantities are rarely known. Thus, errors must be estimated. An uncertainty U is an estimate of an error such that the interval $\pm U$ contains the true value of δ_S 95 times out of 100, i.e., at the 95% confidence level. An uncertainty interval thus indicates the range of likely magnitudes of δ_S but no information about its sign.

Sources of errors and uncertainties in simulation results can be divided into two distinct sources: modeling and numerical. Modeling errors and uncertainties are due to assumptions and approximations in the mathematical representation of the physical problem (such as geometry, mathematical equation, coordinate transformation, boundary conditions, air-water interface, and turbulence models) and incorporation of previous data (such as fluid properties) into the model. Numerical errors and uncertainties are due to numerical solution of the mathematical equations (such as discretization, artificial dissipation, incomplete iterative and grid convergence, lack of conservation of mass, momentum, and energy, internal and external boundary non-continuity, and computer round-off). In considering the development and execution of a CFD code, it is assumed that δ_S is composed of additive modeling and numerical errors.

$$\delta_S = S - T = \delta_{SM} + \delta_{SN} \tag{4}$$

The simulation uncertainty equation follows directly by considering equation (4) as a data reduction equation, as per EFD uncertainty analysis

$$U_S^2 = U_{SM}^2 + U_{SN}^2 \tag{5}$$

where U_S is the uncertainty in the simulation and U_{SM} and U_{SN} are the simulation modeling and numerical uncertainties. It should be noted that correlations between modeling and numerical errors are also possible and should be considered in the future.

There are two types of verification. Code verification is a procedure to find coding mistakes that affect the numerical discretization using, for example, the method of manufactured solutions (MMS) (Roache, 2002; Knupp and Salari, 2003). Solution verification is a process for assessing simulation numerical uncertainties U_{SN} and, when conditions permit, estimating the sign and magnitude δ_{SN} of the simulation numerical error itself and the uncertainties in that error estimate U_{SN}. The most important numerical errors and uncertainties are due to use of iterative solution methods and specification of various input parameters such as spatial and time-step sizes and other parameters (e.g., artificial dissipation). The errors and uncertainties are highly dependent on the specific application (geometry and conditions). The errors due to specification of input parameters are decomposed into error contributions from iteration number δ_I, grid size δ_G, time step δ_T, and other parameters δ_P, which gives the following expressions for the simulation numerical error and uncertainty.

$$\delta_{SN} = \delta_I + \delta_G + \delta_T + \delta_P = \sum_{j=1}^{J} \delta_j \tag{6}$$

$$U_{SN}^2 = U_I^2 + U_G^2 + U_T^2 + U_P^2 = U_I^2 + \sum_{j=1}^{J} U_j^2 \tag{7}$$

Validation is a process for assessing simulation modeling uncertainty U_{SM} by using benchmark experimental data D and, when conditions permit, estimating the sign and magnitude of the modeling error δ_{SM} itself.

$$E = D - S = \delta_D - (\delta_{SM} + \delta_{SN}) \tag{8}$$

$$U_V^2 = U_D^2 + U_{SN}^2 \tag{9}$$

where E is the comparison error, $\delta_D = D - T$ is the difference between an experimental data and the truth and U_V is the validation uncertainty. When

$$|E| < U_V \tag{10}$$

the combination of all the errors in D and S is smaller than U_V and validation is achieved at the U_V interval. If U_V □ $|E|$, the sign and magnitude of $E \approx \delta_{SM}$ can be used to make modeling improvements..

6.3 Factor of safety method for solution verification

Xing and Stern (2010) proposed four steps for solution verification: (a) convergence studies with four possibilities: monotonic convergence, oscillatory convergence; monotonic divergence, and oscillatory divergence; (b) error estimate δ_{SN} with magnitude and sign; (c) uncertainty estimate U that indicates the range of likely magnitudes of δ_{SN}, but no information about its sign; and (d) statistical analysis to establish

that the interval of U at a 95% confidence level bounds the comparison error E.

Most solution verification methods are derived for monotonic convergence when the general Richardson extrapolation (RE) method can be used to estimate the observed order of accuracy p_{RE}, error δ_{RE}, and the numerical benchmark S_C using three systematically refined grids. The uncertainty U is defined as an estimate of an error such that the interval of U, $\pm U$, bounds the true value of δ_{SN} at a specified level of confidence, which is usually 95% for experimental fluid dynamics and CFD. Uncertainty estimates can be written in the general form of

$$U = F_S \left| \frac{\varepsilon_{21}}{r^p - 1} \right| \tag{11}$$

Various solution verification methods differ in the choice of factor of safety F_S and p. The GCI derived by Roache (1998) is currently used and recommended by ASME (Celik, 2008) and AIAA (Cosner et al., 2006). However, as discussed by Xing and Stern (2010; 2011), there are different variants of the GCI method such as the original GCI, GCI_1, GCI_2, GCI_3, and GCI_{OR}, etc. Thus the choice of F_S and p in the GCI method requires user judgment calls, for which no single guideline is currently available. The uncertainty estimate for the original GCI is

$$U_{GCI} = F_S \left| \frac{\varepsilon_{21}}{r^{p_{RE}} - 1} \right| = 1.25 \left| \delta_{RE} \right| \tag{12}$$

The correction factor method (Stern et al., 2001; Wilson et al., 2004) uses a variable factor of safety and was validated for correction factor less than one using a few analytical benchmarks. The factor of safety for correction factor larger than one is obtained by assuming that the factor of safety is symmetric with respect to the asymptotic range where the observed order of accuracy p_{RE} is equal to the theoretical order of accuracy of the numerical scheme p_{th}, $P = p_{RE} / p_{th} = 1$. The uncertainty for the correction factor method is estimated by the sum of the absolute value of the improved error estimate $CF \left| \delta_{RE} \right|$ and the absolute value of the amount of the correction.

$$U_{CF} = \begin{cases} \left[9.6\left(1 - CF\right)^2 + 1.1 \right] \left| \delta_{RE} \right| & 0.875 < CF < 1.125 \\ \left[2\left|1 - CF\right| + 1 \right] \left| \delta_{RE} \right| & 0 < CF \le 0.875 \quad or \quad CF \ge 1.125 \end{cases} \tag{13}$$

The GCI and CF methods have two deficiencies. The first is that the uncertainty estimates for $p_{RE} > p_{th}$ are unreasonably small in comparison to those with the same distance to the asymptotic range for $p_{RE} < p_{th}$. This is due to the fact that the error estimate δ_{RE} for the former is much smaller than that of the latter. The second is that there is no statistical evidence for what confidence level the GCI and CF methods can actually achieve.

Two other recent studies (Eça and Hoekstra, 2006; Rumsey and Thomas, 2008) considered the use of different uncertainty estimates for different ranges of p_{RE} for solutions that show monotonic convergence. These two verification methods were demonstrated for a manufactured solution (Eça and Hoekstra, 2006) and the flow over a backward facing step (Eça and Hoekstra, 2006; Rumsey and Thomas, 2008) without detailed derivation and validation. Statistical samples or analyses were not reported in either of these studies.

Recently, Xing and Stern developed the factor of safety method (Xing and Stern, 2010). It removes the two deficiencies previously discussed for the GCI and CF methods. The best error estimate is used to construct the uncertainty, which is

$$U_{FS} = \begin{cases} \left[FS_1 P + FS_0 \left(1 - P\right) \right] \left| \delta_{RE} \right| & 0 < P \le 1 \\ \left[FS_1 P + FS_2 \left(P - 1\right) \right] \left| \delta_{RE} \right| & P > 1 \end{cases} \tag{14}$$

$FS_0 = 2.45$, $FS_1 = 1.6$, and $FS_2 = 14.8$ are recommended based on statistical analysis.

6.4 Discussion of the factor of safety method

The factor of safety method is the only solution verification method that was validated using statistical analysis, which consists of 25 samples with different sizes based on 17 studies covering fluids, thermal, and structure disciplines. Only the factor of safety method, compared with the GCI and correction factor methods, provides a reliability larger than 95% and a lower confidence limit greater than or equal to 1.2 at the 95% confidence level for the true mean of the parent population of the actual factor of safety. This conclusion is true for different studies, variables, ranges of P values, and single P values where multiple actual factors of safety are available. The number of samples is large and the range of P values is wide such that the factor of safety method is also valid for other applications including results not in the asymptotic range, which is typical in industrial and fluid engineering applications. The factor of safety method has been used to estimate CFD uncertainties in ship hydrodynamics such as the recent CFD Workshop Gothenburg 2010 (Larsson et al., 2010).

Roache presented ten items of discussion of the factor of safety method (Roache, 2011), which were responded item-by-item by Xing and Stern (2011). Additionally, Xing and Stern (2011) evaluated two new variants of the GCI method including GCI_{OR} (Oberkampf and Roy, 2010) and GCI_3 methods and one new variant of the factor of safety method (FS_1 method). Except the original GCI method, all variants of the GCI method have jumps of F_S versus P, which cannot be justified. The FS_1 method is the same as the FS method for $P<1$ but uses p_{th} instead of p_{RE} in the error estimate for $P>1$. The FS_1 method may have an advantage for uncertainty estimates when $P>2$ where the FS and other verification methods likely predict unreasonably small uncertainties due to small error estimates. However, since the current dataset is restricted to $P<2$, the pros/cons of using the FS or FS_1 method cannot be validated. Thus, until additional data is available for $P>2$, all verification methods should be used with caution for such conditions and, if possible, additional grid-triplet studies conducted to obtain $P<2$.

7 V&V FOR CAPTIVE SIMULATIONS

Captive testing in the towing tank is the standard approach in ship design. The CFD ship hydrodynamic efforts started with and mostly focused on captive simulations both to replace the towing tank model testing and to carry out validations against EFD data. The CFD community has developed new procedures for single run captive computations for resistance and for seakeeping in head waves. The resistance procedure is not possible or highly difficult using a physical towing tank suggesting a potential of using CFD to aid the design process (Xing et al., 2008). The single run seakeeping procedure is also applicable for experiments or potential flow and can significantly reduce the costs in all methods (Mousaviraad et al., 2010a). Full-scale computations are carried out with CFD which are rarely done in experiments. Appendages are easily added/removed in CFD simulations and can be used to study the interactive effects between different appendages and the hull. CFD simulations are carried out for unconventional ships and high speed crafts including real waterjet flow computations.

This section focuses on CFD captive V&V efforts including resistance, sinkage and trim in calm water, seakeeping in regular head waves, captive maneuvering including static and dynamic simulations, and stability studies.

7.1 Resistance and propulsion

Prediction of resistance is the oldest application of CFD in ship hydrodynamics and its accuracy has been significantly improved over the last 20 years. In the latest workshop on ship hydrodynamics, Gothenburg 2010, a total of 89 submissions of resistance prediction are documented, which is the largest number in the workshop series and the analysis of the results shows that the statistical variance of all the predictions are substantially smaller than the previous workshops in 2000 and 2005 (2.1% in 2010 compared to 4.7% in 2005) (Larsson & Zou, 2010). An overview of the computational methods including modeling, numerical methods, and HPC, and the applications studied are provided herein, followed by a detailed analysis of V&V efforts.

The dominate modeling approaches for resistance simulations are RANS for turbulence, while some simulations are based on LES or DES, surface capturing methods such as VOF and level-set for free surface, and unstructured or structured multi-block or overset grids (Resistance Committee, ITTC 2011; Larsson & Zou, 2010). Two equation based, isotropic eddy viscosity turbulence models are most popular, especially the family of k-ω models. Wall functions for turbulence modeling are used in some studies, while many simulations resolve the near wall region including the viscous sublayer. The majority of the numerical methods are based on second order schemes, while higher order discretization schemes are seldom used. Gridding techniques include adaptive mesh refinement and overset grids for moving-body and multi-body applications as well as local refinement by embedding blocks of finer grids. The HPC methods have been vastly used in most recent simulations enabling parallel computing for increased grid size of a few to tens of million points to improve the spatial resolution of turbulent boundary layer and wake.

The resistance prediction simulations are carried out for a wide range of applications and conditions. Other than drag, sinkage and trim, local flow fields such as boundary layer and wake, and wave patterns are also predicted by many simulations. Different geometries including tankers, container ships, surface combatants, and small vessels are studied at a range of very small to large Froude numbers. Unconventional ships such as multi hulls, planing hulls, and new concept hulls are included, e.g. Bhushan et al. (2012b) simulations for a SES/ACV ship in deep and shallow water (Fig. 14). Fully appended ships with rudders, bilge keels, shafts, struts, and propellers are also included in the literature. Full-scale resistance predictions including the effects of surface roughness have become of interest in the recent years (e.g. Bhushan et al., 2012c). Mousaviraad et al. (2012) included the effects of hurricane strength head winds in their CFD simulations.

Innovative methods are introduced in CFD studies including a procedure to obtain resistance and propulsion curves for a wide range of velocities in a single run (Xing et al., 2008). The method is based on solving the fluid flow equations using an inertial earth-fixed reference frame, and ramping up the ship speed slowly such that the time derivatives become negligible and the local solution corresponds to a quasi steady-state. Fig. 15 shows the resistance and propulsion curves for Athena.

Self-propulsion computations with rotating propellers to find the propeller rotational speed (RPS) for a given ship speed are carried out recently. Lubke (2005) used prescribed propeller RPS and ship speed for self-propulsion computations of KCS. Carrica et al. (2010a) used a controller to obtain the self-propulsion model point for the KVLCC1 tanker and the ONR Tumblehome surface combatant free to sink and trim, and for self-propulsion at full scale for the KCS containership at even keel. Carrica et al. (2010c) performed self-propulsion point computations of the KCS containership in model scale free to sink and trim with the rotating discretized propeller. A methodology to compute most of the self-propulsion factors using a simple prescribed body force model for the propeller is presented by Fu et al. (2010), including a method to obtain the advance velocity at the self-propulsion point and application to the KCS containership at full-scale.

CFD calm water V&V results are summarized in Table 2. The overall average errors are 3.3% for resistance, 22.2% for sinkage, and 32.8% for trim. For motions, the errors are larger for lower Fr. This could be both due to the measurement uncertainties at low speed model test and small absolute D values. The average errors for Fr<0.2 are 34.7% for sinkage and 54.7% for trim, while for Fr≥0.2 the errors are as small as 9.7% for sinkage and 11% for trim. It must be noted that some studies (e.g. Xing et al., 2008 and Sadat-Hosseini et al., 2010) used dynamic range of sinkage and trim to evaluate errors, resulting in smaller errors for lower Fr. For the limited verification studies the average U_{SN}=2.5%, 6.9% and 6.7%S for resistance, sinkage and trim, respectively, and the average validation uncertainty levels are 2.9%, 14.1% and 8.1%D. The average errors are comparable to average validation uncertainty levels.

7.2 Seakeeping

CFD computations of seakeeping has been rapidly increasing since 2005 when the seakeeping committee of ITTC stated “seakeeping computations are still far from a state of mature engineering science.” While there was only one forward speed diffraction case which involves no motions in the Tokyo 2005 CFD Workshop, several heave and pitch in regular head waves were included in the G2010 Workshop with numerous contributions for each case. Herein, an overview of computational methods and applications are provided, along with a detailed analysis of the V&V results.

The majority of the simulations are URANS, while limited simulations are based on LES or DES. Surface capturing methods such as VOF and level-set are dominant for free surface. Incoming waves are mainly assumed linear and are imposed at the domain boundaries. Structured or unstructured multi-block or overset grids are used for motions. Numerical methods mainly use second order discretization schemes for spatial and temporal terms. The HPC methods are used in almost all simulations allowing for small grid sizes at the free surface and boundary layer and small time steps to capture the motions in waves accurately.

The applications for seakeeping predictions include a wide range of ship types and geometries, wave conditions, Froude numbers, and motion restrictions. Grid sizes ranging from 0.4 M to 71 M points are used with a clear trend toward increasing accuracy with grid size. In G2010 computations were contributed by five groups for KCS pitch and heave in regular head waves under three different conditions using FreSCo, Comet, Open Foam, Wisdam and CFDShip-Iowa. Five groups also contributed for KVLCC2 using Comet, Open Foam, CFDShip-Iowa, Isis, Icare and RIAM-CMEN. A case for pitch and heave fee to surge was include in G2010 for KVLCC2 with three wavelengths with two contributions using CFDShip-Iowa and Comet. Seakeeping for side by side ship-ship interactions for regular head and oblique waves are carried out, as shown in Fig. 16, for Hope and Bobo geometries (Mousaviraad et al., 2011).

Since pitch and heave computations of RAOs can be expensive due to the large number of runs needed for every Froude number at different encounter frequencies, Mousaviraad et al. (2010a) developed an innovative procedure to compute the RAOs for a Froude number in a single run. A harmonic wave group single run procedure is developed and validated for URANS, although the procedure can be implemented using experiments or potential flow. Incoming waves are deterministic wave groups defined by linear superposition of a number of component waves. While the regular wave procedure requires multiple runs, the proposed single run procedure obtains the response amplitude operators (RAO) for a range of frequencies at a fixed speed, assuming linear ship response. This greatly reduces the computational time and expenses, while the results are shown for the presented cases to have the same order of errors as the standard single wave methods if the response is linear.

Following G2010, assessment of CFD predictions for seakeeping in regular head waves separate

capability for 1st order vs. 2nd order terms (Stern et al., 2010). Both steady calm water resistance, sinkage, and trim and unsteady head waves resistance, heave and pitch are analyzed to include added resistance studies. For calm water, resistance is considered 1st order, whereas sinkage and trim 2nd order. Resistance 0th harmonic is 1st order and 0th harmonic heave and pitch are second order. 1st harmonic heave and pitch are considered 1st order while 1st harmonic resistance is 2nd order.

CFD seakeeping V&V results for heave and pitch in regular head waves are summarized in Table 3. The average of the fine grid points is 15 M. Time step studies were included by 3 studies. Resistance was included in only one U_T study using a relatively coarse grid (0.3M) with relatively high uncertainty level (U_T=21%S) compared to average uncertainty of motions (U_T=2.5%S). Comparing motions, heave had generally higher U_T than pitch for almost all studies. For grid studies, three out of five studies considered resistance with average resistance uncertainty of U_G=2%S1, which is smaller than the average time step uncertainty for resistance. Pitch has slightly higher grid uncertainty than heave, with average heave and pitch uncertainty of U_G=4.3%S1, which is slightly larger than that for time step studies. Overall, average simulation numerical uncertainties for seakeeping verification studies are U_{SN}=6.7%D for resistance and U_{SN}=4.9%D for motions. In the view of the average grid size for U_{SN} studies being only about 7M, the solutions are likely far from the asymptotic range and therefore U_{SN} values are optimistic. U_V values are generally dominated by U_D, being 15% for resistance and 10% for motions. Average error values are very large for 2nd order terms (44%D) while for 1st order terms the average is less than 15%. On the average level, validation is achieved only for the 1st harmonic amplitude of heave at 11%D interval.

7.3 Maneuvering

Captive maneuvering experiments and simulations are carried out to obtain coefficients used in system-based models to predict actual 6DOF maneuvers. The simulations include static maneuvering simulations such as pure drift and steady turn, and dynamic planar motion mechanism (PMM) simulations which provide a wide range of derivatives needed in system-based methods than those provided by static computations. Both static and dynamic captive maneuvering simulations, as well as some free model cases were included in the SIMMAN 2008 workshop (Stern et al., 2011a) which was the first workshop on verification and validation of ship maneuvering simulation methods. Herein, an overview of computational methods and applications are provided for CFD captive maneuvering simulations, along with a detailed analysis of the V&V results.

Most of the maneuvering simulations are URANS using 1- and 2-equation isotropic/anisotropic models and Reynolds-stress transport model for turbulence modeling. Free surface is mostly modeled by a surface capturing method (e.g., level-set, volume of fluid), while a few simulations use surface tracking approaches. For numerical methods, spatial discretization is done by finite difference and finite volume methods with structured/unstructured grids. The order of accuracy in time integration is mostly second-order or higher. The divergence-free condition is satisfied either by velocity-pressure correction or an artificial compressibility approach. Analytical weighted re-gridding, mesh morphing, and dynamic overset approaches are used to handle dynamic ship motions. For the high-performance computing, message passing interface (MPI) or open MP is used in many cases as a parallel computing technique. Multigrid technique is also used in some simulations for speeding up computations.

The application of CFD captive maneuvering simulations focus on PMM-type forced motions such as static rudder, static drift, pure sway, pure yaw, and yaw & drift conditions. SIMMAN 2008 included different geometries, i.e. a tanker (KVLCC), a container ship (KCS), and a surface combatant (DTMB 5415). For the KVLCC test case, two stern shape variants named KVLCC1 and KVLCC2 giving different instability loops were included. CFD-based methods were used to simulate forced motions and were compared with PMM/CMT model test data. A total of 16 submissions were received for the forced motion simulations, comprising different CFD-based methods such as RANS, URANS, and DES. It was concluded that finer grids were needed especially for the rudder and appendages and in regions of large vortices, as well as more advanced turbulence and propeller models for improvements in the CFD predictions of static and dynamic PMM maneuvers. Recent results (Bhushan et al., 2011a) for 5415 bare hull 20 deg static drift using 10 to 250 M grid points and DES turbulence modeling have shown that errors in X, Y, and N can be reduced to less than 5%D, which is comparable to errors for straight ahead resistance at the Gothenburg 2000 and Tokyo 2005 CFD workshops. Static and dynamic PMM simulations are also carried out for other geometries, i.e. HTC, MARIN LNG, and KVLCC2M (Toxopeus, 2009; Jacquin et al., 2006). Mousaviraad et al. (2012b) included the effects of head wind on static and dynamic PMM maneuvers in their CFD simulations (e.g. Fig. 17). It has been shown that multiple-run CFD/EFD curve fitting methods can provide better estimates for nonlinear maneuvering derivatives than the single-run method

used here, but statistical convergence of the higher-order Fourier series components is an issue (Sakamoto et al., 2012).

CFD V&V results for captive maneuvering simulations are summarized in Table 4. Following Stern et al. (2011), assessment of CFD predictions for captive maneuvering separate capability for original values of X, Y, and N, slope of forces and moments versus dynamic variables referred to as linear hydrodynamic derivatives, and higher-order terms of the slope referred to as nonlinear hydrodynamic derivatives. The average of the fine grid points is 6 M. The overall average simulation numerical uncertainties are U_{SN}=10%D for X, U_{SN}=12%D for Y, and U_{SN}=4%D for N. For X, the largest numerical uncertainty is for static rudder, while for Y and N largest uncertainties are observed for pure yaw simulations. U_V values are generally in the same order as U_{SN}, being 12% for X, 14% for Y, and 5% for N. Average error values are 15%D for X, 15%D for Y, and 11%D for N. The largest error values are generally observed for pure yaw and static rudder simulations. Overall, the average error for X, Y, and N predictions is 13.6%D. For linear derivatives, the average error is much larger for N′ (40%D) than Y′ (15%D). For nonlinear derivatives, the average error value is about 40%D.

7.4 Intact and damaged ship instability

There are very limited simulations conducted to investigate the ship instability. The intact ship stability is conducted by Sadat-Hosseini et al. (2010) to investigate parametric rolling using CFDShip-Iowa (e.g. Fig. 18). The computations were conducted for the ship free to heave, roll and pitch and with and without bilge keels and for different ship speed and loading in head waves. The results were compared with the experimental data and the predictions from nonlinear dynamic approaches which solve 1DOF roll equation using empirical or experimental values for damping and restoring moment coefficients. The results showed that CFD can predict the parametric rolling for the ship with no bilge keels, similar to EFD. The parameter rolling was observed for the ship without bilge keels when the encounter frequency was about twice of the natural roll frequency of the ship. The large damping coefficient of the ship with bilge keels resulted in no instability. The comparison with nonlinear dynamic approaches showed that the nonlinear dynamic methods could predict parametric rolling fairly well but their results were sensitive to the accuracy of the coefficients. Cho et al. (2006) studied the flooding of a compartment with no motion using FLOW3D solver, a RANSE solver based on finite volume method. The computations were performed for two compartments, the simplified compartment with no internal complexity and the compartment with all the side shells and engine rooms. The grid size was between 0.9-1.3M. Also different inlet shapes were used for the compartments. They compared the results with the experimental data and showed that CFD predicts the loads on the compartment fairly well during the flooding. The results showed that it is necessary to consider the compressibility of air in FLOW3D to predict the flooding rate very well. Gao and Vassalos (2011) used Fluent to predict the roll decay of a damaged ship free to sway and roll. They showed that sway motion has large effect on hydrodynamic coefficients in damage condition. Added moment of inertia and damping from roll decay without sway are significantly larger than those from roll decay with sway. However, they did not validate the results with any experimental data. Gao et al. (2011) developed a NS solver with VOF model to study the motions and flooding for a barge with damaged compartment. The grid size was about 677K. The ship was free to roll, heave and pitch. The comparison with EFD data were conducted for both motions and the water heights inside the compartment. The results showed good agreement with EFD data. The effect of flooding on roll motion was not large due to the strong stability of the barge.

8 VALIDATION FOR FREE RUNNING SIMULATIONS AND SYSTEM IDENTIFICATION

Numerical simulation of free running test cases (maneuvering, course keeping and etc.) is a challenge, due to both the complexity of the physical phenomena involved and the level of capability and resources needed to perform the computations. This type of simulation requires self-propulsion, moving appendages such as rudders, controllers, and in general full 6DOF capabilities in a free surface environment. Thus, there have been a few computations of this type so far. In this section, the computational methods, the applications and the V&V efforts for the free running simulations are reviewed.

The computational methods applied for free running simulations have employed different techniques for modeling, numerical methods and HPC as shown in Table 5 and 6. The free surface is mostly predicted by interface capturing schemes such as single/two phase level set method and volume of fraction technique. For turbulence modeling, the majority of the CFD codes solve two additional equations (i.e. in addition to the momentum and mass conservation equations) for the eddy viscosity, one for the turbulence kinetic energy (k), and one for its dissipation rate (typically ε or ω). Only one CFD code (RANS code developed by INSEAN) solves one additional equation based on Spalart-Allmaras. Also,

some employed the turbulence models based on Reynolds-Stress by solving the equations for the six Reynolds stress components directly. Only DES is applied in this category in which the computational time reduces by employing unsteady RANS equation in the boundary layer and applying LES in the rest of the domain. For most computations, the propulsion is usually implemented as body force and thus the computational grid does not conform to the geometry of the rotating components. The body force is determined by propeller open water curves and applied as a source term to the underlying grid. To solve the rigid body equations it is necessary to obtain the instantaneous forces and moments acting on the object. This is done by integrating the contribution of pressure and viscous forces on each cell on the solid body in all solvers. In most CFD codes the flow is assumed to be incompressible and thus the continuity is enforced using projection method to solve Poisson equation as the governing equation for pressure. The codes mainly adopt finite volume discretization and only one uses finite difference scheme. High order schemes are used for spatial and temporal discretization in all of the solvers. Most of the codes use the structure body fitted grids where the cells are distorted to fit around a complex shape. The majority of the solvers use overset or overlapping grid and the flow parameters is interpolated from one grid to another. The interpolation is done dynamically to form transient moving and sliding grids to account for the relative motions of the ship hull and the appendages. One solver (ICARE) uses structured grid with dynamic overset technique but the moving appendages such as rudders are modeled by external forces. Few codes use unstructured re-gridding for unsteady simulations. The HPC method is used in most of the solvers enabling parallel computing. A few computations are conducted for a fairly large grid size with more than 15M grid points. However, the computations of hundreds of millions of grid points are not yet conducted for free simulations while these types of simulations are reported for captive tests.

The free running computations are conducted for different types of applications including maneuvering, course keeping and stability. The majority of the computations are for maneuvering predictions in calm water. Among the maneuvering computations, mostly are conducted for turning simulations and few are performed for zigzag. Two maneuvering simulations are conducted not only to validate the CFD results but also to estimate the maneuvering coefficients using system identification technique. The course keeping computations are mostly carried out to study the ship stability in regular or irregular following waves and only few computations are conducted for course keeping in calm water. One computation includes the wind effects in the simulation to predict ship course keeping in hurricane. Some simulations are for damaged ship stability in calm water and waves. In these simulations the damaged ship is floated and no rudders are used for course keeping.

8.1 Maneuvering and system identification in calm water and waves

Muscari et al. (2008a,b) used the RANSE code developed at INSEAN (Italian Ship Basin) to simulate the turning maneuvering of KVLCC2 tanker. The free surface in the simulation was neglected and treated as symmetric plane. Thus the vertical motions including heave, pitch and roll were not included in the computations. The simulations were conducted for two different grid sizes of 424K and 3.4M. The results for fine grid showed the average error of 4.8%D for turning maneuver parameters which increases to 8.2%D for coarse grid. The turning maneuver parameters include the advance (A), transfer (TR), tactical diameter (TD) and turning diameter (D) as identified by IMO (International maritime Organization). They showed that the main features of the flow, including the formation of the bilge vortices, were captured even on the coarse mesh. The same RANS code is used by Durante et al. (2010) for turning circle simulation of a tanker with single rudder and twin propellers. The simulations were conducted in full scale and compared with the EFD data which were repeated three times. The body force propeller model was modified to take into account both axial flow reduction at the propeller disk and the side force developed by the propeller. The side force was estimated to be proportional to the thrust and the instantaneous angle between the propeller axis and the ship velocity. Two solutions were computed by using fine (6.2M) and medium (0.77M) grids and the numerical results were compared with the experiments. The prediction errors for turning circle were 4.95%D for fine grid and 9.31%D for coarse grid. Also, the EFD and CFD time history comparisons of ship speed, drift angle and yaw rate showed that the speed was predicted better by medium grid while the drift angel and yaw rate were predicted well by fine grid. The flow field was analyzed in terms of wave pattern, surface pressure and the velocity field. The flow field was characterized by a strong cross flow which generates large vortices including the vortical structures generated at the bilge keels, the keel and from the propeller apparatus. Dubbioso et al. (2012) extended the analysis in Durante et al. (2010) and focused on the stern appendages forces/moments and their contribution to the maneuvering. However, the forces/moments on the appendages were not validated. They showed that the hydrodynamic loads of the appendages reduce the turning quality of the vessel. This is due to the position of the center of pressure of the hull force, which is

shifted towards the stern, proving a stabilizing moment which counteracts the vessel motion. It was also shown that the appendages on the external side of turning develop a higher lateral force with respect to the inner side ones as the appendages in inner side are in wake of the hull. Even though the lateral force of inner side appendages were small, the induced moment was in the same order as that developed by the bare hull. This stresses the extreme importance of the stern appendages on the maneuvering behavior of the vessels.

Jacquin et al. (2006) employed ICARE, the RANS code developed by ECN (Ecole Centrale de Nantes) in France. They performed turning maneuver of a containership (Series 60). They mentioned that the computations were conducted with actual moving rudders and also with simplified condition where a side force was used to mimic the existence of a deflected rudder behind the ship. However, only the free running results of the model with side force were reported. The computations were only conducted to demonstrate the capability of ICARE in free running maneuvering and no validations were shown. The solver ICARE later was used by Ferrant et al. (2008) and Drouet et al. (2008). Ferrant et al. (2008) demonstrated the capability of ICARE for turning circle simulation in regular waves for 5415M, a surface combatant. The rudder was approximated by a time varying side force applied at the rudder location. The Wave is treated using SWENSE (Spectral Wave Explicit Navier-Stokes Equations) approach by combining the description of undisturbed incident waves introduced by a non-linear spectral scheme in potential flow theory and the computation of the non-linear viscous diffracted flow using the free surface RANS solver. Since there is no direct impose of wave condition on free surface, there would be no need to have a fine grid to ensure a good propagation of the waves. Drouet et al. (2008) conducted turning maneuver simulations for Humburg test case and 5415M using ICARE solver. For both geometries, the rudders were modeled by an external side force. For Humburg test case, the simulations were conducted for the model free to horizontal motions (surge, sway and yaw) and also free to all motions. The comparison with EFD data showed better agreement for 3DOF simulations with error of 0.3%D for tactical diameter compared to 5%D for free simulations. For 5415M, the turning maneuver results were reported in calm water and waves but no validation was conducted. For calm water, a model with different bulb forms were considered and showed that the tactical diameter reduces 5% for a bulb form shorter and more immerged than the initial form.

Carrica et al. (2008a) employed CFDShip-Iowa for turning and zigzag maneuver simulations in calm water and waves for 5415M. The body force propeller model was used for the propulsion and the actual rudders were included in the simulations. The results were obtained using both constant propeller rate and constant torque condition for propellers. The total grid points were 7M for calm water increasing to 12M for waves. The simulations were conducted for both model and full scale and no validation was reported. The details of turbulence modeling for the model scale and full scale simulations were discussed later in Bhushan et al. (2009). For model scale simulations, blended k-w was used while for full scale computations the multilayer wall-function models were employed. For zigzag simulations, the full scale case reached the rudder check points faster than that of model scale, indicating a slightly more efficient rudder action in full scale. Since the boundary layer was thicker in the model scale case, the lower velocities at the propeller plane was expected compared to that of full scale. This provided higher velocity reaching the rudders for full scale and consequently better steering capacity. For turning simulations in waves, with constant RPM, the ship was locked in the wave when the wave was following waves providing surf-riding. In the case of constant torque the ship did not have enough power and the following waves could overcome the ship. The validation of calm water turning and zigzag simulations for 5415M was reported in Carrica et al. (2012b). Figure 19 shows the predicted free surface and vortical structures during turning circle reported in Carrica et al. (2012b). The average error of turning and zigzag maneuvers predictions were 5.74%D and 6.83%D, respectively. Mousaviraad et al. (2012a) used CFDShip-Iowa for turning and zigzag maneuvering of a surface effect ship (SES), as shown in Figure 20. The body force propeller model was used in the simulation. The simulations were conducted in both deep and shallow water and in both calm water and waves with the grid size of 8.6-9.3M. It was shown that shallow water increases transfer and tactical diameter in turning maneuvers. However, radius and yaw rate showed no change in shallow and deep water. Also, shallow water reduced the 1st and 2nd overshoot for zigzag. For turning, wave effect is significant on the maneuver of the ship in shallow water. For zigzag, the waves reduce the overshoot angle. Sadat-Hosseini et al. (2011a) and Araki et al. (2012a, b) employed CFDShip-Iowa for a surface combatant (ONR Tumblehome) maneuvering in calm water and waves. The model included all the appendages with grid size of 12.1M in total but the propellers were simulated using body force. The average error for calm water simulations were 1.62%D and 1.88%D for turning and zigzag. The results for waves also showed very good agreement with the EFD data. They also used system identification technique for first time to improve the maneuvering coefficients and their variations induced by waves, rudder forces and wave forces from CFD free running outputs. They

used two system identification methods including extended Kalman filter (EKF) and constrained least square (CLS). The results in calm water showed the average system based prediction errors for maneuvering simulations drop from 16% to 8% by using the maneuvering coefficients and rudder forces found from CFD free running instead of those from captive experiments (see Figure 21). Also, the system based results in waves were significantly improved by tuning the maneuvering coefficients and wave forces in the mathematical model using CFD outputs.

8.2 Course keeping and stability in calm water and waves

Carrica et al. (2008b) and Huang et al. (2008) demonstrated the capability of CFDShip-Iowa for course keeping and the instability of ONR Tumblehome in irregular following waves. The actual rudder was included in the simulation and the propeller was modeled through a body force. Broaching was predicted during the course keeping but the results were not validated. Mousaviraad et al. (2008) demonstrated the capability of CFDShip-Iowa for course keeping in waves in present of significant winds. They simulated course keeping in CAMILLE hurricane for ship in quartering waves with winds hitting the ship at 45 and 225 deg. The results showed the wind has strong effects on ship forces and moments. The case with wind from 45 deg loses control at some instants but regains control while the ship turns to port and cannot be controlled for the case with wind at 225 deg. Sadat-Hosseini et al. (2011b) validated the course keeping and instability of ONR Tumblehome for various speed and heading in regular following waves. The CFD simulation could remarkably predict the instability map. CFD predicted the boundary between periodic motion and surf-riding/broaching at Fr=0.3 for heading less than 30 degrees. Periodic motion was predicted below the boundary (Fr<0.3) whereas surf-riding/broaching was observed above the boundary, in agreement with EFD. However, there were discrepancies in the time histories due to missing EFD initial condition for ship speed and wave phase. The authors later included the actual propeller in the simulation and showed improvement for the time histories of all motions (Carrica et al., 2012a). Also direct integration of forces and moments on all appendages were conducted to investigate the contribution of the appendages on the instability of the ship during the course keeping. The yaw moments showed that the turning moments produced by the appendages were dominated by the rudders, with values one order of magnitude larger than any other appendage. Also, both propellers contributed a net positive turning, helping prevent broaching. The CFD solutions for broaching using both body force and actual propeller are shown in Figures. 22 a and b.

The validation of forces and moments on the appendages in free running simulations were performed by Stern et al. (2011b) and Sadat-Hosseini et al. (2012a). They employed CFDShip-Iowa and ISIS-CFD to study the predictions of course keeping for 5415M in calm water and regular waves. The CFDShip-Iowa simulations included course keeping under either roll decay or forced roll in calm water and course keeping in head and beam waves. For ISIS-CFD computations, the roll decay in calm water was only performed. The moving rudders and stabilizers were included in CFDShip-Iowa while both were fixed in ISIS-CFD. The propeller was modeled as a body force in both solvers. The grid size for CFDShip-Iowa and ISIS-CFD was 6.3-18.6M and 5.9M, respectively. The results showed very good agreement with EFD data using both CFD simulations. Also, the CFD results were compared with potential flow and system based method predictions and confirmed that CFD provides better results than the other methods. Figure 23 shows the grid topology and the instant view of CFDShip-Iowa solution during course keeping in beam waves. Sadat-Hosseini et al. (2012b) extended the validation of forces and moments to irregular wave condition, as shown in Figure 24. The irregular wave was generated by summation of many regular waves with amplitudes computed from the desired wave spectrum and with random phases. A very fine grid was used to resolve all the components of the irregular waves from very small to very large amplitudes. The grid size was about 24M, decomposed into 249 CPUs for parallel processing. The computations were conducted for course keeping of a surface combatant in irregular beam waves for JONSWAP wave spectrum and the results were compared with the experimental data. The results were validated against the experiments not only for the ship motions but also for the loads on the appendages. The correlation between ship motions and input irregular waves were also studied. Comparing the irregular wave results with the results computed from regular wave simulations at several discrete wave length conditions showed that the ship has fairly similar motion in both regular and irregular waves with same wave length condition.

Dreyer and Boger (2010) used OVER-REL_TCURS solver to simulate the overtaking of a submarine and a ship. The OVER-REL_TCURS solver is developed at ARL (Applied Research Laboratory, Pennsylvania State University). The free surface is ignored in the simulation. The body force propeller model was used in the simulation for both the ship and the submarine. The grid size of the ship and submarine was 2.3M and 4.1M, respectively. The comparisons were performed for depth and pitch. Good agreement

with EFD was obtained for locked fin cases but large discrepancies for those cases with moving fins were observed. A few simulations were conducted for the ship with damaged compartment to investigate the stability of the ship under damaged condition.

Strasser et al. (2009) conducted CFD simulation of floating damaged barge. They included the compressibility of the air trapped in the damaged compartment. The time histories of sinkage, trim, heel and water height inside the compartment were compared with EFD data and the results showed very good agreement. Sadat-Hosseini et al. (2012c) employed CFDShip-Iowa for a damaged ship and investigated roll decay and motions with flooding in calm water and waves. The grid size was in range of 6.3-28M, depending on the case. The results were compared with experimental data not only for ship motions but also for the water height inside the compartment to evaluate the flooding rate prediction. The verification study was also conducted, showing that the results were not very sensitive to the numerical uncertainty. Overall CFD showed good agreement with experimental results for both ship motions and water heights inside the compartment for all cases in calm water and waves. CFD results could capture the complex free surface shape inside the compartment generated by the flooded water and the reflected water by the walls inside the compartment (see Figure 25). For roll decay cases, CFD showed that the damping coefficient is larger and roll frequency is smaller for the roll decay under damaged condition.

9 FUNDAMENTAL STUDIES FOR TWO-PHASE FLOWS

Breaking waves, spray formation, and air entrainment around ships are one of the main sources of the underwater sounds and white-water wakes, which are of great importance for signature of ships. These flow phenomena occur on a large range of temporal and spatial scales. At small scales, spray formation and air entrainment in the contact line region depend on the length scales which are orders of magnitude smaller than the length of the ship with correspondingly small time scale. For the large scales, the overall structures include wave breakings along the hull and the induced vortices, instabilities, separations and scars, etc. Understanding the small scale physics and capturing their effects on the large scale features are of primary importance for ship hydrodynamics. Skin-friction drag reduction is of great significance in ship hydrodynamics. One of the important techniques for the drag reduction is to inject gas into the liquid turbulent boundary layer to form bubbles or air layer. In this section, fundamental studies for two-phase flows in ship hydrodynamics are reviewed.

9.1 Flow around surface-piercing object

Experimental and computational studies have been conducted for the flows of a surface-piercing flat plate with focus on the wave induced effects on the flat plate boundary layer below the juncture region (Stern, 1986; Stern et al., 1989; Stern et al., 1993). More recent experimental and computational studies focused on the juncture region and turbulence modeling using towed, two-dimensional laser-doppler velocimetry (LDV) and RANS and large-eddy simulation (LES) methods for flat free surface (Longo et al., 1998; Sreedhar and Stern, 1998a, b). The juncture region experiment (Longo et al.,1998) is extended to include wave effects using servomechanism wave gauges (Kang et al., 2008). It is observed that the interface appears always broken in the contact line region even for the case with a smooth wave field. Air is entrained into the boundary layer at the contact line region due to the interaction of the contact line with the solid surface. A string of bubbles can be generated near the solid wall usually with small bubble sizes. For flows past a blunt leading edge, such as NACA0024 foil, the bow wave breaks and wraps around the bow with similar features to spilling breakers (Metcalf et al., 2006) at a Fr number of 0.37. Wave induced flow separation occurs and reattaches to the foil surface resulting in a wall-bounded separation bubble. The complexity of unsteady, wave-induced, boundary layer separation makes the experimental measurements difficult. With the combined CFD studies (Kandasamy et al., 2009 and Xing et al., 2007), more detailed flow description is provided. Three main instabilities, namely the initial shear-layer instability, Karman-like shedding and flapping of the separation bubble, were found in the unsteady Reynolds-averaged Navier-Stokes (URANS) study (Kandasamy et al., 2009). These instabilities are difficult to be identified in both the DES study (Xing et al., 2007) and experimental study (Metcalf et al., 2006) due to the numerous small-scale vortices in the separation region. There are limitations in both of the two CFD studies. The complicated flow structures at the interface as shown in the experimental images, such as splashing, breaking waves, air entrainment and free surface induced turbulence observed in the experiments, cannot be resolved since a single phase flow solver (air effect is neglected) and relatively less accurate interface modeling methods were used. These unresolved flow structures at the interface might affect the global flow patterns and turbulence. In Suh et al. (2011), flows past an interface piercing circular cylinder is investigated using LES with a focus on the effect of air–water interface on the vortex shedding from the vertical circular cylinder (selected results shown in Fig. 26).

Previous studies are mainly focused on the global structure of ship flows, such as the wave elevation, scars, and vortices. The small scale details of interface breaking, spray formation, and air entrainment are not well understood.

9.2 Bow wave breaking and spray formation

Ship bow waves exhibit both large and small scale features. The most prominent large scale feature is the Kelvin bow wave pattern scaled by Fr; however, for sufficiently large Fr and depending on bow shape, spilling and/or plunging breaking occurs and induces vortices and scars additionally scaled by Re and We. Small Re and We inhibit breaking, i.e., in general model scale flows exhibit reduced breaking compared to full scale, and smaller models display reduced breaking compared to larger models. A recent complementary EFD and CFD study has documented bow wave breaking and induced vortices and scars for model 5415 for Fr = 0.35 using CFDShip-Iowa Version 4 (Olivieri et al., 2007; Wilson et al., 2007a). The most prominent small scale feature is the bow wave crest formation of thin overturning sheets which break up into spray. In the study by Beale et al. (2010), recent in-situ measurement efforts were reviewed and spray formation generated by full-scale naval platforms were examined. Re and We scale effects are large such that replication of full scale phenomena of the small scale features of ship bow waves is difficult even with large models. The extent of the thin sheets is drastically reduced and remains attached, as shown by Stern et al. (1996) for the Series 60.

However, studies for wedge flows by Waniewski et al. (2002) and Karion et al. (2004) display and document the structure of bow waves (thin water sheet formation, overturning sheet with surface disturbance, fingering and breaking up into spray, plunging and splashing, and air entrainment) with valuable experimental data provided such as wave elevation, extent of wave breaking, spray droplets size and number. These two studies are summarized in Table 7. In Waniewski et al. (2002) the bow waves are created by a deflecting plate mounted at an angle in a flume, the towing tank experiments are also conducted with two wedge models. Typical bow wave profile obtained in the towing tank experiment shows a thin liquid sheet is created at the leading edge of the wedge, and it continues to ride up on the side wall. This thin liquid sheet starts to separate from the side wall as it reaches its maximum height. Once the crest reaches its maximum height, an overturning jet is formed and plunges back onto the undisturbed free surface. A large area of splash is generated at the wake of the wedge due to wave plunge and air entrainment. Noblesse et al. (2008) proposed a series of simple analytical relations for a wedge-shaped bow wave based on the experimental measurements and elementary fundamental considerations, which define the main characteristics of a ship bow (wave height, wave crest location and profile, and flow steadiness or unsteadiness) in terms of ship speed U, draught D and waterline entrance angle 2θ. A computational study has been carried out by Broglia et al. (2004) with the results compared with the experimental data (Waniewski et al., 2002). Since a single phase level set method was used for the free surface tracking, the small scale interface structures were not captured. The mechanism of the liquid sheet disturbance, fingering, pinching off drops and spray formation has not been thoroughly studied.

In Wang et al. (2010b), flows around a wedge-shaped bow are numerically simulated with the aim of investigating the wave breaking mechanism and small scale features of ship bow waves. The study (Waniewski et al., 2002) was selected as test cases to validate the capability of the code of CFDShip-Iowa Version 6 (Yang and Stern, 2009; Wang et al., 2009b) for small scale features of ship bow waves. The simulations are carried out using a Cartesian grid solver first with the sharp interface, coupled level set and volume-of-fluid (CLSVOF) and immersed boundaries methods; and an orthogonal curvilinear grid solver (Wang et al., 2012a) is also used in order to increase the grid resolutions near the wall.

The wedge geometry is similar to the large wedge model used by Waniewski et al. (2002). The side length of the wedge is L = 0.75 m, and the height of the wedge is H = 1 m. The half wedge angle is θ = 26º and the flare angle φ = 0º. The sharp edge corners are rounded with an arc of a small radius in order to make the grid orthogonal at the two corners. The grid is 1536×768×848 (one billion) which is refined near the solid surface.

For the case considered here, the water depth is d = 0.0745 m and the upstream velocity is U = 2.5 m/s, the corresponding Reynolds number, $\mathrm{Re} = \rho Ud / \mu = 1.64\times10^5$, and the Froude number, $Fr = U/\sqrt{gd}$ = 2.93. The domain boundary is given by x = [5.33 m, 4.55 m], y = [0.0745 m, 0.6 m], and z = [0 m, 5 m]. Uniform inflow and convective outflow boundary conditions are used. Slip-wall boundary conditions are imposed at all the other boundaries. A uniform velocity field same as the upstream velocity is prescribed to the entire computational domain at t = 0. Figure 27 shows the computed bow wave profile compared with the experimental video image. The overall wave structure is very similar to the experimental observation (Waniewski et al., 2002) as shown in figure, such as the thin liquid sheet at the leading edge of the bow, overturning jet, jet plunging onto the free surface, and splashes at the wake. As the liquid

sheet overturns, the sheet is stretched and fingered up, and some ‘‘cylindrical drops’’ then pinch off from the liquid sheet, when the detached drops impact onto the water surface, a spray region is created. The close-up view of the bow sheet breakup is shown in Fig. 28. In the experimental study conducted by Deane and Stokes (2002), the diameters of most observed bubbles due to the fragmentation process are greater than 2 mm. Mean drop size is 2.3 mm as observed in experiments (Karion et al., 2004). The effective diameters measured in the experiments by Beale et al. (2010) for full-scale ship bow spray are mainly in the range of 1 mm to 2.5 mm. For small size bubbles/droplets, surface tension force is dominant and further fragmentation is difficult. In the present study, the grid spacing is 0.125 mm near the wedge and 1 mm in the plunging region. With the current grid, the minimum drop size is 0.8 mm near the wedge. The droplets and bubbles near the wedge can be effectively captured. Further grid refinement (3 to 4 billion grid points) is needed to increase the resolution in the wake region.

9.3 Plunging wave breaking

Plunging wave breaking is one of the most violent phenomena of air-water interface interactions, producing strong turbulence with large amounts of air bubbles, water droplets, jets and sprays. These phenomena commonly occur in ship flows and are one of the main sources of the underwater sounds and white-water wakes, which are of great importance for signature of ships. Many experimental and computational studies for the plunging wave breaking have been done in the past few decades. Early experimental studies are focused on wave geometric properties (Bonmarin, 1989), wave breaking process (Tallent et al., 1990), energy dissipation (Melville, 1994), jet characteristics and air entrainment (Chanson and Fang, 1997), and turbulence (Chang and Liu, 1999). With the Particle Image Velocimetry (PIV) techniques, more detailed velocity field, turbulence, and void fraction data and analysis have been investigated in recent studies (Melville et al., 2002; Deane and Stokes, 2002; Grue and Jensen, 2006; Kimmoun and Branger, 2007; Blenkinsopp and Chaplin, 2007; Drazen and Melville, 2009). Due to the technical difficulties, the experimental measurements can only be done in the water region, and detailed description of the flow field in the energetic wave breaking region is not available. With the development of the computational fluid dynamics (CFD) technology, detailed wave breaking process and velocity profile can be obtained in both water and air phases (Chen et al., 1999; Watanabe and Saeki, 2002). The early CFD studies are usually 2-D due to the prohibitive computational cost for the 3-D simulations. In the more recent CFD studies (Watanabe et al., 2005; Lubin et al., 2006; Iafrati, 2010), simulations are conducted with the air entrainment, 2-D and 3-D vortex structures, and energy dissipation discussed.

It should be noted that most previous studies on plunging wave breaking are for deep water or sloping beach for which wave plunges forward in the same direction of the mean flow. Yao and Wu (2005) experimentally investigated the shear currents effects on unsteady waves but with a focus on incipient breaking. Moreover, the geometry and conditions in most cases of CFD differ from the experiments even though the experiments are usually used to guide the analysis of CFD. Present interest is ship hydrodynamics for which body-wave interactions are important and the direction of wave breaking is opposite or at an angle to the mean flow. Previous research used model ships in towing tanks focused on scars, vortices and mean and root mean square (rms) wave elevation induced by ship bow and shoulder wave breaking (Miyata and Inui, 1984; Dong et al., 1997; Olivieri et al., 2007), which suggests the presence of underlying coherent structures. A complementary CFD study to the latter study was carried out by Wilson et al. (2007). However, typical plunging wave breaking can hardly be obtained using model ships in towing tanks, and detailed measurements of the wave breaking processes are difficult. Recently, Shakeri et al. (2009) provide detailed measurements and analysis of divergent bow waves using a unique wave maker for simulating 2D + t flow. A numerical study using a 2D + t model has been reported by Marrone et al. (2011) for high speed slender ships. For slender bow ships, 2D + t wave breaking process is similar to deep water and sloping beach studies, i.e., plunges with forward splash-ups. In the early experimental studies by Duncan (1981; 1983), a fully submerged, two-dimensional hydrofoil was towed horizontally to produce breaking waves. These studies are focused on spilling breakers. Greco et al. (2004) investigated the impact flows on ship-deck structures due to head-incoming waves.

In the experimental fluid dynamics (EFD) study by Kang et al. (2012), a quadratic profile bump mounted in a shallow water flume is used to create impulsive sub critical flow conditions where plunging wave breakers are successfully obtained. Ensemble-averaged measurements (relative to the time t_b at which the maximum wave height is reached just before the first plunge) are conducted, including the overall flume flow and 2-D PIV center-plane velocities and turbulence inside the plunging breaking wave and bottom pressures under the breaking wave. The plunging wave breaking that is triggered by the flow over a submerged bump is of relevance to ship hydrodynamics since it includes wave-body interactions and the wave breaking direction is opposite to the mean flow as discussed in Kang et al. (2012). The idea and approach of creating

plunging wave breakers using a submerged bump is obtained collectively from the previous experimental (Cahouet, 1984; Miyata et al., 1985a) and CFD studies (Iafrati et al., 2001; Yang and Stern, 2007; Huang et al., 2007). The CFD results were used as a guide for the test design of the experiments (Ghosh, 2008) and the initial experimental data was used for validation. Subsequently, a complementary CFD study was used to aid in the data analysis simultaneously as the experimental data is used to validate a Cartesian grid, immersed boundary, coupled level set and volume-of-fluid CFD method (Wang et al., 2009b). Wang et al. (2009b) indentified three repeated plunging events each with three sub-events [jet impact (plunge), oblique splash and vertical jet]; however, they used fully impulsive initial conditions and adjusted the initial velocity and water elevation to match Ghosh's (2008) wave breaking position, which precluded detailed temporal validation.

In the study by Koo et al. (2012), impulsive plunging wave breaking downstream of a bump in a shallow water flume is numerically simulated with the aim of providing a detailed quantitative description of the overall plunging wave breaking process. The time-dependent velocity and wave elevation boundary conditions are specified at the inlet and outlet using the exact experimental data provided in Kang et al. (2012). The computational results are compared with the experimental measurements to validate the capability of the code of CFDShip-Iowa Version 6 (Yang and Stern, 2009; Wang et al., 2009b) for wave breaking. The simulations are carried out on a 2D Cartesian grid using the sharp interface, coupled level set and volume-of-fluid (CLSVOF) and immersed boundary methods. In the study by Wang et al. (2012b), a 3D LES of the impulsive plunging wave breaking is performed on an orthogonal curvilinear grid of 768×256×64 (streamwise, vertical, and spanwise) points in order to identify the 3D structures of breaking interface. The constant inlet velocity imposed at the left boundary is u = 0.87 m/s for water and zero for air. The initial interface elevation is 0.2286 m and a uniform velocity field is prescribed in the water domain with the air phase at rest. The overall interface structure of the breaking wave compared with the experimental video images is given in Fig. 29. The major events of the first plunge wave breaking are demonstrated, i.e., maximum height, first plunge, oblique splash, and vertical jet as identified by Wang et al. (2009b) using 2D simulations. On the video images, the entrapped air tube is marked by a circle. As shown in the figure, the computational results match the experiments very well. The 3D spanwise interface structures due to the centrifugal instabilities at the curved flow as observed in the experiments are also captured as shown in Fig. 30.

In a 2D CFD study conducted by Iafrati (2010) for Stokes waves, drops and bubbles in breaking waves are quantitatively estimated with some limitations due to the numerical model adopted in the simulations. Recently, simulation on a large grid of 1920×1280×896 (2.2 billion) was carried out for bubble/droplet size distribution in the breaking waves (Wang et al., 2012d). Figure 31 shows the close-up of the bubble and droplets in breaking waves on the large grid, where detailed small interface structures are well demonstrated.

9.4 Air-layer drag reduction

Bubble drag reduction (BDR) is an important technique that injects gas into the liquid turbulent boundary layer to form bubbles to obtain drag reduction. This technique can substantially reduce skin friction, which has great potential applications in ship hydrodynamics. During the past several decades, a large amount of research has been devoted to the BDR (Merkle and Deutsch, 1992). However, most of the studies were conducted at relatively low Reynolds numbers and small scales. Proper scaling of BDR remains unclear.

In the study by Sanders et al. (2006), a set of BDR experiments were conducted for a large scale flat plate turbulent boundary layer at high Reynolds numbers. It has shown that significant levels of BDR could be achieved only near the air injector, and limited persistence of BDR exists away from the air injector. This short persistence distance of BDR makes it impractical for applications. It has also shown that a layer of gas was formed and persisted along the entire plate at lower flow speeds and higher gas injection rates, which could lead to skin-friction reduction of more than 80%. Elbing et al. (2008) continued the study of Sanders et al. (2006) in an effort to understand the mechanisms underlying the limited persistence of the BDR and the onset conditions for the air layer drag reduction (ALDR). The experimental results indicated that ALDR could be established once the air was injected beyond a critical rate, and more than 80% drag reduction could be obtained over the entire plate. Three distinct regions associated with drag reduction were observed with air injection rate: BDR, transition and ALDR. It was found that the air layer was sensitive to the inflow conditions. In the recent work (Ceccio, 2009), a 1/2 inch (12.7 mm) step was used at the inlet, and the air was injected from the base of the backward-facing step. This greatly enhances the stability of the air layer. The ALDR is a potential alternative to BDR, however, the knowledge of ALDR mechanism is quite limited and more comprehensive studies are needed. Related to ALDR, partial cavity drag reduction (PCDR) is another important technique to reduce skin friction. PCDR needs potentially lower gas flux

compared to ALDR, but un-optimized cavity flow can lead to significant form drag (Ceccio, 2009). Partial cavities are sensitive to flow speed and perturbations from the incoming flow (Amromin and Mizine, 2003).

In the study by Wang et al. (2010a), URANS simulations of ALDR on a large scale flat plate are performed. The simulations are carried out using a sharp interface Cartesian grid solver, with the interface tracked by a coupled level set and volume-of-fluid (CLSVOF) method and turbulence modeled by a Spalart-Allmaras (SA) turbulence model (Spalart and Allmaras, 1992) with a wall function (WF) approach. The experimental data reported by Elbing et al. (2008) is used to validate the simulation results. The simulations are carried out on a two dimensional (2D) computational domain. The Reynolds number is Re = 7.37×10^7 which corresponds to Test 1 in Elbing et al. (2008) with a free stream velocity of 6.7 m/s. It is a challenge for the numerical simulation of such flow since high Reynolds numbers, air-water interface, and two-phase turbulence are involved. The air layer along the entire test plate is successfully achieved and the drag reduction is approximately 100%, which agrees with the experimental findings very well. With reduced air flow rate, BDR is also observed; the computational results also qualitatively match the experiments. The transitional region from BDR to ALDR is also observed in the present simulation. However, the critical air flow rate to form the ALDR is lower in the simulations than in the experiments. Several possible reasons are likely accounting for the low critical air flow rate in the simulations, such as SA-WF turbulence model, three-dimensional instability and surface tension effects. The critical air flow rate does not change much with grid refinement.

In the study by Kim and Moin (2010), DNS of the air layer drag reduction was conducted for a flat plate with a backward-facing step. In their simulations, the Reynolds number is 2.28×10^4 with a free steam velocity of water of 1.8 m/s, which is much lower than that used in the experimental study (Elbing et al., 2008) and CFD study (Wang et al., 2010a). This is because the Reynolds number in the experiment of Elbing et al. (2008) is too high for the direct numerical simulation. The simulation results show that the air layer was stabilized with increased air injection rate, and much larger skin-friction was obtained when the air layer broke up.

10 CONCLUDING REMARKS

10.1 Conclusions

The last thirty or so years have witnessed monumental progress in CFD for ship hydrodynamics: started from solving momentum integral equations, boundary layer equations, and partially parabolic RANS equations, in general with a flat free surface, to full RANS equations for single-phase or two-phase flows around model- or full-scale ships with deformed or broken interfaces, 6DOF motion prediction, and motion controllers. Now computational ship hydrodynamics is to embrace the exascale computing era with LES of multi-scale and multi-physics multi-phase ship flows on billion-point grids, resolving most scales of turbulence and bubbles/droplets at the same time.

In the course of this astronomical progress, there is a clear line of evolution in governing equations. Initial work was mainly focused on the boundary layer portion of the solution domain due to its fundamental importance in ship flows, lack of efficient gridding and solution techniques for high-Re incompressible flows with complex geometries, and limited computing power available at that time. Then steady RANS equations with grid-fitted free-surface conditions became the dominant model in many solvers, some of which are still in use today. Nowadays most solvers solve the unsteady RANS equations for the water flows (and semi- or fully-coupled air flows in some solvers) around ships with the air-water interface embedded in grids. For tomorrow's high-fidelity solvers, there is no doubt that the complete set of governing equations with no or minimum phenomenological modeling will be employed. This means the rigorous implementation of interface jump conditions due to discontinuous density and viscosity and surface tension, fully coupled 6DOF ship motion, fully discretized propulsors, LES with wall models, and environmental effects. Such a list of mathematical formulations might seem to be too sophisticated and unnecessary for some applications well within the capabilities of many current tools, but they are indeed the logical consequence of the above development and required for understanding the temporal-spatial correlations of a much wider spectrum in ship hydrodynamics.

Numerical methods for solving the mathematical models in ship hydrodynamics are mostly finite difference and finite volume methods, although finite element and particle methods are also used by some research groups. In general finite difference methods require complex transformed governing equations and high quality structured grids, which are sometimes quite difficult to generate for complex geometries. Cartesian grid methods can overcome the grid generation problems, but further development is still required for the accurate imposition of boundary conditions, especially for high-Re turbulent boundary layers, at the immersed boundaries. Finite volume methods have gained wide popularity because of their accommodation to polyhedra of arbitrary shape as grid cells and straightforward derivation of discretization schemes

from conservation laws. Computational ship hydrodynamics research codes mostly use multi-block structured grids because of a higher level of accuracy they can provide, although unstructured grids are increasingly applied, especially with commercial or open-source general-purpose application solvers, to ship flows. Most solvers use an inertial reference frame for the flow field and a ship-fixed non-inertial reference frame for ship motion; the latter is also used in some solvers for the flow field but the applications are limited to single ship cases. In general geometry motions in ship flows are treated using deforming, sliding, regenerated, and/or dynamic overset grids; only the last approach provides a good compromise of applicability and efficiency, although conversation property between overlapping grids is still an outstanding issue. Level set and algebraic VOF methods are widely used in many solvers for tracking the air-water interface; but the former are long known of a flawed mass conservation property and the latter are also criticized for giving a diffusive, blurred interface. Geometric VOF methods with various enhancements, such as the constructed distance function, centroids of volume fractions, and tracked surface markers, can provide highly accurate interface position as well as strict mass conservation, and facilitate sharp interface treatment in Navier-Stokes equations; they will be seen in more and more high-fidelity simulations in ship hydrodynamics. For solving the incompressible Navier-Stokes equations, pressure-based and density-based (artificial compressibility) fully coupled methods can provide robust and fast solution, but they demand too much computer memory and are mostly used in steady flow problems. The SIMPLE-family algorithms were initially designed for steady problems too; and their tightly coupled iterative solution procedure for both velocity and pressure greatly restricts the applications of many novel numerical schemes within them including PISO for unsteady problems. On the other hand, fractional-step methods have been applied in high-fidelity simulations for a long time; they also allow different optimized strategies for different terms. High-order schemes including semi-Lagrangian advection schemes can be implemented with ease. On the contrary, most current RANS solvers use first- or second-order temporary and spatial discretization schemes; and applications of higher-order schemes are usually cautioned with robustness issues. Therefore, fractional-step methods will be seen in more and more solvers for ship hydrodynamics applications due to their flexibility in using various higher-order schemes for improving overall accuracy of the solution. In addition, solution adaption strategies can be used to obtain the required level of accuracy with minimized computational cost, in which the h-adaption is the most popular one for its conformability with different types of grids and discretization schemes.

For computational ship hydrodynamics, the most commonly used application area is resistance and detailed local flow field predictions around the hull, followed by seakeeping, manoeuvring and self-propulsion. For seakeeping simulations, wave models are useful for simulating incident waves or sea environments. Winds and air flows are important in applications such as landing-of-aircraft, high speed ships, and wind force applications. Propulsion modeling is performed using body force approach based on the radial distribution body force for finite-bladed propeller. Waterjet propulsion systems have also been modeled using body force method for the pump and by applying axial and vertical reaction forces and pitching reaction moment.

Linear URANS models, in particular two-equation blended k-ε/k-ω model, are the most commonly used turbulence closure for ship hydrodynamics applications. The model performs reasonably well for the model-scale resistance prediction on up to 10M grids. However, they fail to accurately predict the mean vortical and turbulent structures. Currently used anisotropic models show some improvements over the linear models in predicting these features, but are not sufficiently accurate. Wall-functions are a viable option for full-scale ship simulations including wall roughness effects, and perform reasonably well for resistance predictions when compared with ITTC correlation. Thus far, limited LES or hybrid RANS/LES simulations have been performed for ship hydrodynamics. Nonetheless, the simulations emphasize the advantages of these methods over URANS as they reduce dependency on modeling, resolve small scale-scale physics, improve understanding of turbulence and vortical structures, and two-phase flow and air entrainment. They also help in explaining the observation in sparse experimental data and guide experiments. The advances in high performance computing will soon enable calculation on hundreds of millions to billions of grid points on a regular basis. Simulations on tens to hundreds of millions of grid points can help us in obtaining benchmark URANS predictions using the existing model to identify their limitations. Hybrid RANS/LES on hundreds of millions to billions of grid point can help in resolving 90-95% of the turbulence, and can be used to develop accurate anisotropic URANS models for general purpose applications.

For quantitative V&V, there are several problems in using the Richardson extrapolation method. It requires that all solutions should be sufficiently close to the asymptotic range, i.e., within about six percent of the p_{th} of the numerical method. When solutions are not in the asymptotic range, multiple grid-triplet

studies often show oscillatory convergence. In such cases, the estimated order of accuracy p_{RE} approaches p_{th} with oscillations and a wide range of values (Celik 2008). The Richardson extrapolation method requires at least three systematic high-quality grids, which may be too expensive for industrial applications. The oscillatory convergence with grid refinement may be treated using the least-square (Eça and Hoekstra 2002) or response-surface (Logan and Nitta 2006) methods, which requires solutions for more than three grids. There are some issues in using these two methods. The relationship between their estimates for the order of accuracy, error estimate, and numerical benchmark and those for individual grid-triplet studies is not established. They do not discriminate between converging and diverging grid studies and the use of diverging grid studies is not well founded. The requirement of at least four solutions is often too expensive for industrial applications. All the solutions are required to be in the asymptotic range, which is contradictory to the use of solutions that show oscillatory and non-monotonic convergence. They also introduce additional uncertainties due to the least-square fit. The difficulty and computational cost associated with the Richardson extrapolation method may be resolved by the single-grid method (Celik and Hu 2004; Cavallo and Sinha 2007). However, the sensitivity of the solutions to grid spacing and time step is not provided and control of the spatial discretization error as the simulation progresses needs to be further investigated. Additionally, the applicability of the single-grid method to different discretization schemes and turbulence models needs to be validated. The available grid verification methodologies were developed for URANS (Stern et al. 2006; Xing and Stern 2010; Xing and Stern 2011), and cannot be applied straightforwardly to LES and hybrid RANS-LES models due to the coupling of modeling and numerical errors. Thus, new verification methods need to be developed. Very recently, the method of manufactured solutions is used to study the convergence characteristics of numerical solutions of highly non-linear systems of partial differential equations such as the RANS models (Eça *et al*., 2012).

Captive V&V simulations are carried out for a wide range of applications and have shown improvement over the years. Calm water resistance, sinkage and trim simulations have achieved relatively small error values for resistance, averaged at 3.3%D. For sinkage and trim, the error values are larger for smaller Fr<0.2 (44.7%D), while for larger Fr>0.2 the average error value is 10.3%D. The number of seakeeping simulations has increased since 2005, with average fine grid size of 15M. The average error value is relatively small (15%) for 1st order terms while for 2nd order terms the average error is very large (44%D). Captive maneuvering simulations are carried out to obtain coefficients used in system-based models to predict actual 6DOF maneuvers, mostly as part of the SIMMAN 2008 workshop. The average of the fine grid points is 6M with average error value of 13.6%D for forces and moments predictions. In the view of the progress on free running simulations, it is expected that the future challenges and method development efforts for modelling, numerical methods, and HPC will focus on free running rather than captive simulations. However, captive CFD will remain an important tool both for fundamental issues and local flow studies and uncertainty analysis/optimization efforts.

Due to the significant amount of information provided by CFD free running, the free running simulation is the future in computational ship hydrodynamics and captive simulations will be used only for limited purposes. Despite the progress in free running simulations, there are still significant challenges ahead that have to be addressed. The verification study is not performed systematically yet for any computations due to the complex grids structures of the hull and the appendages. The validation studied showed fairly good agreement with EFD data for motions (E=8.46%D). However, the validation for local flow is not conducted yet due to the complexity in the local flow measurement for free running ships. For more computer-intensive applications such as seakeeping and route simulation, an extremely long solution time and a very large operating condition should be covered. For these applications, the speed of current CFD solutions is still far too slow. Thus, using much faster method such as system based method could be considered. However, the mathematical models for these methods should to be improved using high fidelity CFD solutions along with system identification techniques. Furthermore, innovating numerical methods for easier and faster CFD solution is essential. Moreover, taking advantage of faster computers such as next generation of massively parallel multi-core machines should be considered.

Breaking waves, spray formation, and air entrainment around ships are of great importance to ship hydrodynamics. Previous studies are mainly focused on the global structure of ship flows, such as the wave elevation, scars, and vortices. The small scale details of interface breaking, spray formation, and air entrainment are not well understood. With the development of the CFD technology, detailed studies of the two-phase region become possible. In the simulation of the wedge flow, the predicted overall bow wave profile (thin liquid sheet at the leading edge, overturning jet and plunging, and splashes at the wake), plunging jet shape, and surface disturbances on the wave crest are similar to the experimental observations. With 1.0 billion grid points, the droplets and bubbles near the wedge can be

effectively captured. Further grid refinement (3 to 4 billion grid points) is needed to increase the resolution in the wake region. In CFD study of the plunging wave breaking over a submerged bump, the overall interface structure of the breaking wave match the experimental results very well, and the major events of the first plunge wave breaking, i.e., maximum height, first plunge, oblique splash, and vertical jet are also demonstrated. With a large grid of 2.2 billion points, the experimental observed mean droplet/bubble size can be effectively captured. Further grid refinement (up to 16 billion points) is needed in order to capture the minimum drop/bubble size observed in the experiments. 3D structure of the plunging wave breaking over the bump will also be investigated in the future work. In the study of air-layer drag reduction, the air layer along the entire test plate is successfully achieved and the drag reduction is approximately 100%, which agrees with the experimental findings very well. With reduced air flow rate, BDR is also observed; the computational results also qualitatively match the experiments. The critical air flow rate to form the ALDR is lower in the simulations than in the experiments, which needs further investigations in the future work.

10.2 Future directions

The oncoming exascale HPC era is to change our approaches to grand scientific and engineering challenges and to transform modeling and simulation into a specified discipline of predictive science. Central to achieving a predictive science in ship hydrodynamics is the development and application of verified and validated computational methodologies, capable of utilizing exascale HPC platforms and predicting ship resistance and propulsion, seakeeping, and maneuvering, as well as breaking waves, turbulence, fluid-structure interactions, and signature, with quantified uncertainty. High-fidelity, first-principles-based simulations with unprecedented resolution can reveal vast unknown temporal-spatial correlations in multi-scale and multi-physics phenomena that are beyond today's computing capabilities. It is to revolutionize ship hydrodynamics research and along with optimization techniques ship design process. On the other hand, exascale platforms will be dramatically different from current mainstream supercomputers in terms of computing power and parallel architectures; and few codes could make full use of their potentials without major overhauls or even rewrite for minimized dependence on phenomenological/empirical models and substantially improved scalability. To meet the challenges of exascale computing for fundamental studies and simulation-based design in ship hydrodynamics, the next-generation high fidelity solvers have to be developed with focus on improvements of orders of magnitude in accuracy, robustness, and performance.

Current mainstream RANS solvers for ship hydrodynamics are expected to continue performing well for even larger grids of up to a few hundreds of millions of points. However, there will be a threshold that further increase of grid size cannot improve the results anymore because of the inherently limited RANS turbulence models. Of course, it is possible to switch to second moment closure or hybrid RANS/LES such as DES; again, there will be a threshold of accuracy improvements from better turbulence modeling due to the limited orders of accuracy of the discretization schemes. These solvers will replace potential solvers to a large extent in the routine practice of industrial ship design process. And just like the potential solvers are run on today's desktops with one or a few processor cores, these RANS solvers will be very likely to be run on desktops or workstations with a few hundreds of processors cores, including the GPU cores. GPU acceleration capability can be easily obtained by using OpenMP-like compiler directives, such as OpenACC, with a compiler supporting them. This step may not require major changes of the code. However, it is almost sure that computer memory capacity won't increase in a similar scale as the computing power from a many-core processor. In order to achieve the same level of acceptance of potential solvers in ship design process using commodity computers, it will be essential to greatly reduce memory usage in these RANS solvers. Unfortunately, the solution algorithms and discretization schemes in many of these solvers are well-known to require very large amounts of memory, which may become the major issue hindering their daily applications in ship design process. Furthermore, RANS solvers are generally not accurate enough for tackling many fundamental problems related to interfacial phenomena in ship hydrodynamics such as wave breaking, turbulent contact line, bubbly wake, and cavitation, many of which have long been addressed separately using totally different tools without a ship flow context. The modeling of these phenomena in many RANS solvers is usually overly simplified and could not provide much insight into the mechanism behind the problems.

The next-generation, high-fidelity ship hydrodynamics solvers have to be developed aiming at the oncoming exascale computing platforms, and addressing modeling issues, discretization schemes, and HPC memory and scalability restraints at the same time. However, it is not meant to embrace some totally different, novel techniques only showing limited promise in some specific application areas. These new techniques may take several decades to reach the same

level of maturity of some widely accepted algorithms such as MAC grids for variable arrangement, projection methods for velocity-pressure coupling, and VOF methods for interface (volume) tracking. The problem is, the first exascale computer has been projected to become reality before 2020 and it is very likely that these new techniques won't be ready to tackle real world ship hydrodynamics problems by that time. Therefore, it is more sensible to adopt the advanced developments of long-tested modeling formulations and numerical algorithms – this won't be simple tasks by any means – from various research areas. For example, the level set based sharp interface (ghost fluid) method for two phase flows has been around for a while, but it has been seldom implemented and applied in ship flow related studies; geometrical VOF methods with very high accuracy of mass conservation have been rarely used either; similarly, semi-Lagrangian advection schemes have been developed to a very sophisticated level coupling high order accuracy, strongly conservative advection, and unconditional stability in time domain, but expensive, low-order, implicit schemes have been predominated in ship hydrodynamics solvers including commercial and open-source solvers. It is expected that the incorporation of these new algorithms in the high-fidelity solvers to be developed for exascale computers will elevate the state of the art of computational ship hydrodynamics to an unprecedented level, even each numerical technique or solution algorithm is not completely newly invented. In addition, many critical choices can be made during the solver envisagement and design stage by taking into account many characteristic exascale issues such as many-core processors, GPU accelerators, memory constraints, etc. All these considerations are essential for the realization of the next generation, high-fidelity solvers for solving ship hydrodynamics problems on exascale computers.

ACKNOWLEDGMENTS

This research was sponsored by the Office of Naval Research under Grant N000141-01-00-1-7, under the administration of Dr. Patrick Purtell.

REFERENCES

Ahn, H.T., Shashkov, M., "Adaptive moment-of-fluid method," Journal of Computational Physics, Vol. 228, Issue 8, 2009, pp. 2792-2821.

Abdel-Maksoud, M., Menter, F. R., and Wuttke, H., "Numerical Computation of the Viscous Flow around Series 60 CB =0.6 Ship with Rotating Propeller", Proc. 3rd Osaka Colloquium Advanced CFD Applications to Ship Flow And Hull Form Design, Osaka, 1998, pp.25-50.

Amromin, E., and Mizine, I., "Partial Cavitation as Drag Reduction Technique and Problem of Active Flow Control," Marine Technology, Vol. 40, 2003, pp. 181-188.

Araki, M., Sadat-Hosseini, H., Sanada, Y. Tanimoto, K., Umeda, N., and Stern, F., "Estimating Maneuvering Coefficients Using System identification Methods with Experimental, System-based, and CFD Free-running Trial Data", Journal of Ocean Engineering, Vol. 51,2012a, pp. 63-84.

Araki, M., Sadat-Hosseini, H., Sanada, Y., Umeda, N., and Stern, F, "Study of System -based Mathematical Model using System Identification Method with Experimental, CFD, and System-Based Free-Running Trials in Wave", Proceedings of the 11th International Conference on the Stability of Ships and Ocean Vehicles, Athens, Greece, Sept 23-28, 2012b.

ASME Performance Test Codes Committee PTC 61, "V&V 20: Standard for Verification and Validation in Computational Fluid Dynamics and Heat Transfer," 2009.

Aulisa, E., Manservisi, S., Scardovelli, R., "A surface marker algorithm coupled to an area-preserving marker redistribution method for three-dimensional interface tracking," Journal of Computational Physics, Vol. 197, Issue 2, 2004, pp. 555-584.

Baker, T. J., "Automatic Mesh Generation for Complex Three-Dimensional Regions using a Constrained Delaunay Triangulation," Engineering with Computers, Vol. 5, 1989, pp. 161–175.

Balay, S., Buschelman, K., Gropp, W., Kaushik, D., Knepley, M., Curfman, L., Smith, B. and Zhang, H. "PETSc User Manual", ANL-95/11-Revision 2.1.5, 2002, Argonne National Laboratory.

Bardina, J., Ferziger, J., Reynolds, W., "Improved turbulence models based on large eddy simulation of homogeneous, incompressible, turbulent flows," Technical Report TF-19. Department of Mechanical Engineering, Stanford University, Stanford, California, 1983.

Batten, P., Goldberg, U., Chakravarthy, S., "Interfacing statistical turbulence closures with large eddy simulation," AIAA J., Vol. 42(3), 2004, pp. 485–492.

Beale, K.L.C., Fu, T.C., Fullerton, A.M., Drazen, D., Wyatt, D.C., "An Experimental Characterization of Full-Scale Ship Generated Bow Spray," 28th Symposium on Naval Hydrodynamics, Pasadena, California, 12–17 September 2010.

Bhushan, S., Xing, T., Carrica, P., Stern, F., "Model- and Full-Scale URANS Simulations of Athena Resistance, Powering, Seakeeping, and 5415 Maneuvering," Journal of Ship Research, Vol. 53, No. 4, 2009, pp. 179–198.

Bhushan, S., Carrica, P.M., Yang, J., and Stern, F., "Scalability studies and large grid computations for surface combatant using CFDShip-Iowa," International Journal of High Performance Computing Applications, Vol. 25, No. 4, 2011a, pp. 466-287.

Bhushan, S., Hanaoka, A., Yang, J. and Stern, F., "Wall-Layer Modeling for Cartesian Grid Solver Using an Overset Boundary Layer Orthogonal Curvilinear Grid," 49th AIAA Aerospace Sciences Meeting, 2011b.

Bhushan, S., Carrica, P.M., Yang, J., and Stern, F., "Scalability studies and large grid computations for surface combatant using CFDShip-Iowa," International Journal of High Performance Computing Applications, Vol. 25, No. 4, 2011, pp. 466-287.

Bhushan, S, Alam, M.F., Walters DK. "Application of dynamic hybrid RANS/LES model for straight ahead surface combatant vortical and turbulent structure predictions," ParCFD 2012, 22-26 May, 2012a, Atlanta, US.

Bhushan, S., Mousaviraad, S.M., Stern, F., Doctors, L.J., "T-Craft Resistance, Seakeeping and Maneuvering – Part I: Single-Phase Modeling and Verification and Validation for Captive Cases," Submitted to Applied Ocean Research, 2012b.

Bhushan, S., Xing, T., Stern, F., "Vortical Structures and Instability Analysis for Athena Wetted Transom Flow with Full-Scale Validation," Journal of Fluids Engineering, Vol. 134, 2012c, 031201-1 – 18.

Bhushan, S., Walters DK. "A dynamic hybrid RANS/LES modeling framework," Physics of Fluids, Vol. 24, 015103, 2012.

Blenkinsopp, C. E., and Chaplin, J. R., "Void fraction measurements in breaking waves," Proceedings of the Royal Society A 463, 2007, pp. 3151-3170.

Bonmarin, P., "Geometric properties of deep-water breaking waves", J. Fluid Mech.,Vol. 209, 1989, pp.405-433.

Boris, J.P., Grinstein, F.F., Oran, E.S., Kolbe, R.L., "New Insights into Large Eddy Simulation," Fluid Dyn. Res., Vol. 10, 1992, pp. 199-209.

Briley, W., Arabshahi, A, Webster, R.S., and Whitfield, D. L. "Computational Analysis and Advancement of Solid Rocket Motor (SRM) Modeling and Simulation Tools," Monthly Technical Report for period February 2005-July 2006, SPARTA, INC. 25531 CA 92630.

Broglia, R., Di Mascio, A., Muscari, R., "Numerical simulations of breaking wave around a wedge," Proceedings of 25th symposium on naval hydrodynamics, St. John's Newfoundland and Labrador, Canada, 2004.

Brucker, K.A., Dommermuth, D.G., O'Shea, T.T., Yue, D.K.P., Hendrickson, K., Weymouth, G., "Computational Naval Ship Hydrodynamics," In Proceedings of the 2010 DoD High Performance Computing Modernization Program Users Group Conference (HPCMP-UGC '10). IEEE Computer Society, Washington, DC, USA, 64-70, 2010.

Cahouet, J., "Etude numerique er experimentale du problem bidimensionnel de la resistance de vaques non-lineaire," Ph.D. Thesis, ENSTA, 1984, Paris, (in French).

Campana, E., Peri, D., Tahara, Y., Kandasamy, M., and Stern, F., "Optimal ship design algorithms and their application to industrial problems," Transactions SNAME, Vol. 117, 2009, awarded ABS-Captain Joseph H. Linnard Prize for best paper 2009.

Carrica, P.M., Drew, D., Bonetto, F. and Lahey, R.T., Jr., "A polydisperse model for bubbly two-phase flow around a surface ship," Int. J. Multiphase Flow, Vol. 25, 1999, pp. 257–305.

Carrica, P., Wilson, R., Noack, R., and Stern, F., "Ship Motions using Single-Phase Level Set with Dynamic Overset Grids," Computers & Fluids, Vol. 36, 2007, pp. 1415-1433.

Carrica, P.M., Ismail, F., Hyman, M., Shanti Bhushan, S., Stern, F., "Turn and Zig-Zag manoeuvre of a surface combatant using a URANS approach with dynamic overset grids", Proceedings of SIMMAN 2008, 2008a.

Carrica PM, Paik K, Hosseini H, Stern F, "URANS Analysis of a Broaching Event in Irregular Quartering Seas", J. Marine Sci. Tech., 2008b,13, 395-407.

Carrica, P.M., Stern, F., "DES Simulations of the KVLCC1 in Turn and Zigzag Maneuvers with Moving Propeller and Rudder", Proceedings of SIMMAN 2008, 2008.

Carrica PM, Castro A, Stern F, "Self-Propulsion Computations Using Speed Controller and Discretized Propeller with Dynamic Overset Grids", J. Marine Sci. Tech. 15, 2010a, 316-330.

Carrica, P. M. Huang, J., Noack, R., Kaushik, D., Smith, B., Stern, F., "Large-scale DES computations of the forward speed diffraction and pitch and heave problems for a surface combatant," Computers and Fluids, Vo. 39(7), 2010b, pp. 1095-1111.

Carrica, P.M., Fu, H., and Stern, F., "Self-Propulsion Free to Sink and Trim and Pitch and Heave in Head Waves of a Kcs Model", G2010: A Workshop on CFD in Ship Hydrodynamics, Chalmers, Gothenburg, December 8-10, 2010c.

Carrica, P., Sadat-Hosseini, H., and Stern, F., "CFD Analysis of Broaching for a Model Surface Combatant with Explicit Simulation of Moving Rud-

ders and Rotating Propellers," Computers & Fluids, Volume 53, 2012a, pp. 117-132.

Carrica, P.M., Ismail, F., Hyman, M., Bhushan, S., Stern, F., "Turn and Zigzag Maneuvers of a Surface Combatant Using a URANS Approach with Dynamic Overset Grids," Journal of Marine Science and Technology, 2012b.

Castiglione, T., Stern, F., Bova, S., Kandasamy, M., 2011, "Numerical investigation of the seakeeping behavior of a catamaran advancing in regular head waves," Ocean Engineering, Volume 38, Issue 16, Pages 1806–1822.

Cavallo, P. A., and Sinha, N., "Error quantification for computational aerodynamics using an error transport equation," Journal of Aircraft, 44(6), 2007, pp. 1954-1963.

Ceccio, S.L, "Evaluation of Air Cavity Lubrication at High Reynolds Numbers," Air Layer Drag Reduction Program Review Meeting, Stanford University, Stanford, California, September 15, 2009.

Celik, I. B., Ghia, U., Roache, P. J., Freitas, C.J., Coleman, H., Raad, P. E. , "Procedure for Estimation and Reporting of Uncertainty Due to Discretization in CFD Applications," Journal of Fluids Engineering, 130(7), 2008, p. 078001.

Celik, I., and Hu, G., "Single Grid Error Estimation Using Error Transport Equation," Journal of Fluids Engineering, 126(5), 2004, p. 778.

Chang, K. A. and Liu, P. L. F., "Experimental investigation of turbulence generated by breaking waves in water of intermediate depth," Physics of Fluids 11, 1999, pp. 3390-3400.

Chanson, H., Fang L., "Plunging jet characteristics of plunging breakers," Coastal Engineering, 31, 1997, pp. 125-141.

Chen, G., Kharif, C., Zaleski, S., Li J., "Two-dimensional Navier-Stokes simulation of breaking waves," Physics of Fluids ,11, 1999, pp. 121-133.

Cho, S., Hong, S., Kim, Y., " Investigation of dynamic characteristics of the flooding water of the damaged compartment of an ITTC RoRo-Passenger", J. of the Soc. of Naval Architects of Korea, Vol. 43, Issue 4, 2006, pp.451-459

Choi, H. and Moin, P., "Effects of the computational time step on numerical solutions of turbulent flow", J. Comput. Phys., Vol. 113, 1994, pp. 1-4.

Cohen, J., Molemaker, J., "A Fast Double Precision CFD Code using CUDA," 21st Parallel CFD Conference, May 18-22, Moffett Field, California, USA, 2009, pp. 252-256.

Cosner, R. R., Oberkampf, W. L., Rumsey, C. L., Rahaim, C., and Shih, T., "AIAA Committee on standards for computational fluid dynamics: status and plans," AIAA paper, 889, 2006.

Deane, G.B., Stokes, M.D., "Scale dependency of bubble creation mechanisms in breaking waves," Nature, Vol. 418, 2002, pp. 839–844.

Di Mascio, A., Broglia, R., Muscari, R., On the application of the single-phase level set method to naval hydrodynamic flows, Computers and Fluids, 36 (5), 2007, pp. 868-886.

Dommermuth, D.G., O'Shea, T.T. , Wyatt, D.C., et al., An application of Cartesian-grid and volume-of-fluid methods to numerical ship hydrodynamics, in: Proc. Nineth Int. Conf. Numer. Ship Hydrodynamics, Ann Arbor, MI, 2007.

Dong, R. R., Katz, J. and Huang, T. T., "On the structure of bow waves on a ship model," Journal of Fluid Mechanics, 346, 1997, pp.77-115.

Dong, S., Shen, J., "A time-stepping scheme involving constant coefficient matrices for phase-field simulations of two-phase incompressible flows with large density ratios," Journal of Computational Physics, Vol. 231, Issue 17, 2012, pp. 5788-5804.

Dong, S., Shen, J., "An unconditionally stable rotational velocity-correction scheme for incompressible flows," Journal of Computational Physics, Vol. 229, Issue 19, 2010, pp.7013-7029.

Drazen, D. A. and Melville, W. K., "Turbulence and mixing in unsteady breaking surface waves," Journal of Fluid Mechanics, 628, 2009, pp. 85-119.

Drazen, Fulletron, Fu, Beale, O'Shea, Bruker, Dommermuth, Wyatt, Bhushan, Carrica and Stern, "A comparison of model-scale experimental measurements and computational predictions for a large transom-stern wave," 28th Symposium on Naval Hydrodynamics, Pasadena, California, 12-17 September 2010.

Dreyer, J.J. and Boger, D.A., "Validation of a Free-Swimming, Guided Multibody URANS Simulation Tools", 28th Symposium on Naval Hydrodynamics, Pasadena (Ca), 2010.

Drouet, A., Jacquin, E. et al., "Simulation of unsteady ship maneuvering on calm water and in waves using free-surface RANS solver", 27th Symposium on Naval Hydrodynamics, Seoul, South Korea, 2008.

Dubbioso, G., Durante, D., Broglia, R., Mauro, S., "Comparison of experimental and CFD results for a tanker-like vessel", Proceeding of MARSIM 2012, 2012.

Ducan, J.H., "An experimental investigation of breaking waves produced by a towed hydrofoil," Proc. R. Soc. London Ser. A, 377, 1981, pp. 331-348.

Ducan, J.H., "The breaking and nonbreaking wave resistance of a two-dimensional hydrofoil," Journal of Fluid Mechanics, 126, 1983, pp. 507-520.

Durante, D., Broglia, R., Muscari, R. and Di Mascio, A., "Numerical simulations of a turning circle maneuver or a fully appended hull", 28th Symposium on Naval Hydrodynamics, Pasadena (Ca), 2010.

Eça, L., and Hoekstra, M., "An Evaluation of Verification Procedures for CFD Applications," 24th Symposium on Naval Hydrodynamics, Fukuoka, Japan, 2002.

Eça, L., and Hoekstra, M., "Discretization uncertainty estimation based on a least squares version of the grid convergence index," Proc. Proceedings of the Second Workshop on CFD Uncertainty Analysis, Instituto Superior Tecnico, 2006.

Eça, L., Vaz, G., Hoekstra, M., "Assessing Convergence Properties of RANS Solvers with Manufactured Solutions," European Congress on Computational Methods in Applied Sciences and Engineering (ECCOMAS 2012), Vienna, Austria, 2012.

Elbing, B.R., Winkel, E.S., Lay, K.A., Ceccio, S.L., Dowling, D.R., and Perlin, M., "Bubble-Induced Skin-Friction Drag Reduction and the Abrupt Transition to Air-Layer Drag Reduction," J. Fluid Mech., Vol. 612, 2008, pp. 201-236.

Enright, D., Fedkiw, R., Ferziger, J., Mitchell, I., "A Hybrid Particle Level Set Method for Improved Interface Capturing," Journal of Computational Physics, Vol. 183, Issue 1, 2002, pp. 83-116.

Falgout, R.D., Jones, J.E., and Yang, U.M., "The design and implementation of HYPRE, a library of parallel high performance preconditioners", in Numerical Solution of Partial Differential Equations on Parallel Computers, A.M. Bruaset and A. Tveito, eds., Springer-Verlag, Vol. 51, 2006, pp. 267-294.

Ferrant P., Gentaz L., Monroy C., Luquet R., Ducrozet G., Alessandrini B., Jacquin E. and Drouet A., "Recent Advances Towards the Viscous Flow Simulation of Ships Manoeuvring in Waves", Proc. of 23rd International Workshop on Water Waves and Floating Bodies, Jeju, Korea, April 2008.

Fossen, T. I., "Guidance and Control of Ocean Vehicles," (John Wiley & Sons Ltd.), 1994.

Fu, H., Michael, T., Carrica, P.M., "A Method to Perform Self-Propulsion Computations with a Simplified Body-Force Propeller Model", G2010: A Workshop on CFD in Ship Hydrodynamics, Chalmers, Gothenburg, December 8-10, 2010.

Fureby, C. Towards the use of large eddy simulation in engineering, Progress in Aerospace Sciences, Vol. 44, 2008, pp. 381–396.

G2010, Gothenburg 2010 A Workshop on CFD in Ship Hydrodynamics, Chalmers, Gothenburg, December 8-10 2010.

Gao, Q., Vassalos, D., " Numerical Study of the Roll Decay of Intact and Damaged Ships", 12th International Ship Stability Workshop, 2011.

Gao, Z., Gao, Q., Vassalos, D., "Numerical simulation of flooding of a damaged ship", Ocean Engineering, Vol, 38, 2011, pp. 1649-1662.

Gatski, T., Jongen, T., "Nonlinear eddy viscosity and algebraic stress models for solving complex turbulent flows," Progress in Aerospace Sciences, Vol. 36(8), 2000, pp. 655–682.

Ghosh, S., "Free surface instabilities and plunging breaking wave downstream of a bump in shallow water open channel flume," Ph.D. Thesis, 2008, The University of Iowa, USA.

Gibou, F., Min, C., "Efficient symmetric positive definite second-order accurate monolithic solver for fluid/solid interactions," Journal of Computational Physics, Vol. 231, Issue 8, 2012, pp. 3246-3263.

Gicquel, L.Y.M., Staffelbach, G., Cuenot, B., Poinsot, T., "Large eddy simulations of turbulent reacting flows in real burners: the status and challenges," Journal of Physics: Conference Series, Vol. 125, 2008, 012029.

Gilmanov, A., Sotiropoulos, F., and Balaras, E., "A general reconstruction algorithm for simulating flows with complex 3d immersed boundaries on Cartesian grids", J. Comput. Phys., Vol. 191, 2003, pp. 660-669.

Girimaji, S., Jeong, E., Srinivasan, R., 2006. "Partially averaged Navier-Stokes method for turbulence: Fixed point analysis and comparison with unsteady partially averaged Navier-Stokes," Journal of Applied Mechanics, Vol. 73, 2006, pp. 422-429.

Greco, M., Landrini, M., Faltinsen, O.M., "Impact flows and loads on ship-deck structures," Journal of Fluids and Structures, 19 (3), 2004, pp.251–275.

Grue, J., Jensen, A., "Experimental velocities and accelerations in very steep wave events in deep water," European Journal of Mechanics B/Fluids 25, 2006, pp. 554-564.

Hanjalic, K., "Will RANS Survive LES? A view of perspective," Journal of fluids engineering, Vol. 127, 2005, pp. 831-839.

Heredero, P. A., Xing, T., and Stern, F., "URANS and DES for Wigley hull at extreme drift angles," Journal of Marine Science and Technology, **15**(4), 2010, pp. 295-315.

Hino, T. Ohashi, K, Kobayashi, H. "Flow Simulations Using Navier-Stokes Solver Surf", Proc. of G2010 Workshop, 2010.

Hoekstra M., "Numerical Simulation of Ship Stern Flows with a Space-marching Navier-Stokes Method," PhD Thesis, Delft 1999.

Horiuti K., "A new dynamic two-parameter mixed model for large-eddy simulation," Physics of Fluids, Vol. 9(11), 1997, pp. 3443– 3464.

Horiuti, K., "Roles of non-aligned eigenvectors of strain-rate and subgrid-scale stress tensors in turbulence generation", Journal of Fluid Mechanics, Vol. 491, 2003, pp. 65-100.

Hough, G. and Ordway, D., "The generalized actuator disk", Developments in Theoretical and Applied Mechanics, 1965, 2:317-336.

Hu, C. and Kashiwagi, M., "Numerical and experimental studies on three-dimensional water on deck with a modified Wigley model", Proc. 9th Inter. Conf. Numer. Ship Hydrodynamics, Ann Arbor, Michigan, 2007.

Hu, C., Kashiwagi, M., "CIP Based Cartesian Grid Method for Prediction of Nonlinear Ship Motions", Proc. of G2010 Workshop, 2010a.

Hu, C-H., Sueyoshi, M., Kashiwagi, M., "Numerical Simulation of Strongly Nonlinear Wave-Ship Interaction by CIP based Cartesian Grid Method," International Journal of Offshore and Polar Engineering, 2010b (June), Vol. 20, No.2, pp.81-87

Huang J., Carrica P., Stern F., "Semi-coupled air/water immersed boundary approach for curvilinear dynamic overset grids with application to ship hydrodynamics", International Journal Numerical Methods Fluids, Vol. 58, 2008, pp. 591-624.

Huang, J., Carrica, P., Stern, F., "Coupled ghost fluid/two-phase level set method for curvilinear body-fitted grids," International Journal Numerical Methods Fluids, Vol. 55, Issue 9, November 2007, pp. 867-897.

Huang, J., Carrica, P., Stern, F., "Numerical Study of a Ship Exhaust Plume with Waves and Wind," International Journal Numerical Methods Fluids, Vol. 68, Issue 2, January 2012a, pp. 160-180.

Huang, J., Carrica, P. M. and Stern, F. A geometry-based level set method for curvilinear overset grids with application to ship hydrodynamics. International Journal Numerical Methods Fluids, Vol. 68, 2012b, pp. 494-521.

Hunt, J.C.R., Wray, A. A., Moin, P. "Eddies, streams, and convergence zones in turbulent flows, in: Its Studying Turbulence Using Numerical Simulation Databases", Vol. 2, Proceedings of the 1988 Summer Program (SEE N89-24538 18-34), 1988, pp. 193–208.

Iafrati, A., "Air-water interaction in breaking wave events: quantitative estimates of drops and bubbles," In: Proceedings of 28th Symposium on Naval Hydrodynamics, Pasadena, California, 12-17 September 2010.

Iafrati, A., Di Mascio, A., Campana, E. F., "A level set technique applied to unsteady free surface flows," International Journal for Numerical Method and Fluids, 35, 2001, 281-297.

Ismail, F., Carrica, P.M., Xing, T., Stern, F., 2010, "Evaluation of linear and nonlinear convection schemes on multidimensional non-orthogonal grids with applications to KVLCC2 tanker," Int. J. Numer. Meth. Fluids, Vol. 64, pp. 850–886.

ITTC 2011, The specialist Committee on computational fluid dynamics, Proceedings of 26th International Towing Tank Conference, Rio de Janeiro, Brazil, 28 August – 3 September, 2011.

Jacquin, E., Guillerm, P.E., Drouet, A., Perdon, P., and Alessandrini, B., 2006, "Simulation of unsteady ship maneuvering using free-surface RANS solver," 26th Symposium on Naval Hydrodynamics, Rome, Italy.

Jemison, M., Loch, E., Sussman, M., Shashkov, M., Arienti, M., Ohta, M., Wang, Y., "A Coupled Level Set-Moment of Fluid Method for Incompressible Two-Phase Flows," Journal of Scientific Computing, in press, 2012, 10.1007/s10915-012-9614-7.

Jeong, J. Hussain, F., "On the identification of a vortex", Journal of Fluid Mechanics, Vol. 285, 1995, pp. 69–94.

Jiang, G.-S. and Peng, D., "Weighted ENO schemes for Hamilton-Jacobi equations", SIAM J. Sci. Comp., Vol. 21, 2000, pp. 2126-2143.

Jiang, G.-S. and Shu, C.-W., "Efficient implementation of weighted ENO schemes", J. Comput. Phys., Vol. 126, 1996, pp. 202-228.

Jimenez, J. "Turbulent Flows over Rough Walls," Annual Review of Fluid Mechanics, Vol. 36, 2004, pp. 173-196.

Kalitzin, G., Medic, G., Iaccarino, G., Durbin, P. "Near-wall behavior of RANS turbulence models and implications for wall functions," Journal of Computational Physics, Vol. 204, 2005, pp. 265-291.

Kandasamy, M., He, W., Takai, T., Tahara, Y., Peri, D., Campana, E., Wilson, W., and Stern, F., "Optimization of Waterjet Propelled High Speed Ships -Jhss and Delft Catamatran," 11th International Conference on Fast Sea Transportation, FAST 2011, Honolulu, Ha wa ii, USA, September 2011.

Kandasamy, M., Ooi, S.K., Carrica, P., & Stern, F., "Integral force/moment water-jet model for CFD simulations," Journal of Fluids Engineering, 132, 2010, 101103-1 - 9.

Kandasamy, M., Xing, T., Stern, F., "Unsteady Free-Surface Wave-Induced Separation: Vortical Structures and Instabilities", Journal of Fluids and Structures, Vol. 25, Issue 2, 2009, pp. 343-363.

Kang, D.H., Longo, J., Marquardt, M., and Stern, F., "Solid/free-surface juncture boundary layer and wake with waves", Proc. 27th ONR Symposium on Naval Hydrodynamics, Seoul, Korea, 2008.

Kang, D., Ghosh, S., Reins, G., Koo, B., Wang, Z., and Stern, F., "Impulsive plunging wave breaking downstream of a bump in a shallow water flume—Part I: Experimental observations," Journal of Fluids and Structures, Vol. 32, 2012, pp. 104-120.

Karion, A., Fu, T. C., Sur, T.W., Rice, J.R., Walker, D.C. and Furey, D.A., "Experiment to examine the effect of scale on a breaking bow wave", Carderock Division, Naval Surface Warfare Center, Hydromechanics Research and Development report, 2004, NSWCCD-50-T R-2004/060.

Karman, Jr., S.L., and Wilson, R., 2008, "Hierarchical Unstructured Mesh Generation with General Cutting for Free Surface Simulations," Proceedings of the 27th ONR Symposium on Naval Hydrodynamics, Seoul, Korea, 5-10 Oct. 2008.

Kassinos, S. C., Langer, C. A., Kalitzin, G. Iaccarino, G., "A simplified structure-based model using standard turbulence scale equations: computation of rotating wall-bounded flows," International Journal of Heat and Fluid Flow, Vol. 27(4), 2006, pp. 653–660.

Kaushik, D., Balay, S. Keyes, D., Smith, B., "Understanding the Performance of Hybrid MPI/OpenMP programming Model for Implicit CFD Codes," 21st Parallel CFD Conference, May 18-22, Moffett Field, California, USA, 2009, pp. 174-177.

Kerwin, J.E., Lee, C.S., "Prediction of Steday and Unsteady Marine Propeller Performance by Numerical Lifting-Surface Theory", SNAME Transactions, Vol. 86, 1978, pp.218-253.

Kim, D, Moin, P., "Direct numerical study of air layer drag reduction phenomenon over a backward-facing step," Center for Turbulence Research, Annual Research Briefs, 2010, pp. 351-363.

Kim, S.-E., Choudhury D., "A near-wall treatment using wall functions sensitized to pressure gradient, Separated and Complex Flows," ASME, FED-Vol. 217, 1995, 273-280.

Kimmoun, O. and Branger, H., "A particle image velocimetry investigation on laboratory surf-zone breaking waves over a sloping beach," Journal of Fluid Mechanics, 588, 2007, pp. 353-397.

Knupp, P. M., and Salari, K., Verification of computer codes in computational science and engineering, CRC Press, 2003.

Koo, B., Wang, Z., Yang, J., and Stern, F., "Impulsive plunging wave breaking downstream of a bump in a shallow water flume—Part II: Numerical simulations," Journal of Fluids and Structures, Vol. 32, 2012, pp. 121-134.

Kraichnan, R.H. "Eddy viscosity in two and three dimensions," J. Atmos. Sci., Vol. 33, 1976, pp. 1521–1536.

Kremenetsky, M. and Kodiyalam, S., "Parallel Performance of CFD Algorithm and the Ubiquitous Need for HPC with High Fidelity, Multidisciplinary Analysis and Optimization (MDO)." 21st Parallel CFD Conference, May 18-22, Moffett Field, California, USA, 2009, pp .338-342.

Larsson, L. Stern F. Visonneau, M (Editors), Proceedings of G2010 Workshop on Numerical Ship Hydrodynamics, 2010.

Larsson, L., and Zou, L., 2010, "CHAPTER 2 - Evaluation of Resistance, Sinkage and Trim, Self Propulsion and Wave Pattern Predictions," Gothenburg 2010 workshop on CFD in Ship Hydrodynamics.

Larsson, L., Stern, F., and M. Visonneau, "CFD in Ship Hydrodynamics – Results of the Gothenburg 2010 Workshop," Proc. IV International Conference on Computational Methods in Marine Engineering, 28-30 September 2011, Lisbon, Portugal.

Lentine, M., Grétarsson, J.T., Fedkiw, R., "An unconditionally stable fully conservative semi-Lagrangian method," Journal of Computational Physics, Vol. 230, Issue 8, 2011, pp. 2857-2879.

Leonard, B. P., "A stable and accurate modelling procedure based on quadratic interpolation", Comput. Methods Appl. Mech. Engrg., Vol. 19, 1979, pp. 58-98

Li, T., and Matusiak, J., "Simulation of a modern surface ship with a wetted transom in a viscous flow," Proc. of the 11th International Offshore and Polar Engineering Conference, Stavanger, Norway, June 17-22, 2001, pp. 570-576.

Lilly, D. K., 1992. "A proposed modification of the Germano subgrid-scale closure method," Physics of Fluids A, Vol. 4, 1992, pp. 633-635.

Lin, S. P., Reitz, R. D., Drop and spray formation from a liquid jet, Annual Review of Fluid Mechanics, Vol. 30, 1998, pp. 85-105.

Liovic, P., Lakehal, D., "Multi-physics treatment in the vicinity of arbitrarily deformable gas–liquid interfaces," J. Comput. Phys., 222, 2007, pp. 504–535.

Liu, S., Kermani, A., Shen, L. and Yue, D., "Investigation of coupled air-water turbulent boundary layers using direct numerical simulations," Phys. Fluids, 21, 2009, 062108.

Logan, R. W. and Nitta, C.K., "Comparing 10 Methods for Solution Verification, and Linking to Model Validation," Journal of Aerospace Computing, Information, and Communication, 3(7), pp. 354-373, 2006.

Longo, J., Huang, H.P., and Stern, F., "Solid-fluid juncture boundary layer and wake", Experiments in Fluids, Vol. 25(4), 1998, pp. 283-297.

Longo, J., Shao, J., Irvine, M., and Stern, F., "Phase-averaged PIV for the nominal wake of a surface ship in regular head waves", J. Fluids Eng., Vol.129, 2007, pp.524-540.

Longuet-Higgins, M., "On the Disintegration of the Jet in a Plunging Breaker", Journal of Physical Oceanography, Vol. 25, 1995, pp. 2458–2462.

Lubin, P., Vincent, S., Abadie, S., Caltagirone, J. P., "Three-dimensional large eddy simulation of air entrainment under plunging breaking waves," Coastal Engineering, 53, 2006, pp.631-655.

Lübke, L.O., "Numerical Simulation of the Flow around the Propelled KCS", Proc. CFD Workshop Tokyo 2005, Tokyo, Japan.

Marcum, D. L., "Generation of Unstructured Grids for Viscous Flow Applications," AIAA Paper 95-0212, 1995.

Marrone, S., Colagrossi, A., Antuono, M., Lugni, C., and Tulin, M.P., "A 2D + t SPH model to study the breaking wave pattern generated by fast ships," Journal of Fluids and Structures, 27, 2011, pp. 1199-1215.

Mattor, N., Williams, T.J., and Hewett, D.W., "Algorithm for solving tridiagonal matrix problems in parallel," Parallel Comput., Vol. 21, 1995, pp. 1769-1782.

Melville, W. K., "Energy dissipation by breaking waves," Journal of Physical Oceanography, 24, 1994, 2041-2049.

Melville, W. K., Veron, F. and White, C. J., "The velocity field under breaking waves: coherent structures and turbulence," Journal of Fluid Mechanics, 454, 2002, pp. 203-233.

Meneveau, C., Katz, J., "Scale-invariance and turbulence models for large-eddy simulations," Annual Review of Fluid Mechanics, Vol. 32, 2000, pp. 1–32.

Menter, F. R. Egorov, Y., 2010. "The scale-adaptive simulation method for unsteady turbulent flow predictions. Part 1: Theory and model description" Flow, Turbulence and Combustion, Vol. 85, 2010, pp. 113-127..

Menter, F.R. Two-Equation Eddy-Viscosity Turbulence Models for Engineering Applications. AIAA Journal, Vol. 32 (8), 1994, pp. 1598-1605.

Merkle, C., and Deutsch, S., "Microbubble Drag Reduction in Liquid Turbulent Boundary Layers," Appl. Mech. Rev., Vol. 45, No. 3, 1992, pp. 103-127.

Metcalf, B., Longo, J., Ghosh, S., Stern, F., "Unsteady free-surface wave-induced boundary-layer separation for a surface-piercing NACA 0024 foil: towing tank experiments", J. Fluids Struct., Vol. 22, 2006, pp. 77-98.

Min, C., Gibou, F., "A second order accurate level set method on non-graded adaptive Cartesian grids," Journal of Computational Physics, Vol. 225, Issue 1, 2007, pp.300-321.

Min, C., Gibou, F., "A second order accurate projection method for the incompressible Navier–Stokes equations on non-graded adaptive grids," Journal of Computational Physics, Vol. 219, Issue 2, 2006, pp. 912-929.

Miyata, H. and Inui, T., "Nonlinear ship waves," Advances in Applied Mechanics, 24, 1984, pp. 215-288.

Miyata, H., Matsukawa, C., and Kajitani, H., "Shallow water flow with separation and breaking wave," Autumn meeting of Naval Architecture, 1985a, Japan.

Miyata, H., Nishimura, S., Masuko, A., "Finite difference simulation of nonlinear waves generated by ships of arbitrary three-dimensional configuration," Journal of Computational Physics, Vol. 60, Issue 3, 1985b, pp. 391-436.

Mousaviraad, S.M., Carrica, P.M., Huang, J., and Stern, F., "CFD Prediction of Ship Response to Severe Ocean Waves and Wind", 27th Symposium on Naval Hydrodynamics, Seoul, South Korea, 2008.

Mousaviraad, S.M., Carrica, P.M., and Stern, F., "Development and Validation of Harmonic Wave Group Single-Run Procedures for RAO with Comparison to Regular and Transient Wave Group Procedures Using URANS," Ocean Engineering, Vol. 37, Issues 8-9, June 2010, pp.653-666.

Mousaviraad, S.M., "CFD prediction of ship response to extreme winds and/or waves," PhD diss., University of Iowa, 2010.

Mousaviraad, S.M., Sadat-Hosseini, S.H., Carrica, P.M., Stern, F., "URANS Studies of Ship-Ship Interactions in Calm Water and Waves for Replenishment and Overtaking Conditions", Second International Conference on Ship Maneuvering in Shallow and Confined Water: Ship-to-Ship Interaction, Trondheim, Norway, 18-20 May 2011.

Mousaviraad, S.M., Bhushan, S., Stern, F., "CFD prediction of free-running SES/ACV deep and shallow water maneuvering in calm water and waves", Proceeding of MARSIM2012, 2012a.

Mousaviraad, S.M., Cook, S.S., Carrica, P.M., Toda, Y., Stern, F., "Complimentary EFD and CFD on Effects of Headwinds on Towing Tank Resistance and PMM Tests for ONR Tumblehome," 29th Symposium on Naval Hydrodynamics, 2012b, Gothenburg, Sweden.

Muscari, R., Broglia, R., Di Mascio, A, "Trajectory prediction of a self-propelled hull by unsteady RANS computations", 27th Symposium on Naval Hydrodynamics, Seoul, Korea, 2008a.

Muscari, R., Broglia, R., Di Mascio, A, "ANALYSIS OF THE FLOW AROUND A MANOEUVRING VLCC", Proceedings of the ASME 27th International Conference on Offshore Mechanics and Arctic Engineering, Estoril, Portugal, 2008b.

Muscari R., Felli M., Di Mascio A., "Numerical and experimental analysis of the flow around a propeller behind a fully appended hull", 28th Symposium on Naval Hydrodynamics, Pasadena, California, 2010.

Noack, R.W. "SUGGAR: a general capability for moving body overset grid assembly," 17th AIAA Computational Fluid Dynamics Conference, 2006, Toronto, Ontario, Canada.

Noblesse, F., Delhommeau G., Guilbaud, M., Hendrix, D., Yang, C., "Simple analytical relations for ship bow waves," Journal of Fluid Mechanics, Vol. 600, 2008, pp. 105-132.

Oberkampf, W. L. and C. J. Roy. Verification and Validation in Scientific Computing, Cambridge Univ Pr., 2010.

Oh, K.J., Kang, S.H., "Full Scale Reynolds Number Effects for the Viscous Flow around the Ship Stern," Computational Mechanics, Vol. 9, 1992, pp. 85-94.

Oger, G., Doring, M., Alessandrini, B., Ferrant, P., "Two-dimensional SPH simulations of wedge water entries," Journal of Computational Physics, Vol. 213, Issue 2, 2006, pp. 803-822.

Olivieri, A., Pistani, F., Wilson, R., Campana, E., and Stern, F., "Scars and vortices induced by ship bow wave breaking", J. Fluids Eng., Vol. 129, 2007, pp. 1445-1459.

Olsson, E., Kreiss, G., "A conservative level set method for two phase flow," Journal of Computational Physics, Vol. 210, Issue 1, 2005, pp. 225-246.

Orihara, H. and Miyata, H., "A Numerical Method for Arbitrary Ship Motions in Arbitrary Wave Conditions using Overlapping Grid System," Proceedings of the 8th International Conference on Numerical Ship Hydrodynamics, Busan, KOREA, 2003.

Park I. R. and Chun H. H., "A Study on the Level-Set Scheme for the Analysis of the Free Surface Flow by a Finite Volume Method", Journal of the Society of Naval Architects of Korea, 36, No. 2, (1999), pp.40-49.

Patel, V. C., "Perspective: Flow at high Reynolds number and over Rough surfaces- Achilles Heel of CFD," Journal of Fluids Engineering, Vol. 120, 1998, pp. 434-444.

Paterson, E.G., Wilson, R.V., and Stern, F., "General-Purpose Parallel Unsteady RANS Ship Hydrodynamics Code: CFDSHIP-IOWA," Iowa Institute of Hydraulic Research, The University of Iowa, IIHR Report No.432, November 2003, 105 pp.

Peng, D., Merriman, B., Osher, S., Zhao, H., and Kang, M., "A PDE-based fast local level set method", J. Comput. Phys, Vol. 155, 1999, pp. 410-438.

Peregrine, D. H., "Breaking Waves on Beaches", Ann. Rev. of Fluid Mech., Vol. 15, 1983, pp. 149-178.

Phillips, A.B., Turnock, S.R., and Furlong, B., 2009, "Evaluation of manoeuvring coefficients of a self-propelled ship using a blade element momentum propeller model coupled to a Reynolds averaged Navier Stokes flow solver," Ocean Engineering, Vol. 36, pp. 12 17–1225.

Piomelli, U., Balaras, E., "Wall-layer models for large-eddy simulations," Ann. Rev. Fluid Mech., Vol. 34, 2002, pp. 349–374 .

Piomelli, U., Balaras, E., Pasinato, H., Squaires, K.D., Spalart, P.R., "The inner-outer layer interface in large-eddy simulations with wall-layer models," Int. J. Heat Fluid Flow, Vol. 24, 2003, pp. 538–550.

Pope S. B., "Turbulent Flows," Cambridge University Press: Cambridge, MA, 2000.

Pope, S. B., "The calculation of turbulent recirculating flows in general orthogonal coordinates", J. Comput. Phys., Vol. 26, 1978, pp. 197-217.

Posa, A., Lippolis, A., Verzicco, R., Balaras, E., "Large-eddy simulations in mixed-flow pumps using an immersed-boundary method," Computers & Fluids, Vol. 47, Issue 1, 2011, pp. 33-43.

Qiu, J.-M., Shu, C.-W., "Conservative high order semi-Lagrangian finite difference WENO methods for advection in incompressible flow," Journal of Computational Physics, Vol. 230, Issue 4, 2011, pp. 863-889.

Queutey P, Visonneau M., "An interface capturing method for free-surface hydrodynamic flows," Computers & Fluids, Vol. 36(9), 2007, pp. 1481–1510.

Rabenseifner, R., Wellein, G., "Communication and Optimization Aspects of Parallel Programming Models on Hybrid Architectures," The International Journal of High Performance Computing Applications, Vol. 17(1), 2003, pp. 49-62.

Rhee S.H., Stern F., "RANS model for spilling breaking waves," J Fluid Eng, Vol. 124, 2002.

Ripley, M. D., and Pauley, L. L., "The unsteady structure around a surface piercing strut," Physics of Fluids A, **5**(12), 1993, pp. 3099-3106.

Roache, P. J., "Verification and Validation in Computational Science and Engineering," Hermosa Publishers, New Mexico, 1998.

Roache, P. J., "Code Verification by the Method of Manufactured Solutions," Journal of Fluids Engineering, 124(1), 2002, pp. 4-10.

Roache, P. J.. "Discussion:"Factors of Safety for Richardson Extrapolation"(Xing, T., and Stern, F., 2010, ASME J. Fluids Eng., 132, p. 061403)." Journal of Fluids Engineering **133**, 2011, p. 115501.

Robinson-Mosher, A., Schroeder, C., Fedkiw, R., "A symmetric positive definite formulation for monolithic fluid structure interaction," Journal of Computational Physics, Volume 230, Issue 4, 2011, pp. 1547-1566.

Rosenfeld, M., Kwak, D., Vinokur, M., "A Fractional Step Solution Method for the Unsteady Incompressible Navier-Stokes Equations in Generalized Coordinate Systems," J. Comp. Phys., Vol. 94, 1991, pp. 102-137.

Rumsey, C. L., and Thomas, J. L., "Application of FUN3D and CFL3D to the Third Workshop on CFD Uncertainty Analysis," NASA Report No. TM-2008-215537, 2008.

Rung, T., Wöckner, K., Manzke, M., Brunswig, J., Ulrich, C., Stück, A., Challenges and perspectives for maritime CFD applications. Jahrbuch der Schiffbautechnischen Gesellschaft, 103. Band; 2009.

Sadat-Hosseini, H., Stern, F., Olivieri, A., Campana, E., Hashimoto, H., Umeda, N., Bulian, G., Francescutto, A., "HEAD-WAVES PARAMETRIC ROLLING", Ocean Engineering, Vol. 37, Issue 10, 2010, Pages 859-878.

Sadat-Hosseini, H., Araki M., Umeda N., Sano M., Yeo D. J., Toda Y., Stern F., "CFD, system-based method, and EFD investigation of ONR tumble-home instability and capsize with evaluation of the mathematical model", 12th International Ship Stability Workshop, 2011a, pp.135-145.

Sadat-Hosseini, H., Carrica, P., Stern, F., Umeda, N., Hashimoto, H., Matsuda, A., "CFD, System-Based and EFD Study of Ship Dynamic Instability Events: Surf-riding, Periodic Motion, and Broaching," Ocean Engineering, Vol. 38, Issue 1, January 2011b, pp. 88-110.

Sadat-Hosseini, H., Stern F., Toxopeus S., Visonneauc M., Guilmineau E., Lin W.M., and Grigoropoulos G., "CFD, potential flow, and system-based simulations of course keeping in calm water and seakeeping in regular waves for 5415m", 2012a, In preparation to Ocean Engineering.

Sadat-Hosseini, H., Stern F., Toxopeus S., "CFD simulations of course keeping in irregular waves for 5415M", Report No. 3, 2012b.

Sadat-Hosseini, H., Kim, D.H, Lee, S.K., Rhee, S.H., Carrica, P., Stern, F., "CFD and EFD study of Damaged Ship Stability in Regular Waves", Proceedings of the 11th International Conference on the Stability of Ships and Ocean Vehicles, 23-28 September 2012c, Athens, Greece.

Sadat-Hosseini, H., Wu P.C., Carrica P., Kim H., Toda Y., Stern F., "CFD Simulation and Validation of Added Resistance of KVLCC2 with Fixed and Free Surge Conditions in Short and Long Head Waves", 2012d, Under review, Ocean Engineering.

Sagaut, P. and Deck, S., "Large eddy simulation for aerodynamics: status and perspectives," Phil. Trans. R. Soc. A., Vol. 367, 2009, pp. 2849.

Sakamoto, N., Carrica, P.M., and Stern, F., (2012), "URANS Simulation of Static and Dynamic Maneuvering for Surface Combatant: Part1-Verification and Validation of Forces, Moment and Hydrodynamic Derivatives", Journal of Marine Science and Technology, in press.

Sanders, W.C., Winkel, E.S., Dowling, D.R., Perlin, M., and Ceccio, S.L., "Bubble Friction Drag Reduction in a High-Reynolds-Number Flat-Plate Turbulent Boundary Layer," J. Fluid Mech., Vol 552, 2006, pp. 353-380.

Sanada, Y., Tanimoto, K., Sano, M., Yeo, D-J, Gui, L., Toda, Y., and Stern, F., "Trajectories and Local Flow Field Measurements around ONRTH in Maneuvering Motions," Proceedings 29th Symposium Naval Hydrodynamics, Gothenburg, Sweden, 26-31 August 2012.

Sato Y, Miyata H, Sato T, "CFD Simulation of 3D Motion of a Ship in Waves: Application to an Advancing Ship in Regular Heading Waves," J. Marine Sci. Tech. Vol. 4, 1999, pp. 108-116.

Schumann, U. "Stochastic backscatter of turbulence energy and scalar variance by random subgrid-scale fluxes," Proc. R. Soc. Lond. A, Vol. 451, 1995, pp. 293–318.

Shakeri, M., Tavakolinejad, M., and Duncan, J. H., "An experimental investigation of divergent bow waves simulated by a two-dimensional plus temporal wave marker technique," Journal of Fluid Mechanics, 634, 2009, pp. 217-243.

Shalf, J. "Hardware Trends," Panel discussion presentation in 21st Parallel CFD Conference, May 18-22, Moffett Field, California, USA, 2009.

Shibata, K. Koshizuka, S., Tanizawa, K., "Three-dimensional numerical analysis of shipping water onto a moving ship using a particle method," J. Marine Sci. Tech., Vol. 14(2), 2009, pp. 214-227.

Shirani E, Jafari A, Ashgriz N, "Turbulence models for flows with free surfaces and interfaces", AIAA Journal, Vol. 44(7), 2006, pp. 1454-1462.

Shu, C. W. and Osher, S., "Efficient implementation of essentially non-oscillatory shock-capturing schemes," J. Comp. Phys., Vol. 77, 1988, pp. 439-471.

Shur, M., Spalart, P. R., Strelets, M. Kh., Travin, A. 2008. "A hybrid RANS-LES approach with delayed-DES and wall-modeled LES capabilities," International Journal of Heat and Fluid Flow, Vol. 29, 2008, pp. 1638.

Sigurdson, L. W., 1995, "The structure and control of turbulent reattaching flow," Journal of Fluid Mechanics, **248**, pp. 139-165.

Simpson, R. L., 2001, "Junction flows," Annual Review of Fluid Mechanics, **33**, pp. 415-443.

Simonsen, C., and Stern, F., 2010, "CFD Simulation of KCS Sailing in Regular Head Waves," Proceedings of Gothenburg 2010 workshop, Report No. R-10:122, pp. 473-478, Chalmers University of Technology, Sweden.

Simonsen, C., and Stern, F., 2005, "RANS Maneuvering Simulation of Esso Osaka With Rudder and a Body-Force Propeller," Journal of Ship Research, Vol. 49, No. 2, 2005, pp. 98-120.

So, R.M.C. and Lai, Y.G., "Low-Reynolds-number modelling of flows over a backward-facing step," Journal of Applied Mathematics and Physics, Vol. 39, 1988, pp. 13-27.

Spalart, P. R., "Detached-Eddy Simulation," Annual Review of Fluid Mechanics, Vol. 41, 2009, pp. 181.

Spalart, P. R., Allmaras, S. R., "A One-Equation Turbulence Model for Aerodynamic Flows," AIAA Paper 92-0439, 1992.

Sreedhar, M. and Stern, F., "Large Eddy Simulation of Temporally Developing Juncture Flows," International Journal of Numerical Methods in Fluids, Vol. 28, No. 1, 1998a, pp. 47-72.

Sreedhar, M. and Stern, F., "Prediction of Solid/Free-Surface Juncture Boundary Layer and Wake of a Surface-Piercing Flat Plate at Low Froude Number," ASME Journal of Fluids Engineering, Vol. 120, 1998b, pp. 354-362.

Starke, B, van der Ploeg, A. Raven?H, "Viscous free surface flow computations for self-propulsion conditions using PARNASSOS", Proc. of G2010 Workshop, 2010.

Stern, F., "Effects of Waves on the Boundary Layer of a Surface-Piercing Body," Journal of Ship Research, Vol. 30, No. 4, 1986, pp. 256-274.

Stern, F., Yoo, S.Y., and Patel, V.C., "Interactive and Large-Domain Solutions of Higher-Order Viscous-Flow Equations," AIAA Journal, Vol. 26, No. 9, September 1988a, pp. 1052-1060, IIHR Reprint #753.

Stern, F., Kim, H.T., Patel, C., Chen, H.C., "A viscous-flow approach to the computation of propeller-hull interaction", Journal of Ship Research, vol. 32, no. 4, 1988b.

Stern, F., Hwang, W.S., and Jaw, S.Y., "Effects of Waves on the Boundary Layer of a Surface-Piercing Flat Plate: Experiment and Theory," Journal of Ship Research, Vol. 33, No. 1, 1989, pp. 63-80.

Stern, F., Choi, J.E., and Hwang, W.S., "Effects of Waves on the Wake of a Surface-Piercing Flat Plate: Experiment and Theory," Journal of Ship Research, Vol. 37, No. 2, 1993, pp. 102-118.

Stern, F., Kim, H.T., Zhang, D.H., Toda, Y., Kerwin, J., and Jessup, S., "Computation of Viscous Flow Around Propeller-Body Configurations: Series 60 CB = 0.6 Ship Model," Journal of Ship Research, Vol. 38, No. 2, 1994, pp. 137-157.

Stern, F., Longo, J., Zhang, Z.J., and A.K. Subramani, "Detailed bow-flow data and CFD of a Series 60 CB = .6 ship model for Froude number .316", J. Ship Res., Vol. 40, 1996, pp. 193-199.

Stern, F., Wilson, R. V., Coleman, H. W., and Paterson, E. G., 2001, "Comprehensive Approach to Verification and Validation of CFD Simulations—Part 1: Methodology and Procedures," Journal of Fluids Engineering, 123(4), pp. 793-802.

Stern, F., Wilson, R., Longo, J., Carrica, P., Xing, T., Tahara, Y., Simonsen, C., Kim, J., Shao, J., Irvine, M., Kandasamy, K., Gosh, S., and Weymouth, G., "Paradigm for Development of Simulation Based Design for Naval Hydrodynamics," 8th International Conference on Numerical Ship Hydrodynamics, September 22-25, 2003, Busan, Korea.

Stern, F., Wilson, R., Shao, J., "Quantitative approach to V&V of CFD Simulations and Certification of CFD Codes," Int. J. Numer. Methods Fluids, Vol. 50, 2006a, pp. 1335–135.

Stern, F., Xing, T., Muste, M., Yarbrough, D., Rothmayer, A., Rajagopalan, G., Caughey, D., Bhaskaran, R. Smith. S., Hutching, B., and Moeykens, S., "Integration of Simulation Technology into Undergraduate Engineering Courses and Laboratories," International Journal Learning Technology, Vol. 2, No. 1, January 2006b, pp. 28-48.

Stern, F., Carrica, P., Kandasamy, M., Gorski, J., O'Dea, J., Hughes, M., Miller, R., Kring, D., Milewski, W., Hoffman, R., and Cary, C., 2007, "Computational Hydrodynamic Tools for High-Speed Sealift," Transactions of The Society of Naval Architects and Marine Engineers, 114, pp. 55–81.

Stern, F., Bhushan, S., Carrica, P., Yang, J., "Large Scale Parallel Computing and Scalability Study for Surface Combatant Static Maneuver and Straight Ahead Conditions using CFDShip-Iowa," 21st Parallel CFD Conference, May 18-22, Moffett Field, California, USA, 2009, pp. 52-56.

Stern, F., Sadat-Hosseini, H., Mousaviraad, M., Bhushan, S., "CHAPTER 4 - Evaluation of Seakeeping Predictions," Gothenburg 2010 workshop on CFD in Ship Hydrodynamics, 2010.

Stern, F., Agdrup, K., Kim, S.Y., Hochbaum, A.C., Rhee, K.P., Quadvlieg, F., Perdon, P., Hino, T., Broglia, R., and Gorski, J., "Experience from SIMMAN 2008—The First Workshop on Verification and Validation of Ship Maneuvering Simulation Methods," Journal of Ship Research, Vol. 55, No. 2, 2011a, pp. 135-147.

Stern, F., Toxopeus, S., Visonneau, M., Guilmineau, E., Lin, W.M., Grigoropoulos, G., "CFD, Potential Flow, and System-Based Simulations of Course Keeping in Calm Water and Seakeeping in Regular Waves for 5415M", AVT-189 Specialists' Meeting, Portsdown West, UK, 2011b.

Stern, F., Yoon, H., Yarbrough, D., Okay, M., Oztekin, U., and Roszelle, B., "Hands-On Integrated CFD Educational Interface for Introductory Fluids Mechanics: Invited Paper," International Journal Aerodynamics, 2012, in press.

Strasser, C., Jasionowski, A. and Vassalos, D., "Calculation of the Time-to-Flood of a Box-Shaped Barge using CFD", Proc. 10th Int'l Conf. Stability of Ships & Ocean Vehicles, St. Petersburg, Russia, 2009, pp. 733–740.

Suh, J., Yang, J., and Stern, F., "The effect of air-water interface on the vortex shedding from a vertical circular cylinder," Journal of Fluids and Structures, Vol. 27, No. 1, 2011, pp. 1-22.

Sussman, M., "A parallelized, adaptive algorithm for multiphase flows in general geometries," Comp. Struct., Vol. 83, 2005, pp. 435-444.

Sussman, M., Dommermuth, D., "The numerical simulation of ship waves using Cartesian grid methods," in: Proc. 23rd Symposium on Naval Hydrodynamics, Val De Reuil, France, 2000.

Sussman, M., Puckett, E.G., "A Coupled Level Set and Volume-of-Fluid Method for Computing 3D and Axisymmetric Incompressible Two-Phase Flows," Journal of Computational Physics, Vol. 162, Issue 2, 2000, pp. 301-337.

Sussman, M., Smereka, P. and Osher, S., "A level set approach for computing solutions to incompressible two-phase flow," J. Comp. Phys., Vol. 114, 1994, pp. 146-159.

Tahara, Y., Stern, F., and Rosen, B., "An Interactive Approach for Calculating Ship Boundary Layers and Wakes for Nonzero Froude Number," Journal of Computational Physics, Vol. 98, No. 1, January 1992, pp. 33-53, IIHR Reprint #892.

Tahara, Y. and Stern, F., "Large-Domain Approach for Calculating Ship Boundary Layers and Wakes and Wave Fields for Nonzero Froude Number," Journal Computational Physics, Vol. 127, No. 2, September 1996, pp. 398-411, IIHR Reprint #1210.

Tahara, Y., Katsuui, T., Himemno, Y. 2002 Computation of ship Viscous flow at full scale Reynolds number, Journal of the Soc. Naval Architects of Japan, Vol. 92, 2002, pp. 89-101.

Tahara, Y., Wilson, R Carrica, P., "Comparison of Free-Surface Capturing and Tracking Approaches in Application to Modern Container Ship and Prognosis for Extension to Self-Propulsion Simulator", Proc. of CFD Workshop Tokyo 2005, Tokyo, Japan.

Takai, T., Kandasamy, M. and Stern, F., 2011, " Verification and validation study of URANS simulations for an axial waterjet propelled large high-speed ship," Journal of Marine Science and Technology, 2011, Volume 16, Issue 4, pp 434-447.

Tallent, J. R., Yamashita, T., and Tsuchiya, Y., "Transformation Characteristics of Breaking Waves", Wave Water Kinematics, Vol. 178, 1990, pp. 509-523.

Temmerman, L., Leschziner, M. A., Hadziabdic, M., Hanjalic, K., "A Hybrid Two-Layer URANS-LES Approach for Large-Eddy Simulation at High Reynolds Numbers," Int. J. Heat Fluid Flow, Vol. 26, 2005, pp. 173–190.

Thompson, J. F.; Warsi, Z. U. A., Mastin, C. W. "Numerical Grid Generation: Foundations and Applications," North-Holland, Elsevier, 1985.

Toutant, A., Chandesris, M., Jamet, D., Lebaigue, O., "Jump conditions for filtered quantities at an under-resolved discontinuous interface Part 1: theoretical development," Int. J. Multiphase Flow, 35 (12), 2009, pp. 1100-1118

Toxopeus, S., 2009, "Deriving mathematical manoeuvring models for bare ship hulls using viscous flow calculations," J. Mar Sci Technol, Vol. 14, pp. 30–38.

von Kerczek, C.H., Christoph, G., and Stern, F., "Further Developments of the Momentum Integral Method for Ship Boundary Layers," SAI Report #8413046, May 1984, 38 pp.

Wackers, J., Koren, B., Raven,.H.C..van der Ploeg, A, Starke, A.R. Deng, G.B., Queutey, P., Visonneau, M, Hino, T. Ohashi K., 2011 "Free-Surface Viscous Flow Solution Methods for Ship Hydrodynamics," Archives of Computational Methods in Engineering, Vol. 18(1), 2011, pp. 1-41.

Wackers, J., Deng G., Leroyer, A., Queutey, P., Visonneau, M., Adaptive grid refinement for hydrodynamic flows, (2012) Computers and Fluids, 55 ,pp. 85-100.

Wallin, S., Johansson, A. V., "Modeling Streamline Curvature Effects in Explicit Algebraic Reynolds Stress Turbulence Models," International Journal

of Heat and Fluid Flow, Vol. 23, 2002, pp. 721–730.

Wang, Y., Simakhina, S., Sussman, M., "A hybrid level set-volume constraint method for incompressible two-phase flow," Journal of Computational Physics, Vol., 231, 2012, pp. 6438–6471.

Wang, Z., Yang, J., Stern, F., "An improved particle correction procedure for the particle level set method," Journal of Computational Physics, Vol. 228, Issue 16, 2009a, pp. 5819-5837.

Wang, Z., Yang, J., Koo, B., and Stern, F, "A coupled level set and volume-of-fluid method for sharp interface simulation of plunging breaking waves", Inter. J. Multiphase Flow, Vol. 35, 2009b, pp. 227-246.

Wang, Z., Yang, J., Stern, F., "URANS Study of Air-Layer Drag Reduction in a High-Reynolds-Number Flat-Plate Turbulent Boundary Layer", 40th Fluid Dynamics Conference and Exhibit 28, June - 1 July 2010a, Chicago, Illinois.

Wang, Z., Yang, J., Stern, F., "Numerical simulations of wave breakings around a wedge-shaped bow," 28th Symposium on Naval Hydrodynamics, Pasadena, California, September 12-17, 2010b.

Wang, Z., Suh, J., Yang, J., and Stern, F., "Sharp Interface LES of Breaking Waves by an Interface Piercing Body in Orthogonal Curvilinear Coordinates," 50th AIAA Paper, January 2012a.

Wang, Z., Yang, J., Stern, F., "A new volume-of-fluid method with a constructed distance function on general structured grids," Journal of Computational Physics, Vol. 231, Issue 9, 2012b, pp. 3703-3722.

Wang, Z., Yang, J., Stern, F., "A simple and conservative operator-splitting semi-Lagrangian volume-of-fluid advection scheme," Journal of Computational Physics, Vol. 231, Issue 15, 2012c, pp. 4981-4992.

Wang, Z., Yang, J., Stern, F., "Parallel LES of breaking wave over an immersed bump in orthogonal curvilinear coordinates," ParCFD 2012, 22-26 May, 2012d, Atlanta, US.

Wang, Z., Suh, J., Yang, J., Stern, F., "Sharp Interface Large-Eddy Simulation of Breaking Waves by an Interface Piercing Body in Orthogonal Curvilinear Coordinates", Journal of Computational Physics (in preparation), 2012e.

Wang, Z.J., Parthasarathy, V. "A fully automated Chimera methodology for multiple moving problems," International Journal for Numerical Methods in Fluids, Vol. 33, 2000, pp. 919-938.

Waniewski, T., "Air entrainment by bow waves", Doctoral dissertation, 1999, California Institute of Technology, Pasadena, California.

Waniewski, T.A., Brennen, C.E. and Raichlen, F., "Bow wave dynamics," J. Ship Res., Vol. 46, 2002, pp. 1–15.

Watanabe, Y. and Saeki, H., "Velocity field after wave breaking," International Journal for Numerical Method and Fluids, 39, 2002, pp.607-637.

Watanabe, Y., Saeki, H., Hosking, R., "Three-dimensional vortex structures under breaking waves," Journal of Fluid Mechanics, 545, 2005, pp.291-328.

Weymouth, G., Wilson, R., and Stern, F., 2005, "RANS CFD predictions of pitch and heave ship motions in head seas", Journal of Ship Research, Vol. 49, pp. 80–97.

Wilson, R., Carrica, P. and Stern, F., "Simulation of ship breaking bow waves and induced vortices and scars", Int. J. Num. Meth. Fluids, Vol. 54, 2007a, pp. 419-451.

Wilson, R.V., Nicholas, D.S., Mitchell, B., Karman, S.L., Betro, V.C., Hyams, D.G., Sreenivas, K., Taylor, L.K., Briley, W.R., and Whitfield, D.L., 2007b, "Simulation of a surface combatant with Dynamic Ship Maneuvers," 9th International Conference on Numerical Ship Hydrodynamics, Ann Arbor, Michigan.

Wilson, R., Shao, J., and Stern, F., 2004, "Discussion: Criticisms of the" Correction Factor" Verification Method," Journal of Fluids Engineering, 126, pp. 704-706.

Xing, T., Kandasamy, M., and Stern. F., "Unsteady Free-Surface Wave-Induced Separation: Analysis of Turbulent Structures Using Detached Eddy Simulation and Single-Phase Level Set," Journal of Turbulence, Vol. 8, No. 44, 2007, pp. 1-35.

Xing, T., Carrica, P., and Stern, F., 2008, "Computational Towing Tank Procedures for Single Run Curves of Resistance and Propulsion," ASME J. Fluids Eng., 130(2), pp. 1–14.

Xing, T., Carrica, P. M., Stern, F., "Large-scale RANS and DDES computations of KVLCC2 at drift angle 0 degree." Proceedings of Gothenburg 2010: A Workshop on CFD in Ship Hydrodynamics, Gothenburg, Sweden, 2010.

Xing, T. and Stern, F., "Factors of Safety for Richardson Extrapolation," ASME J. Fluids Eng, Vol. 132 (6), June 2010, pp.061403.

Xing, T., Carrica, P., Stern, F., 2011, "Developing Streamlined Version of CFDShip-Iowa-4.5," IIHR Technical Report No. 479.

Xing, T., and Stern, F., 2011, "Closure to "Discussion of 'Factors of Safety for Richardson Extrapolation'" (2011, ASME J. Fluids Eng., 133, p. 115501)," ASME Journal of Fluids Engineering, 133(11), p. 115502.

Xing, T. Bhushan, S., and Stern, F. "Vortical and Turbulent Structures for KVLCC2 at Drift Angle

0, 12, and 30 Degrees," in press, Ocean Engineering, 2012.

Xiu, D., Karniadakis, G.E., "A Semi-Lagrangian High-Order Method for Navier–Stokes Equations," Journal of Computational Physics, Vol. 172, Issue 2, 2001, pp. 658-684.

Yamazaki, R. 1"On the propulsion theory of ships on still water introduction", Memoirs of the Faculty of Engineering, Kyushu University, 27, 4, 1968.

Yang, J., Balaras, E., "An embedded-boundary formulation for large-eddy simulation of turbulent flows interacting with moving boundaries," Journal of Computational Physics, Vol. 215, Issue 1, 2006, pp. 12-40.

Yang, J. and Stern, F., "Large-eddy simulation of breaking waves using embedded-boundary/level-set method," In: 45th AIAA Aerospace Sciences Meeting and Exhibit, Reno, Nevada, USA, 2007, AIAA Paper 2007-1455.

Yang, J., Sakamoto, N., Wang, Z., Carrica, P.M. and Stern, F., "Two phase level-set/immersed-boundary Cartesian grid method for ship hydrodynamics", Proc. 9th Inter. Conf. Numer. Ship Hydrodynamics, Ann Arbor, Michigan, 2007.

Yang, J., Preidikman, S., and Balaras, E., "A strongly-coupled, embedded-boundary method for fluid-structure interactions of elastically mounted rigid bodies", J. Fluids Struct., Vol. 24, 2008a, pp. 167-182.

Yang, J., Bhushan, S., Suh, J., Wang, Z., Koo, B., Sakamoto, N., Xing, T., Stern, F., Large-eddy simulation of ship flows with wall-layer models on Cartesian grids, Proc. 27th Symposium on Naval Hydrodynamics, 2008b, Seoul, Korea

Yang, J. and Stern, F., "Sharp Interface Immersed-Boundary/Level-Set Method for Wave-Body Interaction," Journal of Computational Physics, Vol. 228, Issue 17, September 2009, pp. 6590-6616.

Yang, J., Wang, Z., Yeon, S-M, Koo, B., and Stern, F., "High-fidelity curvilinear-grid two-phase flow solvers for ship hydrodynamics," Proceedings 29th Symposium Naval Hydrodynamics, Gothenburg, Sweden, 26-31 August 2012.

Yang, J. and Stern, F., "A simple and efficient direct forcing immersed boundary framework for fluid–structure interactions," Journal of Computational Physics, Vol. 231, Issue 15, 2012, pp. 5029-5061.

Yao, A. F. and Wu, C. H., "Incipient breaking on unsteady waves on sheared currents," Physics of Fluids, 17, 2005, 082104-1–082104-10.

Zhang Z.-R., "Verification and validation for RANS simulation of KCS container ship without/with propeller", Journal of Hydrodynamics, 22(5), 2010, pages 932-939.

Zlatko Zlatev, Z., Milanov., E., Chotukova, V., Sakamoto, N. and Stern, F., 2009, "Combined model-scale EFD-CFD investigation of the maneuvering characteristics of a high speed catamaran," 10th International Conference on Fast Sea Transportation FAST 2009, Athens, Greece.

Table 1: Summary of instability studies available in the literature for canonical cases (shown by Grey shadow) and those performed using CFDShip-Iowa V4 for geometries of ship hydrodynamics interest.

Instability	Scaling Parameters Length (Velocity) scales	Geometry	Vortex	$St=fU/L$	Comments
Karman-like	Half wake width (Shear layer velocity)	Cylinders and backstep	Separation bubble	0.07 – 0.09	• Caused by the interaction of two opposite vortices initiated by shear layer instability • Free-surface reduces both *f* and *St* • Responsible for transom wave unsteadiness for wetted transom flow • Averaged St ~ 0.088 for ship flows, higher end of the canonical flow range
		Surface Piercing NACA 0024	Wave induced separation	0.0685±4.3%	
		Barehull Athena	Transom Vortex shedding	0.088 – 0.148	
		Appended Athena		0.103±4.4%	
		Transom-Model		0.075	
		Wigley Hull at β = 45° and 60°	Intersection of hull and tip vortices	0.08±4.2%	
		KVLCC2 at β = 30°	Leeward bow vortices	0.0735	
		Barehull 5415 at β=0°	Port and Starboard Sonar dome	NA	
		5415 with BK at β=20°	Leeward sonar dome separation	0.132	
Horseshoe	Obstacle Thickness (Freestream velocity)	Cylinder/airfoil junction with Flatplate	Horshoe vortex separation	0.17-0.28	• Associated with two vortex system and show dual peak spectra • St increases with obstacle angle of attack, and sweep angle
		Appended Athena	Rudder-Hull intersection	0.146±3.9%	
			Strut-Hull intersection	0.053±2%	
Shear-layer	Momentum thickness (Shear layer velocity)	Airfoils and Cylinders	Boundary layer separation	0.0056±2%	• Associated with boundary layer (BL) separation • St varies inversely with the non-dimensional adverse pressure gradient • St ~ 0.001 – 0.003 for ship flows are lower than those for canonical case
		Surface Piercing NACA 0024	Free-surface separation	0.00384±0.5%	
		Appended Athena	BL separation at strut-hull intersection	0.0067±3%	
		Wigley Hull at β =60°	BL separation at leeward keel	0.0003	
		KVLCC2 at β = 30°	BL separation at leeward bow	0.00101	
		Barehull 5415 at β=0°	Sonar dome separation	NA	
		5415 with BK at β=20°	Leeward Sonar dome separation	0.0016 – 0.0059	
Flapping	Reattachment length (Freestream velocity)	Cylinder, Backstep, Square Rib	Separation bubble	0.073 – 0.12	• Exhibits a periodic enlargement and shrinkage of recirculation region • St has wide range
		Surface Piercing NACA 0024	Free-surface separation bubble	0.28	
		Barehull Athena	Wake growth and decay	0.144	
Helical	Distance along vortex core (Freestream velocity)	Delta Wing	Tip vortex	0.75-1.35	• Vortices for static drift case show helical streamline pattern • Limited studies show good correlation with delta wing tip vortex scaling • Confirm the identity of these instabilities by comparing with slender fuselage vortices
		Wigley Hull at β =60°	Leeward keel vortices	NA	
		KVLCC2 at β = 30°	Leeward Fore-body Side	1.25-1.35	
			Leeward Fore-body Bilge	1.35-1.45	
			Leeward Aft-body bilge	1.8-2.25	
		5415 with BK at β=20°	Windward BK vortex	1.2 – 1.4	
			Fore-body keel vortex	0.95 – 1.15	
Free-surface instability	NA	Bare hull Athena	Rooster tail wave breaking	NA	• Occurs for dry transom flow • Shoulder waves traveling towards centerline
		Transom-model			
Vortex induced motions	Ship length (Freestream velocity)	Wetted Transom appended Athena	Associated with transom vortex shedding	2.19	• Unsteady pitch and heave motions due to Karman-like transom vortex shedding

Table 2 Summary of calm water resistance, sinkage and trim CFD V&V studies

Reference	Geometry	Fr	Grid	Resistance			Sinkage			Trim		
				$\|E_{CT}\|$%D	U_{SN}%S	U_D%D	E_s%D	U_{SN}%S	U_D%D	$\|E_t\|$%D	U_{SN}%S	U_D%D
Carrica et al. (2007)	5415	0.28	3M	4.3		0.64	7.4		4.71	10.4		4.7
		0.41		1.5		0.61	1.5		2.93	1.11		0.87
Xing et al. (2011)	5415	0.28	1.3M	3.7		0.64	9.5		4.71	2.2		4.7
		0.41		4.5		0.61	4.5		2.93	19.3		0.87
Xing et al. (2008)	Bare hull Athena	0.2 - 1.0	1M	2.1	2.53	1.5	7.7	1.6	29.3	9.6	15.3	8.1
	Propelled Appended Athena	0.2 - 0.84	2.2M	4.5			8.1			5		
Sadat-Hosseini et al. (2010)	ONR Tumblehome	0 - 0.6, Roll f = 10°	3.3M	2.6	0.42		3.62	2.3		14.15	2.4	
		0 - 0.6, Roll f = 20°	3.3M	2.5			2.47			10.03		
Stern et al. (2007)	HSSL-Delft catamaran	0.2 - 0.65	-	8			23			17		
Castiglione et al. (2011); Zlatev et al. (2009)	Delft catamaran	0.18 - 0.75	5.4M	5.2			18.5			16.1		
Kandasamy et al. (2010)	DTMB 5594	0.511	1.8M	0.78			0.8			14.3		
	5594, Water Jet self-propelled	0.511	1.8M	4.6			9			13.7		
Takai et al. (2011)	JHSS, Bare hull	0.34	29M	2.2	3.6	5.8	11.6			13.7		
	JHSS, Water Jet self-propelled	0.34	13M	0.2	1.1	1.2	10.27			27.4		
Ismail et al. (2010)	KVLCC2, FX_{st}	0.0 (double tanker)	4.6M	3.45	3.79	0.7						
Bhushan et al. (2009)	Athena bare hull with skeg at full-scale	0.48	4.8M	4.8	1.6	1.5	9.5	15.5	29.3	6.8	2.6	8.1
		0.8		3.14			32.3			5.3		
	Self-propelled fully appended Athena at full-scale	0.432, 0.575, 0.839					23			4.9		
Bhushan et al. (2012c)	Full-scale appended Athena (DES), FXσt	0.25	43M	4.22	5.28	1.5						
Bhushan et al. (2012b)	T-Craft (SES/ACV)	0.2, 0.4, 0.6	14.7M	7.8	1.5		9.8	8.3		14.7	6.3	
Mousaviraad et al. (2012)	Fully appended ONR Tumblehome in head winds	0.2, 0.3, 0.4	10.2M	4.5			3.1			3.3		
Gothenburg 2010 (Stern et al., 2010)	KVLCC2, FX_{st}	0.1423		1.7								
	KVLCC2, FX_{st}	0.26		0.8								
	5415, FX_{st}	0.138 - 0.41		2.5								
	KVLCC2, FR_{zq}	< 0.2		2.1			33.3			7.5		
	KCS, FR_{zq}	< 0.2		1.64			55.6			30.5		
		> 0.2					7.5			3.62		
	5415, FR_{zq}	< 0.2		3			31.4			164.6		
		> 0.2					8.8			23		
Average		< 0.2		3.3	2.5	1.5	34.7			54.7		
		> 0.2					9.7	6.9	12.3	11.0	6.7	4.6

Table 3 Summary of seakeeping in regular head waves CFD V&V studies

Study	Geom.	Grid (M)	Code	λ/L (ak)	Fr	V&V Method	U_T (%S_1) (0^{th} amp, 1^{st} amp, 1^{st} phase)			U_G (%S_1) (0^{th} amp, 1^{st} amp, 1^{st} phase)			U_{SN} (%D) (0^{th} amp, 1^{st} amp, 1^{st} phase)			*Reported* U_V (%D) (0^{th} amp, 1^{st} amp, 1^{st} phase)			E%D for amp, E%2π for phase (0^{th} amp, 1^{st} amp, 1^{st} phase)				
							C_T	z	θ	C_T	z	θ	C_T	z	θ	C_T	z	θ	C_T	z	θ	1^{st} order	2^{nd} order
Weymouth et al. (2005)	Wigley	0.11-0.29	CFDShip-Iowa V3	1.25 (0.018)	0.3	Correction Factor	-	-	-	-	-	-	-	-	-	-	-	-	-	-	-	*4.4*	*0.8*
							21.4	6.0	0.7	2.8	0.7	1.3	21.6	6.0	1.5	21.8	6.5	2.9	0.8	6.6	2.3		
							-	-	-	-	-	-	-	-	-	-	-	-	-	-	-		
							21.4	6.0	0.7	2.8	0.7	1.3	21.6	6.0	1.5	21.8	6.5	2.9	0.8	6.6	2.3		
							9.4			1.6			9.7			10.4			**3.2**			***2.6***	
Carrica et al. (2007)	DTMB 5512	0.38-2.96	CFDShip-Iowa V4	1.5 (0.025)	0.28	Correction Factor	-			2.0	-	-	2.0	-	-	2.0	-	-	-	21.3	3.3	*1.8*	*12.3*
										-	-	-	-	-	-	-	-	-	-	2.8	2.7		
										-	-	-	-	-	-	-	-	-	-	0.3	1.2		
										2.0	-	-	2.0	-	-	2.0	-	-	-	8.1	2.4		
										2.0			2.0			2.0			**5.3**			***7.0***	
Simonsen et al. (2010)	KCS	1.8-3.8	CFDShip-Iowa V4	1.15 (0.025)	0.26	Correction Factor	-			-	-	-	-	-	-	-	-	-	5.6	-5.1	143.8	*15.3*	*55.5*
										1.5	10.3	2.6	1.5	10.3	2.6	10.5	10.3	2.6	82.3	82.3	-10.1		
										-	-	-	-	-	-	-	-	-	1.1	1.1	-2.6		
										1.5	10.3	2.6	1.5	10.3	2.6	10.5	10.3	2.6	*29.7*	26.1	43.7		
										4.8			4.8			7.8			**33.2**			***35.4***	
Castiglione et al. (2011)	DELFT Cat.	0.7-5.4	CFDShip-Iowa V4	1.806 (0.025)	0.75	Correction Factor	-	-	-	-	-	-	-	-	-	-	-	-	-	-	-	*4.8*	-
							-	1.5	0.5	-	3.3	1.7	-	3.6	1.7	-	4.4	3.0	-	9.4	0.1		
							-	-	-	-	-	-	-	-	-	-	-	-	-				
							-	1.5	0.5	-	3.3	1.7	-	3.6	1.7	-	4.4	3.0	-	9.4	0.1		
							1.0			2.5			2.7			3.7			**4.8**			***4.8***	
Mousaviraad et al. (2010a)	DTMB 5512	2.8-22.1	CFDShip-Iowa V4	0.839-2.977 (0.025)	0.34	Factor of Safety	-	-	-	-	-	-	-	-	-	-	-	-	-	-	-	*3.4*	-
							-	5.7	2.2	-	4.9	4.9	-	9.1	5.6	-	9.2	5.8	-	3.8	2.2		
							-	2.0	2.8	-	2.8	4.8	-	3.4	5.6	-	9.1	14.1	-	2.3	5.3		
							-	3.8	2.5	-	3.9	4.9	-	6.2	5.6	-	9.1	9.9	-	3.0	3.8		
							3.2			4.4			5.9			9.5			**3.4**			***3.4***	
Carrica et al. (2010)	DTMB 5512	71	CFDShip-Iowa V4 (DES)	1.5 (0.025)	0.41	-	-			-			-			-			-	6.5	12.5	*4.5*	*9.5*
																			-	4.3	2.5		
																			-	6.2	5.0		
																			-	5.7	6.7		
																			6.2			***7.0***	
Gothenburg 2010 (Stern et al., 2010)	KVLCC2; KCS	Avg.= 2.6	Various				-	-	-	1.9	2.0	8.9	1.9	2.0	8.9	8.7	9.6	22.3	18.5	54.0	54.0	*14.6*	*44.0*
							21.4	4.4	1.1	2.2	4.8	2.6	11.6	6.5	2.9	21.6	11.0	5.3	47.7	10.0	10.0		
							-	2.0	2.8	-	2.8	4.8	-	3.4	5.6	-	5.7	7.2	20.3	17.3	17.3		
							21.4	3.2	2.0	2.0	3.2	5.4	6.7	4.0	5.8	15.1	8.8	11.6	28.8	27.1	27.1		
							8.9			3.5			5.5			11.8			**27.7**			***29.3***	
Average (Average fine grid=15M)							-	-	-	2.0	2.0	8.9	2.0	2.0	8.9	5.3	9.6	22.3	12.0	19.2	53.4	*8.2*	*31.7*
							21.4	4.4	1.1	2.2	4.8	2.6	11.6	7.1	2.9	17.9	8.3	3.9	43.6	17.0	1.4		
							-	2.0	2.8	-	2.8	4.8	-	3.4	5.6	-	7.4	10.7	10.7	5.4	5.2		
							21.4	3.2	2.0	2.1	3.2	5.4	6.8	4.2	5.8	11.6	8.4	12.3	*22.1*	13.9	20.0		
							8.9			3.6			5.6			10.8			**18.7**			***20.0***	

Table 4 Summary of forced motions maneuvering CFD V&V studies

Study	Geom.	Fine Grid (M)	Code	*Fr*	Conditions	Forces & Moments									Linear Derivative		Nonlinear Derivative
						X			Y			N			Y′	N′	
						U_{SN} %D	U_V %D	*E* %D	U_{SN} %D	U_V %D	*E* %D	U_{SN} %D	U_V %D	*E* %D	*E* %D	*E* %D	*E* %D
Ismail et al. (2010)	KVLCC2	4.6	CFDShip-Iowa V4	0.0 (double tanker)	Static Drift, β=12°	2.5	2.6	13.2	0.1	0.7	4.6	2.2	2.5	2.8			
Toxopeus (2009)	HTC, MARIN LNG, KVLCC2M	3.8	PARNASSOS	EFD: 0.13-0.18; CFD: 0.0	Static Drift, β up to 30°										20.6	8.9	
					Pure Yaw, γ up to 0.6										21.9	30.8	
Phillips et al. (2009)	KVLCC2	2.1	ANSYS CFX	EFD: 0.14; CFD: 0.0	Static Rudder, δ=10°	17.5	18.8	6.3	1.4	2.9	11.9	0.5	2.5	3.7			
Bhushan et al. (2011)	DTMB 5415	250	CFDShip-Iowa V4 (DES)	0.28	Static Drift, β=20°	0.4	7.9	4.6	0.6	4.2	3.7			1.4			
Jacquin et al. (2006)	KVLCC2M		ICARE	0.0 (double tanker)	Static Drift, β up to 12°			2.6			4.6			9.2			
	HTC			0.132, 0.238	Static Drift, β up to 30°			10.5			7.3			14.3			
Sakamoto et al. (2012)	DTMB 5415	20	CFDShip-Iowa V4	0.28	Static Drift, β=10°	8.4	9.7	9.4			5.4			3.1	4.9	4.4	
					Pure Yaw, γ=0.3	7.6	10.0	17.1	34.5	37.4	34.0	10.1	10.9	8.8	35.2	7.7	
					Pure sway, β_{max} up to 10°			8.0			9.2			4.5	4.8	4.9	
					Yaw & Drift			21.6			10.0			7.9	15.4	91.3	
Wilson et al. (2007)	DTMB 5415	7.1	Tenasi	0.28	Pure sway			31.0			5.0			24.0			
Mousaviraad et al. (2012)	Fully appended ONR Tumblehome in head winds	10.2	CFDShip-Iowa V4.5	0.2, 0.3, 0.4	Static Drift, β up to 11.7°			0.8			2.9			7.7			
					Pure sway, β_{max}=10°			7.4			2.7			14.6			
					Pure Yaw, ψ_{max} up to 17.7°			5.6			5.9			3.2			
					Yaw & Drift; β=10°, ψ_{max}=8.9°			4.2			2.3			4.1			
SIMMAN 2008; Stern et al. (2011)	KVLCC1, KVLCC2, KCS, 5415	Avg.=5.1	Various URANS solvers	Various	Static Rudder, δ=10°			27.0			55.0			29.0	14.5	59.0	
					Static Drift, β up to 12°			18.1			7.0			10.1	14.5	59.0	
					Pure Sway			21.3			15.4			15.4	8.0	8.0	49.0
					Pure Yaw			32.8			25.7			25.7	23.0	23.0	32.0
Average					Static Rudder	17.5	18.8	16.6	1.4	2.9	33.4	0.5	2.5	16.4	14.5	59.0	
					Static Drift	3.8	6.7	8.4	0.4	2.5	5.1	2.2	2.5	6.9	13.3	24.1	
					Pure Sway			16.9			8.1			14.6	6.4	6.4	49.0
					Pure Yaw	7.6	10.0	18.5	34.5	37.4	21.9	10.1	10.9	12.5	26.7	20.5	32.0
					Yaw & Drift			12.9			6.1			6.0	15.4	91.3	
					AVERAGE	9.6	11.8	14.7	12.1	14.3	14.9	4.3	5.3	11.3	15.3	40.3	40.5
						|E|=13.6									**27.8**		**40.5**

Table 5 Summary of CFD simulations for maneuvering and system identification

										Turning Circle E%D				Zigzag E%D		
Type	Author	Code	Method	Propulsion	Rudder	Grid	Geometry	Cases	DOF	A	TR	TD	D	1st overshoot	2nd overshoot	Ave.
Maneuver	Muscari et al. (2008a,b)	RANSE code developed at INSAEN	Finite Volume, Spalart and All-Maras, no free surface,dynamic overset Grid	Body force propeller	Actual rudder	424K	KVLCC2	turning	3DOF (double model)	6.2	11.2	7.2				8.20
						3.4M				8.4	5.3	0.8				4.83
Maneuver	Bhushan et al. (2009)	CFDShip-Iowa	Finite difference, k-w, level set, dynamic overset grid	Body force propeller	Actual rudder	7M	5415M	zigzag	6DOF	No data						
Maneuver	Carrica and Stern (2008)	CFDShip-Iowa	Finite difference, DES, level set, dynamic overset grid	Actual propeller	Actual rudder	5.6M	KVLCC1	zigzag	6DOF					30.6	36	33.30
						14.9M		turning		8	24		0.65			10.88
Maneuver	Carrica et al. (2008a,2012a)	CFDShip-Iowa	Finite difference, k-w, level set, dynamic overset grid	Body force propeller	Actual rudder	7M	5415M	zigzag and turning	6DOF	2.6	9.5	5.18	5.69	6.97	6.69	6.11
						12M		turning in waves		No data						
Maneuver	Drouet et al. (2008)	ICARE developed by ECN, France	Finite volume, k-w, VOF, dynamic grid	Body force propeller	Side force	-	5415M	turning	6DOF	No data						
							Humburg test case		3DOF			0.3				0.30
									6DOF			5				5.00
Maneuver	Ferrant et al. (2008)	ICARE developed by ECN, France	Finite volume, k-w, VOF, dynamic overset grid	Body force propeller	Side force	-	5415M	Turning in waves	6DOF	No data						
Maneuver and SI	Araki et al. (2012a)	CFDShip-Iowa	Finite difference, k-w, level set, dynamic overset grid	Body force propeller	Actual rudder	12.1M	OT	zigzag and turning	6DOF	1.23	2.29		1.34	1.54	2.23	1.73
Maneuver and SI	Araki et al. (2012b)	CFDShip-Iowa	Finite difference, k-w, level set, dynamic overset grid	Body force propeller	Actual rudder	12.1M	OT	zigzag and turning in wave	6DOF	Not reported						
Maneuver	Jacquin et al. (2006)	ICARE developed by ECN, France	Finite volume, k-w, VOF, dynamic overset grid	Body force propeller	Side force	-	S60	turning	6DOF	No data						
Maneuver	Durante et al. (2010) Dubbioso et al. (2012)	RANSE code developed at INSAEN	Finite Volume, Spalart and All-Maras, no free surface, dynamic overset Grid	Body force propeller	Actual rudder	6.2M	Tanker	turning	6DOF	7.35	3.15	5.24	4.06			4.95
						0.77M				10.6	9.42	4.96	12.26			9.31
Maneuver	Mousaviraad et al. (2012)	CFDShip-Iowa	Finite difference, k-w, level set, dynamic overset grid	Body force propeller	Actual rudder	8.6-9.3M	SES/ACV	turning and zigzag in calm water and waves for deep and shallow	6DOF	No data						
									Total	**6.34**	**9.27**	**4.10**	**4.80**	**13.04**	**14.97**	**8.46**

Table 6 Summary of CFD simulations for course keeping and stability

Type	Author	Code	Method	Propulsion	Rudder	Grid	Geometry	Cases	DOF	Comparison with EFD
Course Keeping and Stability	Sadat-Hosseini et al. (2011)	CFDShip-Iowa	Finite difference, k-w, level set, dynamic overset grid	Body force propeller	Actual rudder	3.7M	OT	broaching in following regular waves	6DOF	Time history of motions
Course Keeping and Stability	Mousaviraad et al. (2008)	CFDShip-Iowa	Finite difference, k-w, level set, dynamic overset grid	Body force propeller	Actual rudder	3.7M	OT	hurricane CAMILLE	6DOF	no EFD data
Course Keeping and Stability	Carrica et al. (2008b) and Huang et al. (2008)	CFDShip-Iowa	Finite difference, k-w, level set, dynamic overset grid	Body force propeller	Actual rudder	3.7M	OT	broaching in irregular waves	6DOF	no EFD data
Course Keeping and Stability	Carrica et al. (2012b)	CFDShip-Iowa	Finite difference, k-w, level set, dynamic overset grid	Actual propeller	Actual rudder	21M	OT	broaching in following regular waves	6DOF	Time history of roll, pitch and yaw
Stability	Strasser et al. (2009)	-	Finitie volume, compressible, k-e,VOF, grid re-meshing	No propeller	No rudder	-	damaged barge	flooding in calm water	6DOF	Time history of motions and water height
Stability	Sadat-Hosseini et al.(2012)	CFDShip-Iowa	Finite difference, k-w, level set, dynamic overset grid	No propeller	No rudder	6.3-20M	damaged SSRC	roll decay and motions with flooding in calm water and waves	6DOF	Time history of motions and water height
Course Keeping	Stern et al. (2011)	CFDShip-Iowa	Finite difference, k-w, level set, dynamic overset grid	Body force propeller	Actual rudder	6.3-18.6M	5415M	roll decay with no fins or passive fins	6DOF	Time history of 6DOF motions, BK, fin and rudder forces
		ISIS-CFD developed by Fluid Mechanics Laboratory, France	Finite volume, k-w, VOF, unstructured grid	Body force propeller	Fixed rudder	5.9M		roll decay, forced roll and motions in waves		
Course keeping	Dreyer and Boger (2010)	OVER-REL_TCURS, ARL	Finite volume, Spalart and All-Maras, VOF, dynamic overset grid	Body force propeller	Actual fins	6.4M	submarine and ship	overtaking	6DOF	Time history of pitch and depth for submarines

Table 7 Experimental studies of bow wave breaking

		Waniewski et al. (2002)	Karion et al. (2004)
Experiment Setup	Geometry	*Deflecting plate in small & large flumes* *Wedge in a towing tank* *Half wedge angle* θ*=13˚ & 26˚* *Dihedral angle* φ*=0˚* (for *small flume,* φ*=0˚ to 15˚*)	*Bow wedge (Model No. 5605) in deep water towing basin* *Bow entrance angle* θ*=20˚ & 40˚* *Flare angle* φ*=20˚ & 0˚*
	Facility	*Small flume: 40 m long, 1.09 m wide* *Large flume:2.65 m long, 0.459 m wide* *Towing tank: 126m long, 7.5 m wide, and 3.7 m deep*	*Deep water towing basin: 575 m long, 15.5 m wide, and 6.3 to 6.5 m deep.*
	Approaches	*Contact line measured using free surface probes in the flumes* *Bow wave profile measured using videos in towing tank*	*Quantitative visualization (QViz) technique for the wave free surface* *High-speed video camera for spray of droplets*
	Test conditions	*Small flume:* $Re=1.1\times10^4$ *to* 1.6×10^4*; Fr=2.57 to 6.46* *Large flume:* $Re=1.4\times10^5$ *to* 2.0×10^5*; Fr=2.57 to 3.29* *Towing Tank:* $Re=0.43\times10^5$ *to* 7.0×10^5*; Fr= 1.27 to 7.77*	$Re= 4.1\times10^5$ *to* 7.0×10^6*; Fr= 0.2 to 1.4* *We= 11 to 2800*
Experimental Results & observations		*1. Bow wave profile: mainly wave elevation* *2. Plunging jet shape: jet thickness & impingement angle* *3. Scaling analysis* *4.Free surface disturbance* *5. Air entrainment (separate paper)*	*1.Contour plots of free surface elevation* *2. Surface fluctuations* *3.Surface roughness measurement* *4.Extent of breaking* *5. Spray droplets formation, number, size*
Summary		*1. The bow wave flow is highly nonlinear, there appears to be no satisfactory analytical solution.* *2. The wave is weakly dependent on dihedral angle and depends on the bow half-angle.* *3. Surface disturbances were observed, which are likely gravity waves on the surface of the bow wave. They seem to be responsible for the breakup of the jet into strings of droplets and for the periodic nature of the bubble clouds produced by the wave breaking process.*	*1. Wave breaking occurs when both Froude and Reynolds numbers exceed a critical level.* *2. A critical Webber number must be exceeded for spray generation to occur.* *3. Scaling the maximum wave heights by the quantity (* $Fr^{1.5}D$*), collapses the data fairly well.*

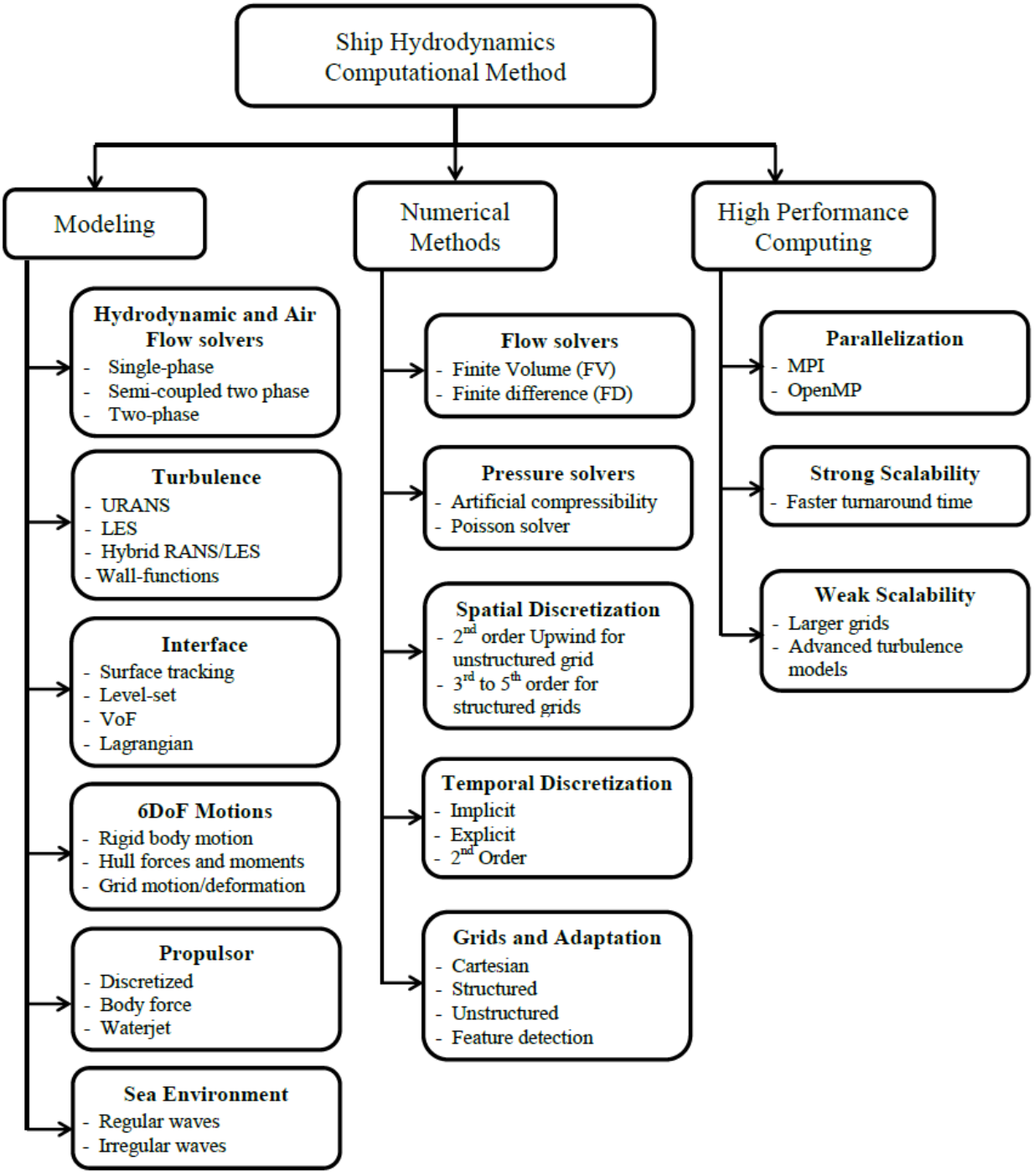

Fig. 1. Flow chart demonstrating the components of the ship hydrodynamics computational methods.

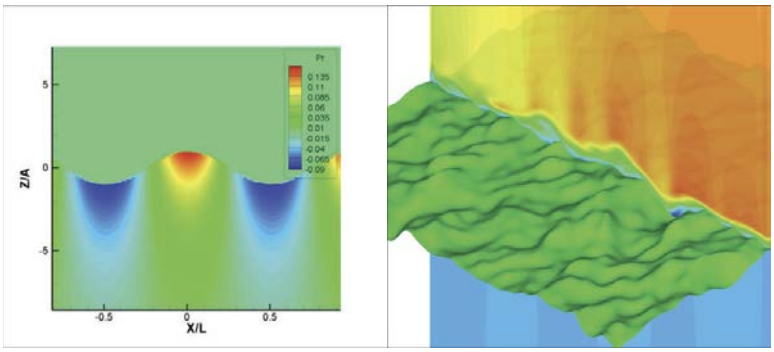

(a)

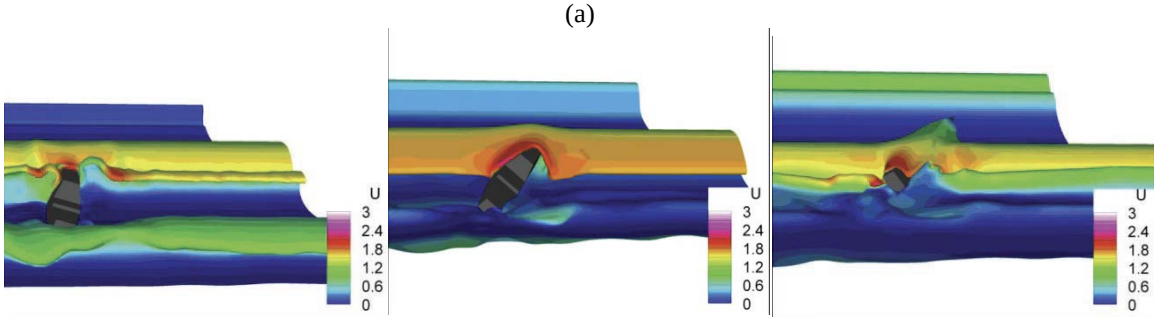

(b)

Fig. 2. Examples for sea modeling: a) exact potential solution for a linear wave component and generated random seas inside the computational domain, b) snapshots of ship in three sisters rogue waves simulations.

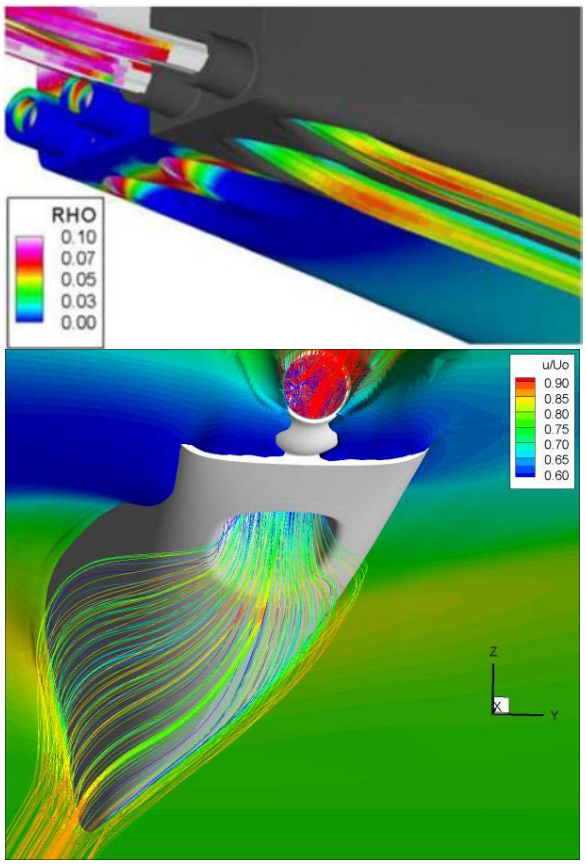

Fig. 3. Waterjet flow modeling for JHSS at Fr=0.34 (top) and Delft catamaran at Fr=0.53 (bottom).

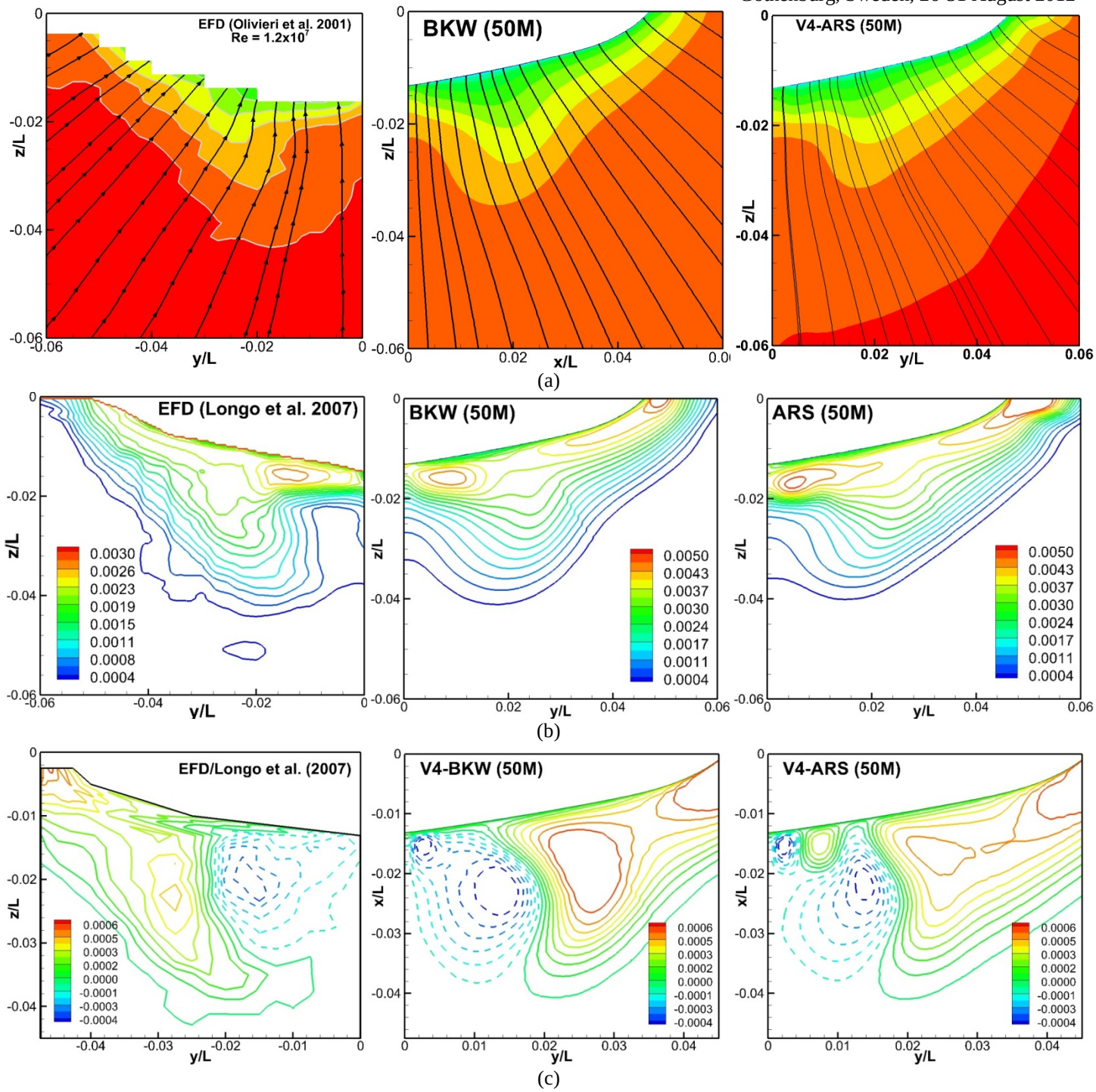

Fig. 4. CFDShip-Iowa V4 predictions for (a) streamwise velocity profile and cross-plane velocity streamline, (b) turbulent kninetic energy and (b) shear stress $\overline{u'v'}$ at nominal wake plane x/L=0.935 using isotropic (BKW) and anisotropic (ARS) models for straight ahead 5415 simulations on 50M grid at $Re = 5.13\times10^6$, $Fr = 0.28$ are compared with experimental data (EFD).

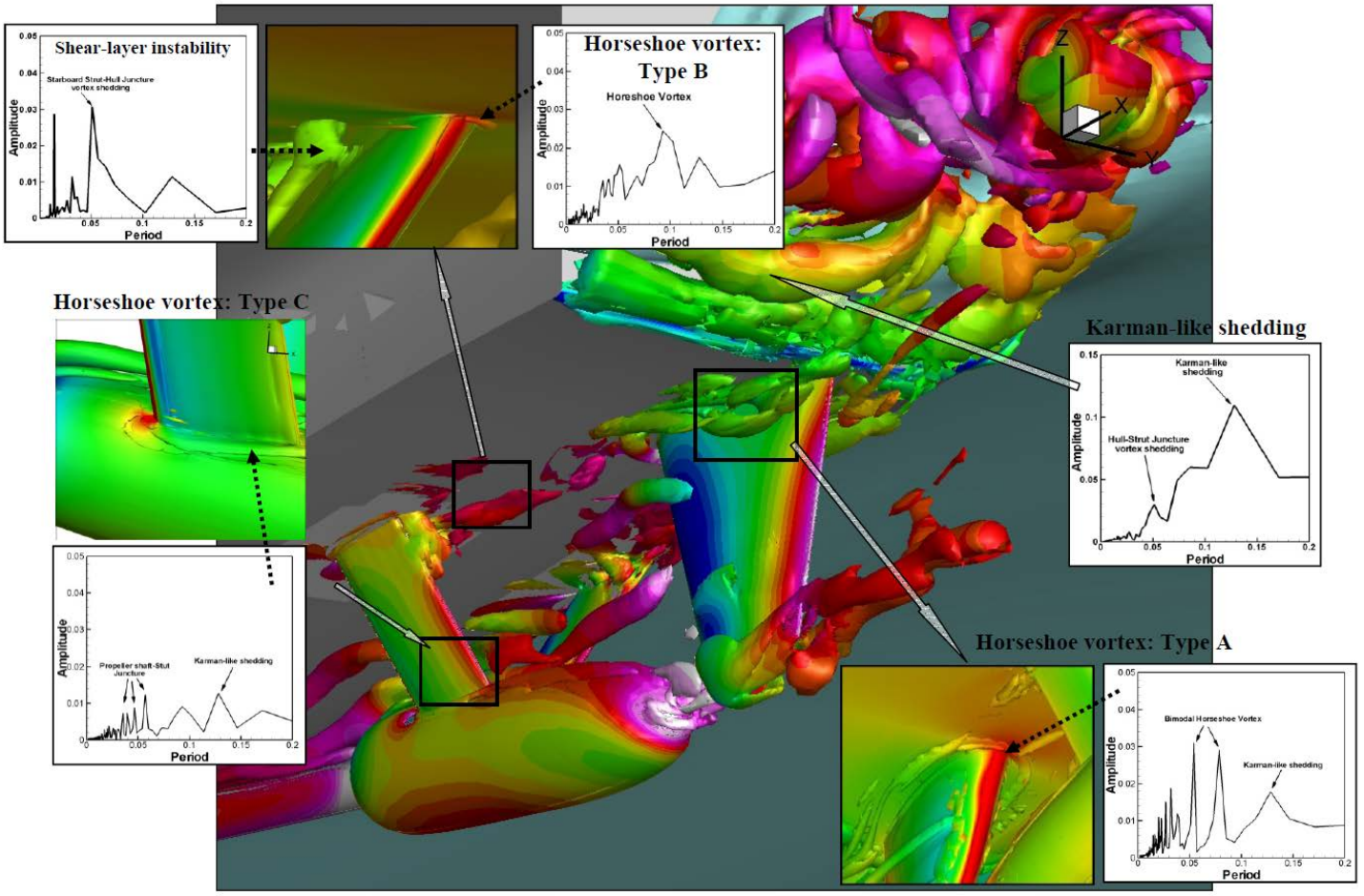

(a)

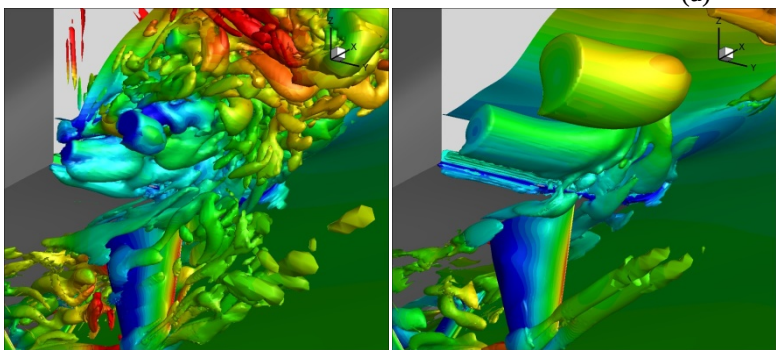

(b) 50M grid-DES

(c) 9M grid, URANS

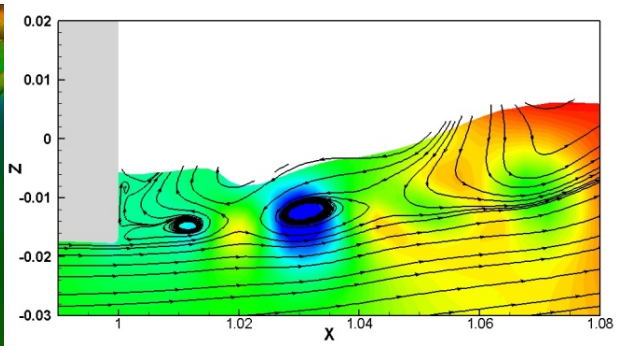

(d) 9M grid-DES

Fig. 5. (a) Isosurfaces of Q=300 for instantaneous solution DES solution on 9M grid. Inset figures are obtained using averaged solution. Three different types (A, B and C) of juncture vortices are marked and associated dominant frequency modes are shown. Contours are of the absolute pressure with levels from -0.5 to 0.1 at an interval of 0.02. Vortical structures at the transom corner obtained using (b) DES on 50M grid and (c) URANS on 9M grid. (d) Instantaneous flow separation at Y = 0.01 plane is shown for DES on 9M grid.

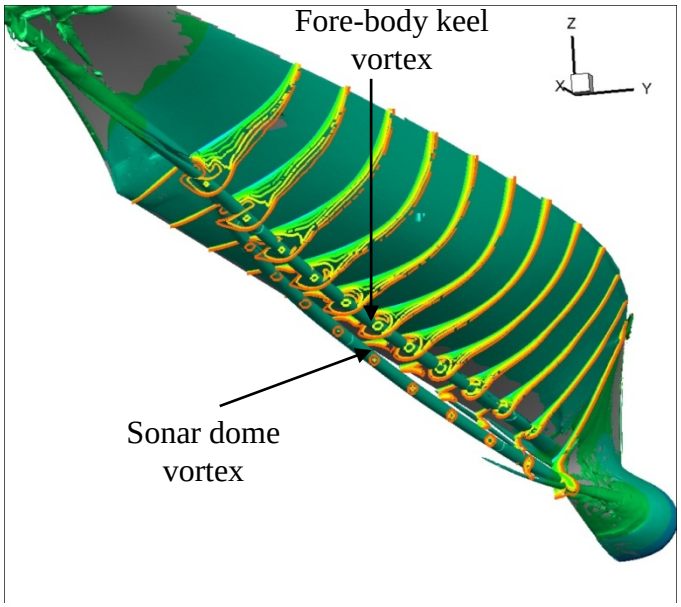

(a)

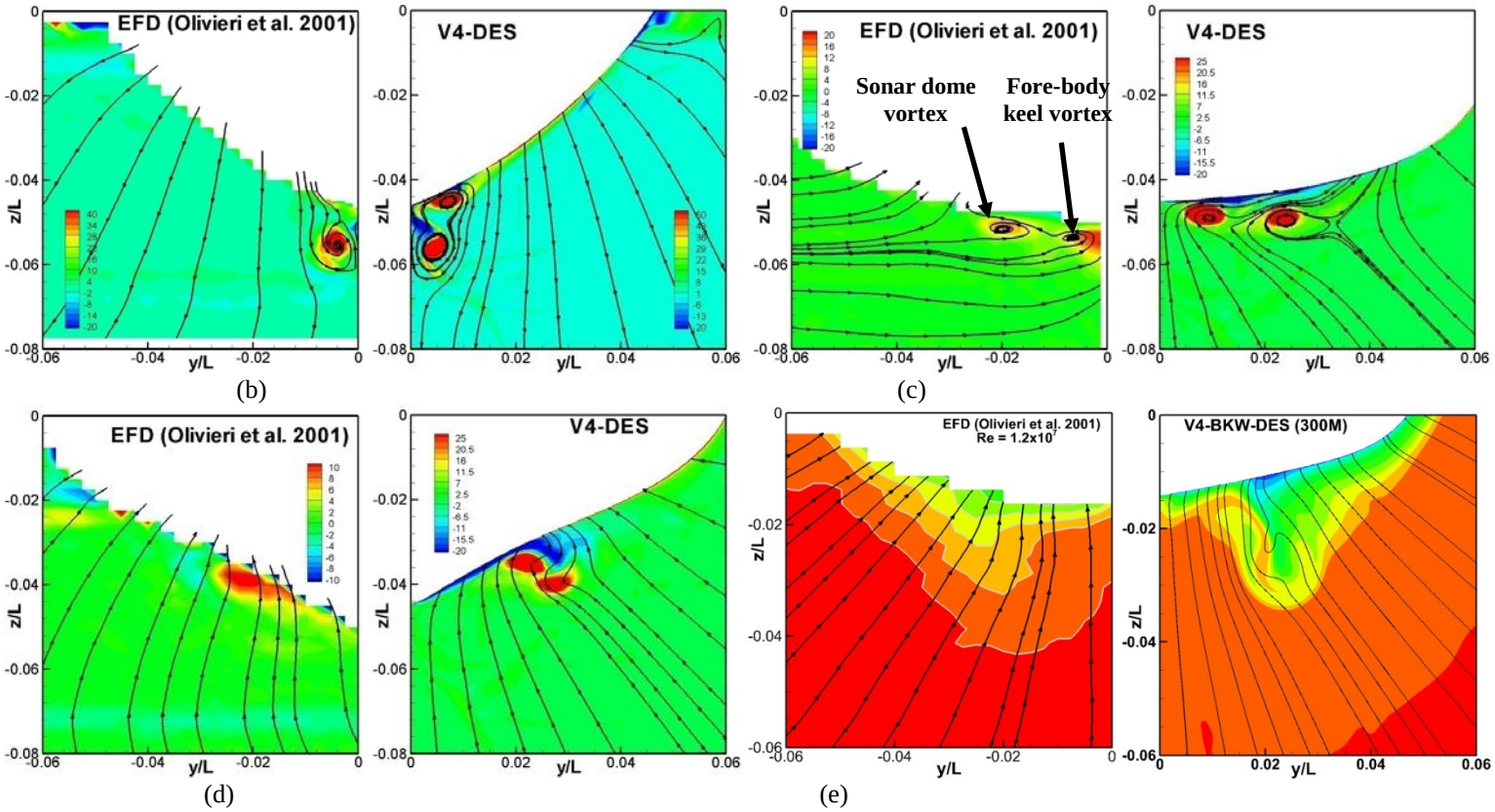

(b) (c) (d) (e)

Fig. 6. (a) Vortical structures predicted by CFDShip-Iowa V4 using DES model on 300M grid for straight ahead 5415 at Re = 5.13×10^6, Fr = 0.28. The flow does not show small scale turbulent structures, but resolves vortical structures and their interaction with the boundary layer very well. Contours of the streamwise vorticity at (b) x/L = 0.2, (c) x/L = 0.6 and (d) x/L = 0.8 are compared with experimental data. (e) Streamwise velocity profile and cross-plane velocity streamline at nominal wake plane is compared with experimental data.

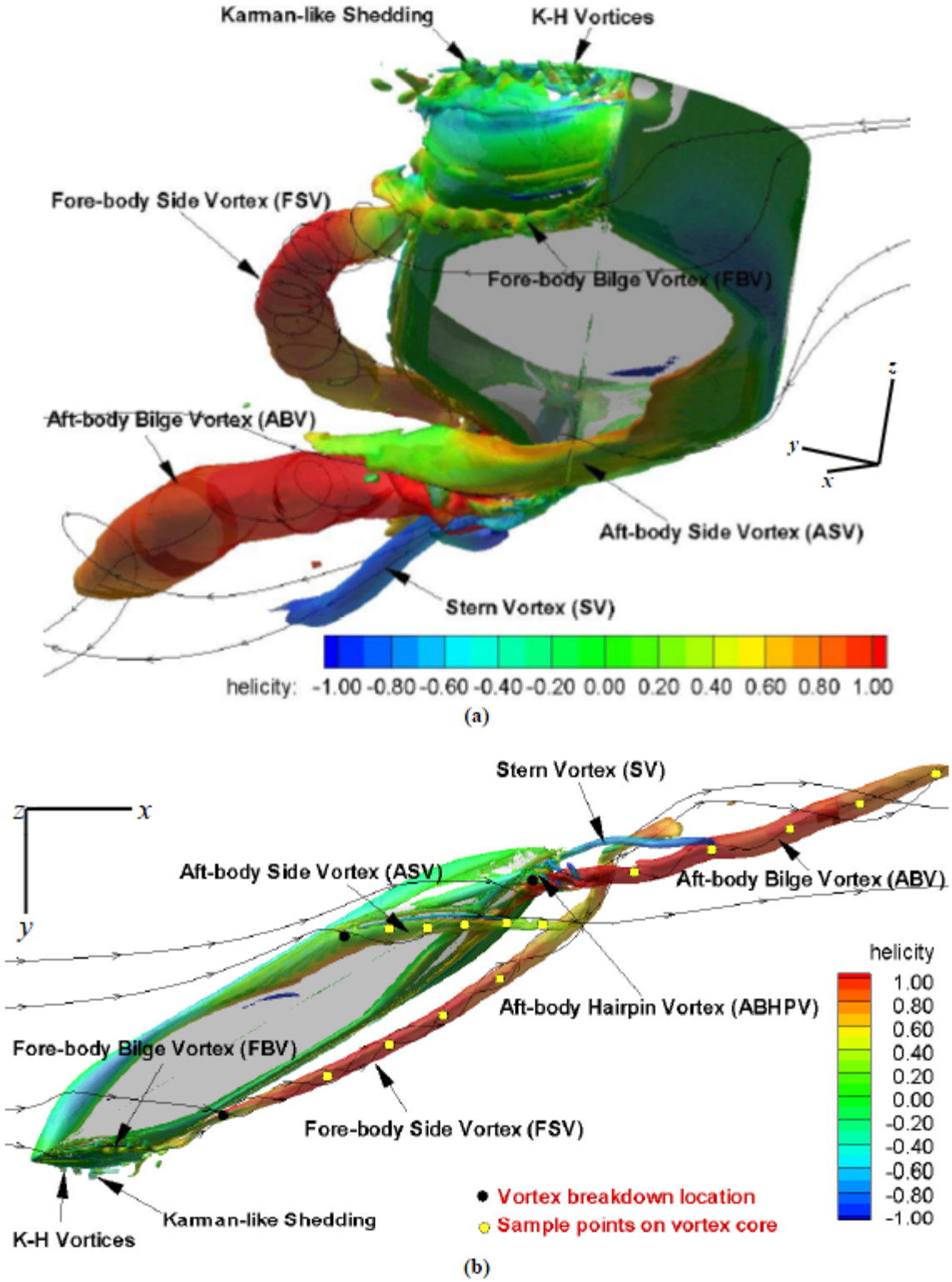

Fig. 7. Vortex system of KVLCC2 (isosurface of $Q = 200$ colored by helicity) at $_0\beta = 30$: (a) bow view and (b) bottom view.

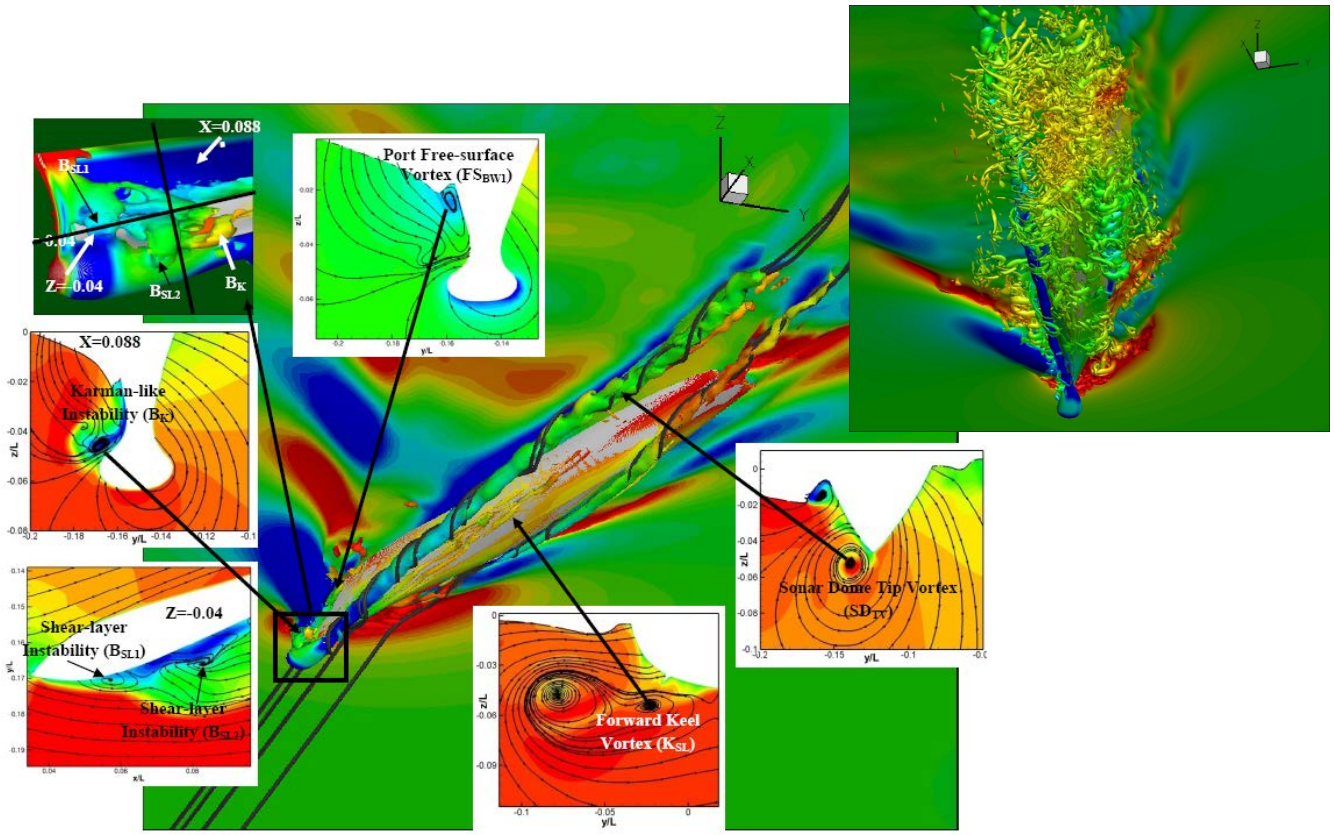

(a)

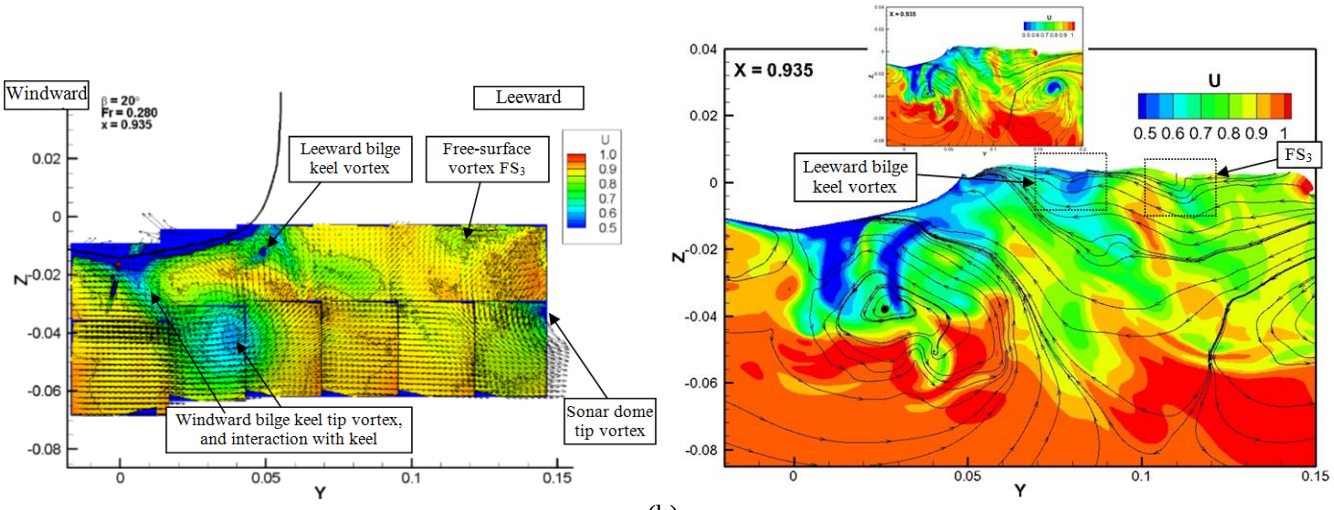

(b)

Fig. 8. (a) Large scale vortical structures and instabilities are identified for 5415 at β = 20° static drift using CFDShip-Iowa V4 DES simulations. The inset on right topmost corner shows the small scale structures predicted on 250M grid. (b) Initial comparison of streamwise velocity contour and cross flow vectors and wake at X=0.935 shows very good agreement with the ongoing experiments.

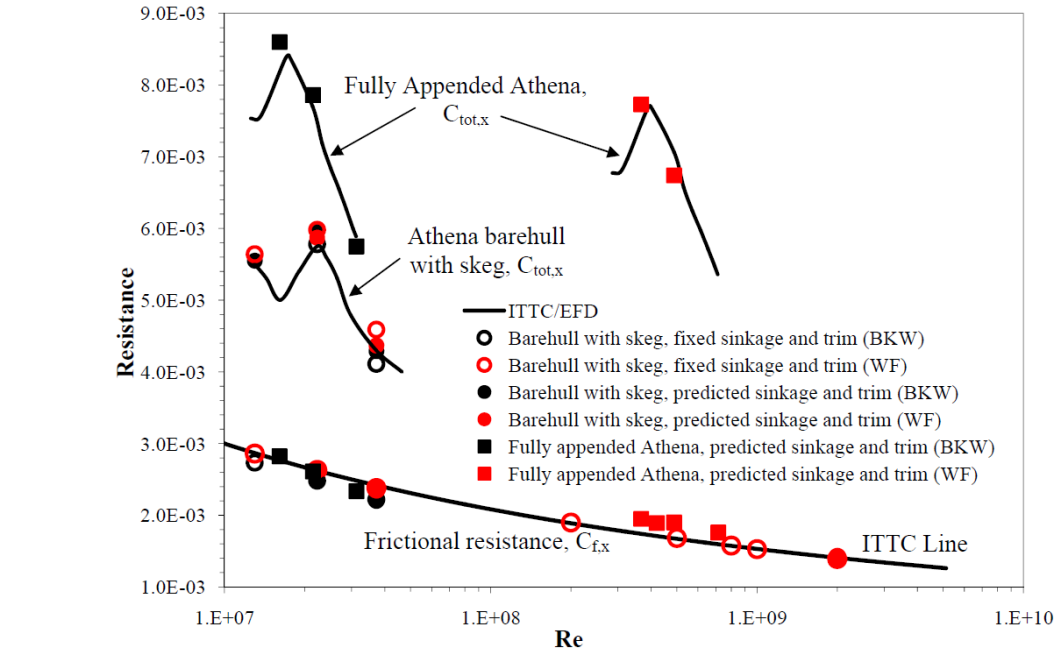

(a)

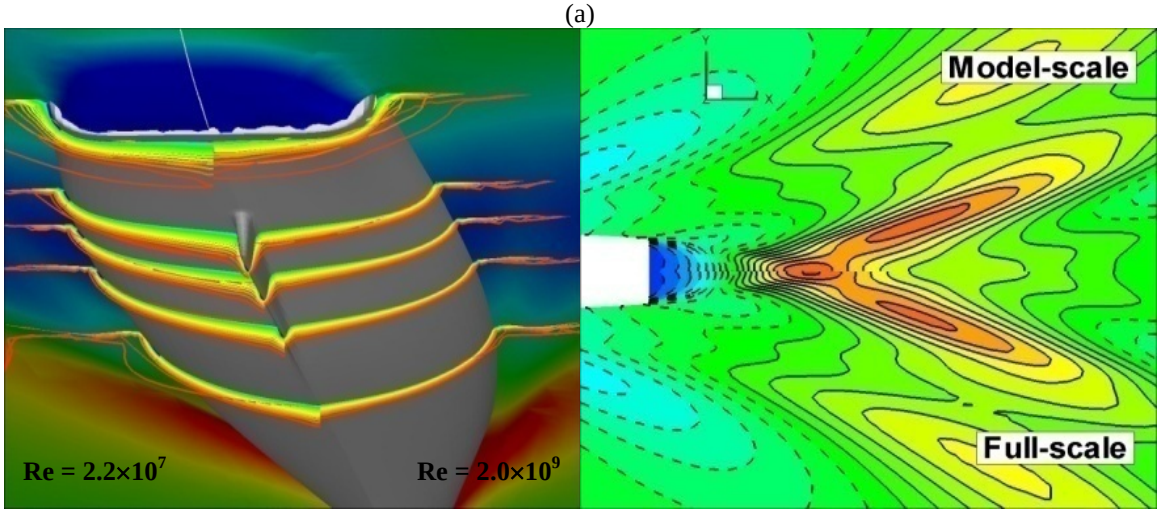

(b) (c)

Fig. 9. (a) Fully appended and barehull Athena resistance predictions for model and full scale using near wall turbulence model (BKW) and wall-functions (WF) are compared with experimental data and ITTC line. Local flow field for model and full scale barehull Athena: (b) boundary layer profiles colored by streamwise velocity; and (c) transom free surface wave elevation contour for *Fr*=0.48. As expected, the full-scale boundary layer is thinner than in model-scale, and the free surface elevation pattern is not significantly affected by the Reynolds number.

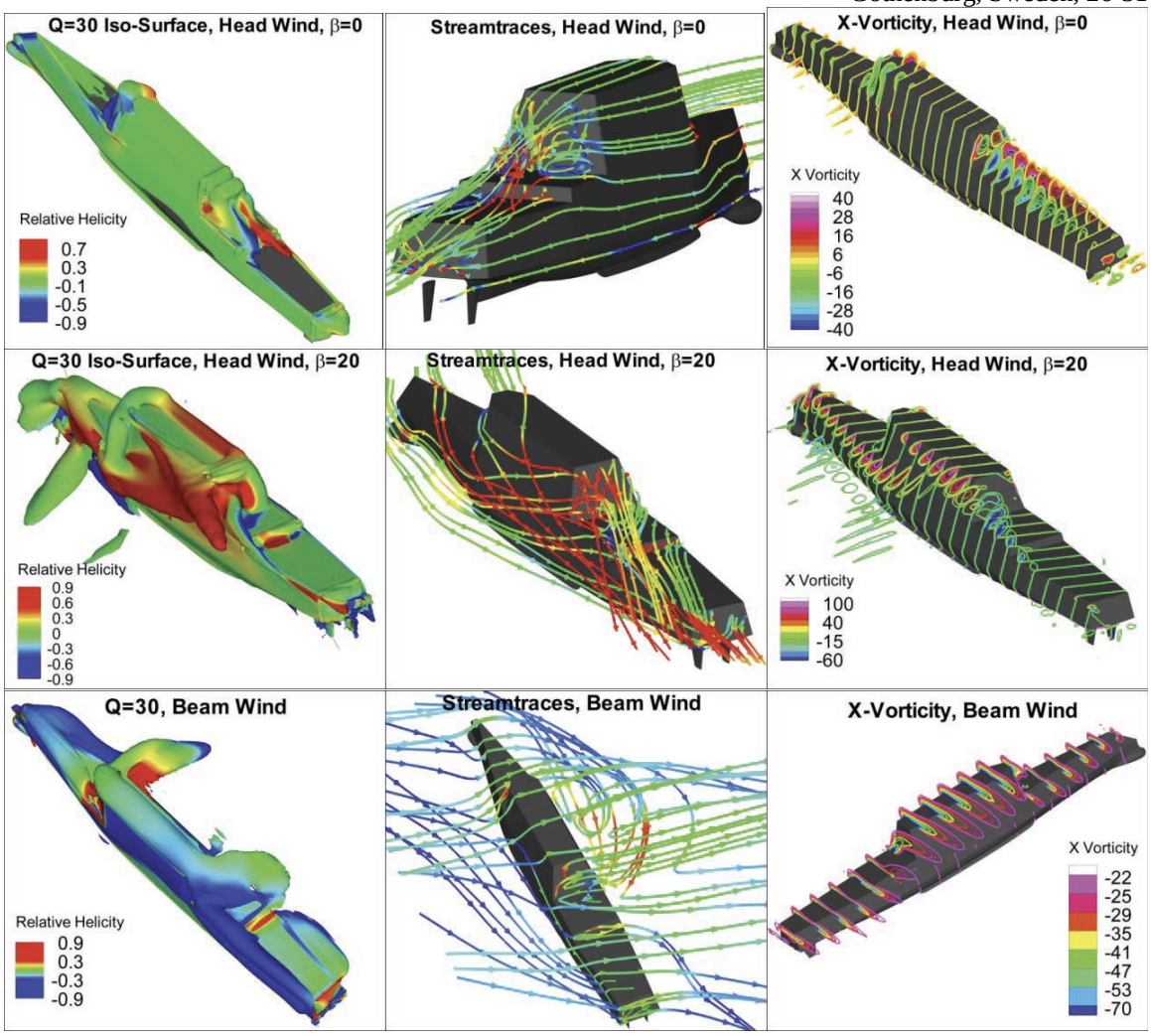

Fig. 10. Examples of air flow modeling for ONR Tumblehome in static conditions

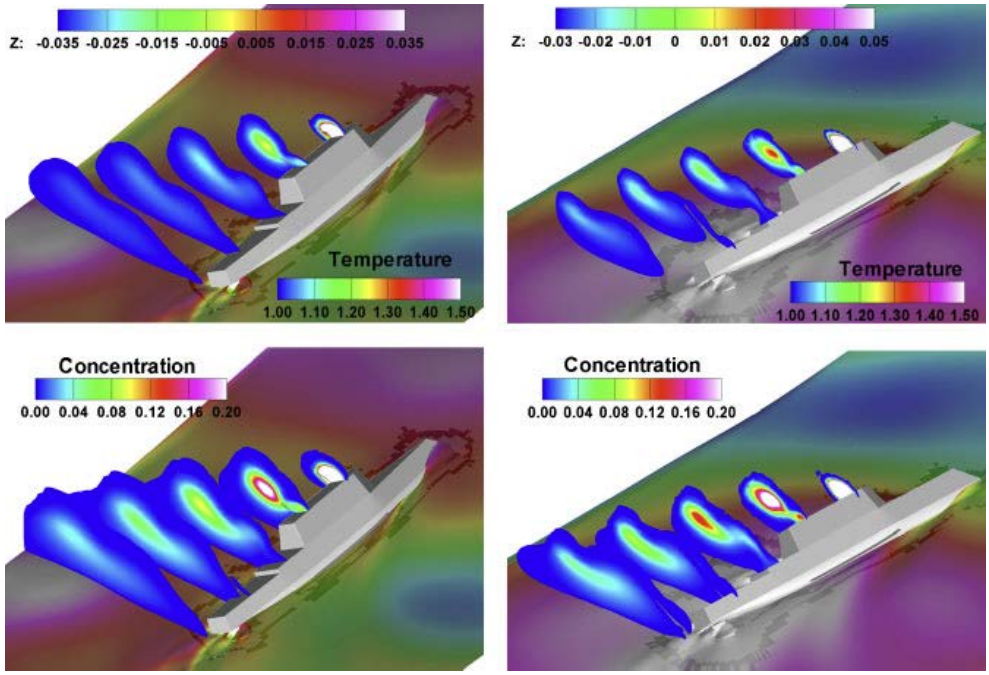

Fig. 11. Examples of CFDShip-Iowa ship exhaust plumes simulations for ONR Tumblehome during a broaching event.

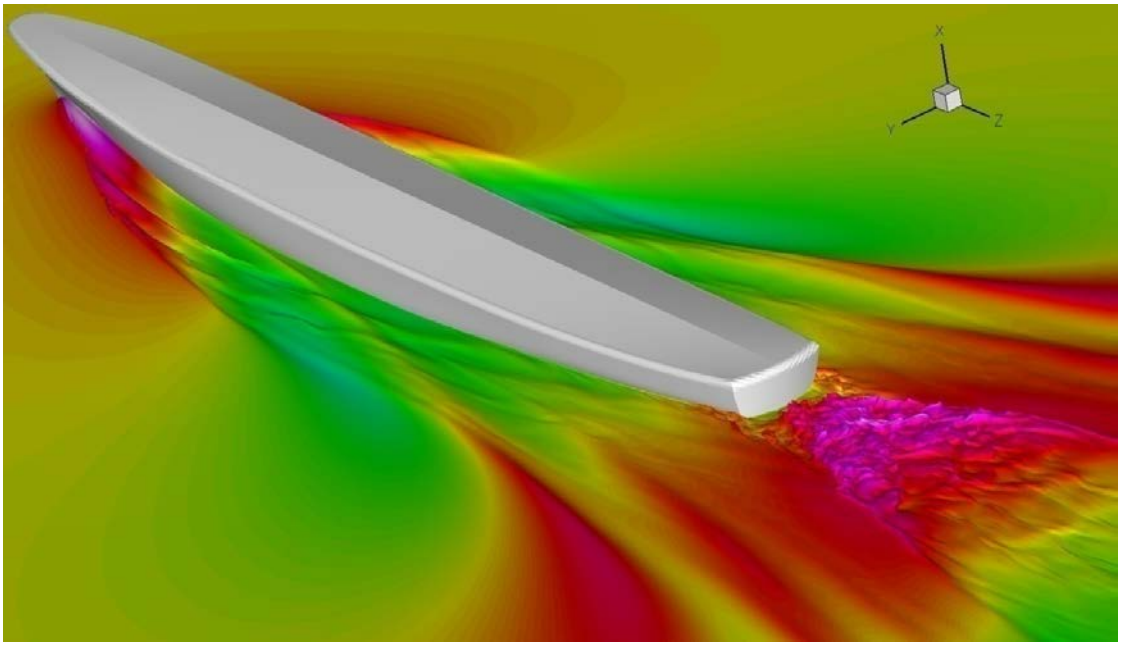

Fig. 12. Instantaneous air/water interface colored by elevation for DTMB 5512 at Fr = 0.41

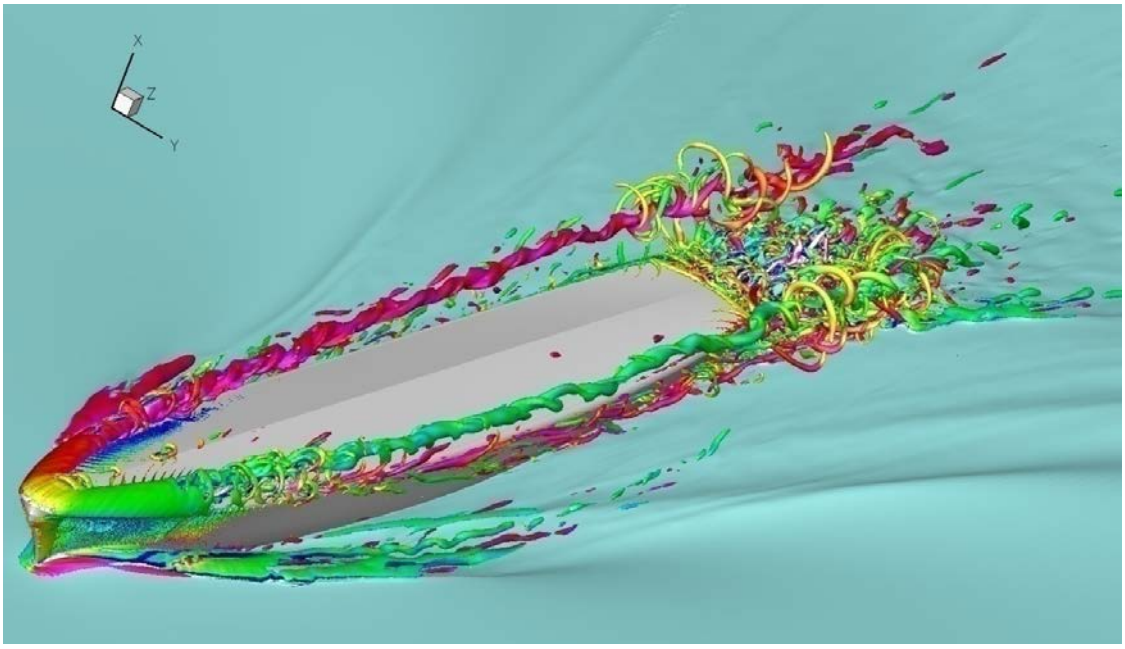

Fig. 13. Instantaneous vortical structures colored by streamwise vorticity for DTMB 5512 at Fr = 0.41 for air phase, Q = 500.

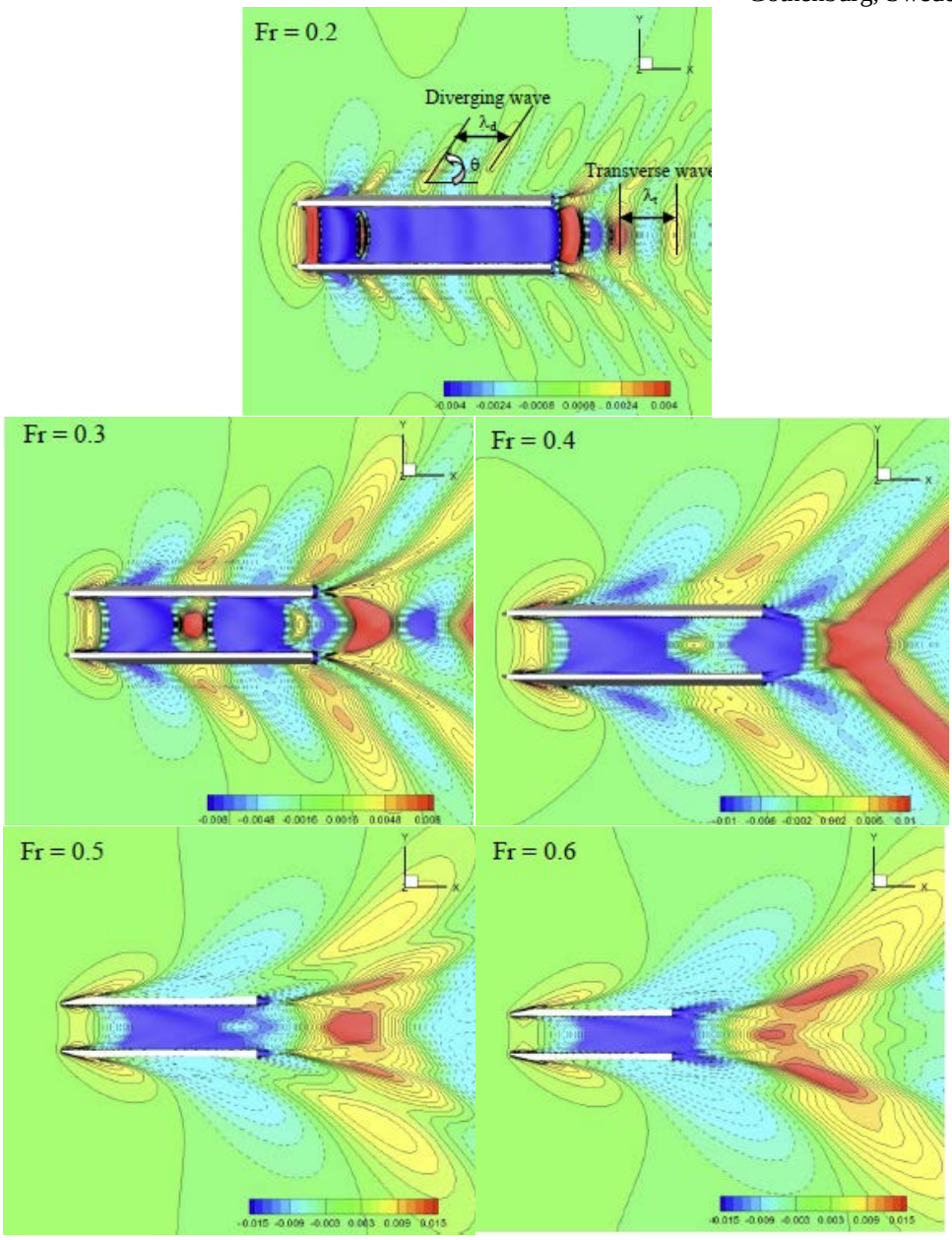

Fig. 14. URANS free-surface wave elevations for calm water resistance, sinkage and trim computations of T-Craft (ACV/SES) at Fr = 0.2 – 0.6 (Bhushan et al., 2012b).

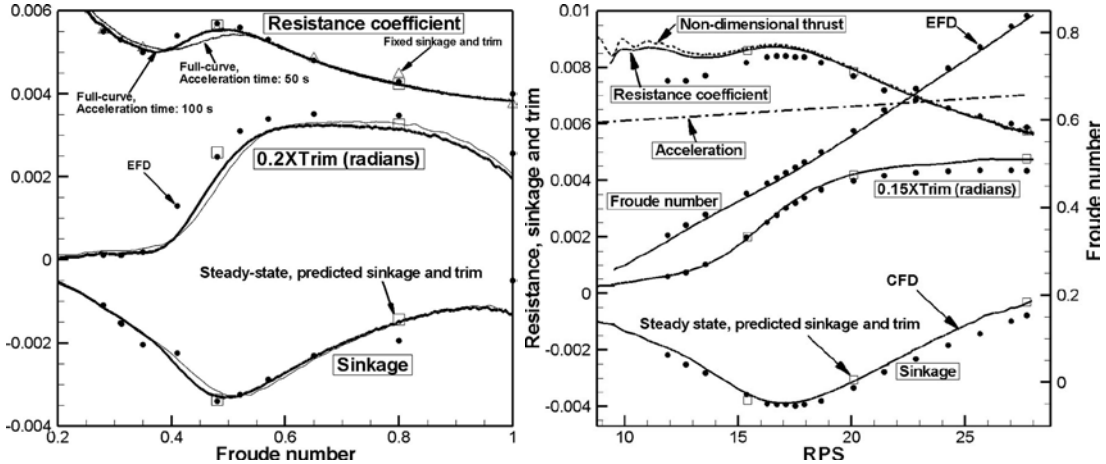

Fig. 15. Resistance and propulsion curves for Athena obtained using the single-run procedure (Xing et al., 2008).

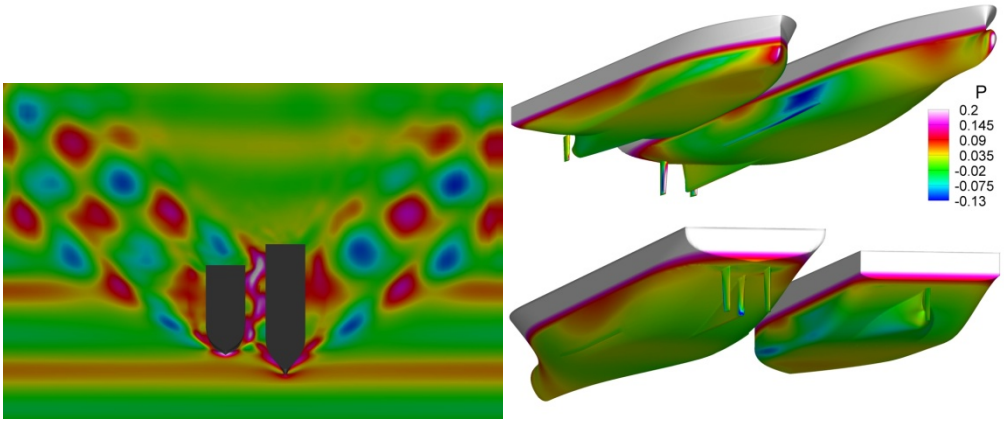

Fig. 16. Free surface and hull pressure distributions at an instance during regular head wave simulation for side by side ship-ship interactions for Hope and Bobo (Mousaviraad et al., 2011).

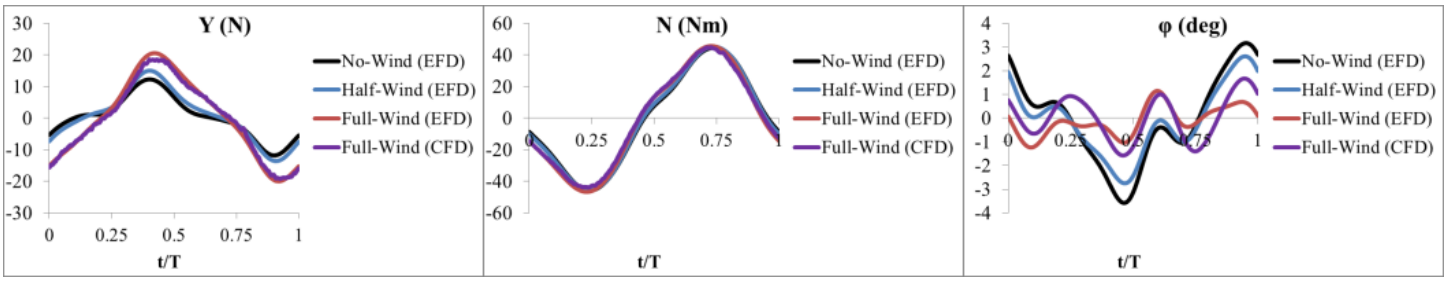

Fig. 17. Captive pure yaw maneuvering for ONR Tumblehome including wind effects (Mousaviraad et al., 2012b).

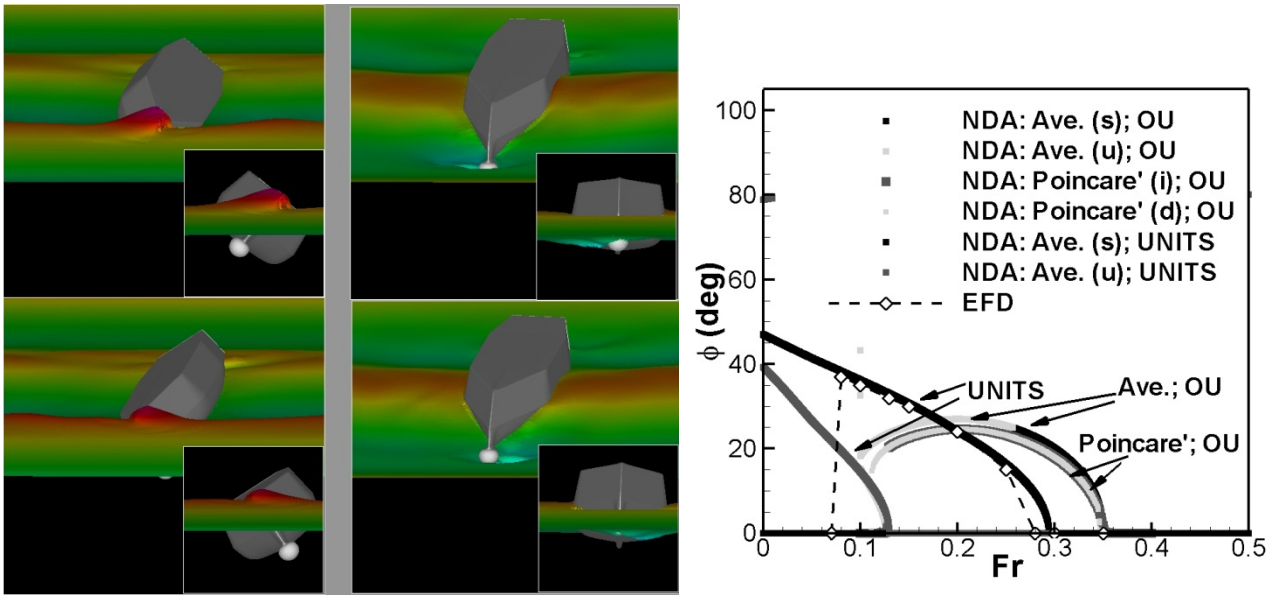

Fig. 18. Parametric rolling studies for ONR Tumblehome (Sadat-Hosseini et al., 2010).

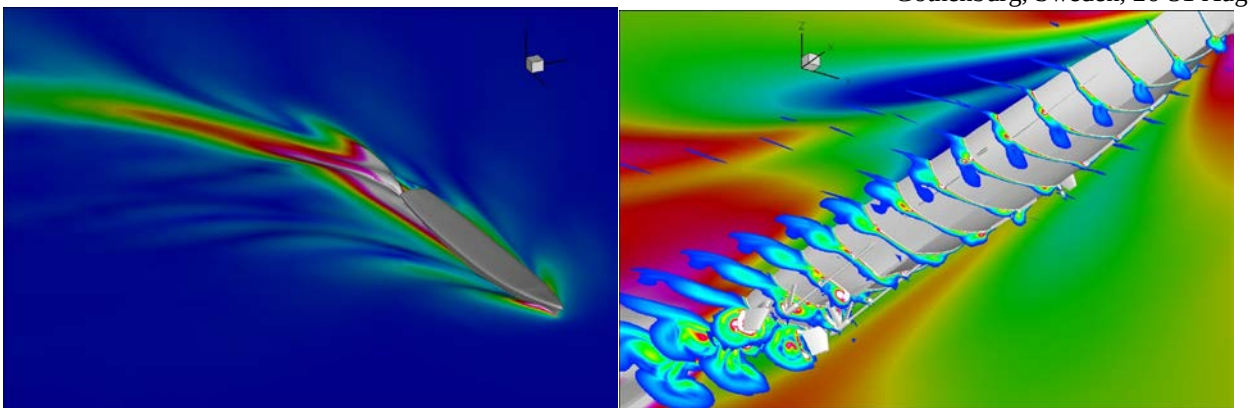

Fig. 19. Free surface colored with the absolute velocity and Isocontours of total vorticity during turning circle maneuvering in calm water for 5415M with body force propeller model (Carrica et al., 2012b)

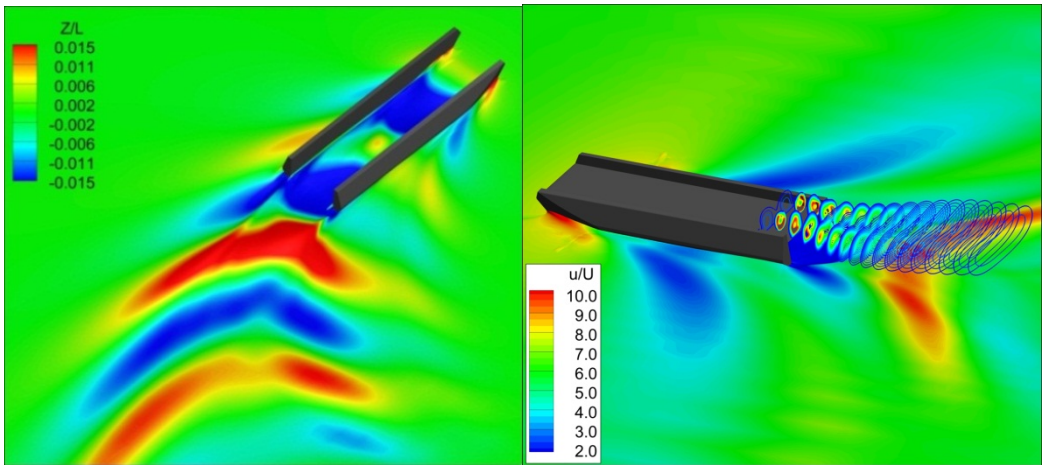

(a) (b)

Fig. 20. Free running simulations for T-Craft (SES/ACV): (a) turning circle in calm water with water jet propulsion; (b) straight ahead free running with air-fan propulsion (Mousaviraad et al., 2012a)

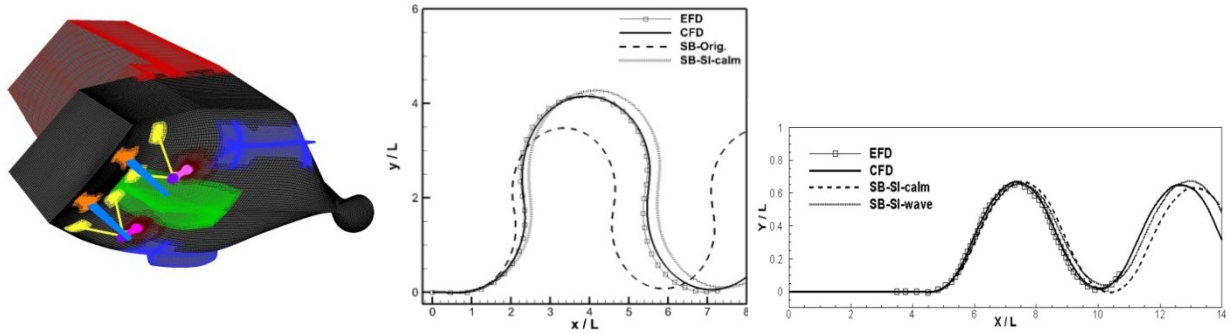

(a) (b) (c)

Fig. 21. Improving system based predictions using CFD outputs along with system identification technique: (a) The grid topology for CFD model of free running ONR Tumblehome with body force propeller model; (b) Improved system based prediction for zigzag simulation in calm water; (c) Improved system based prediction for zigzag in following waves (Araki et al., 2012a,b).

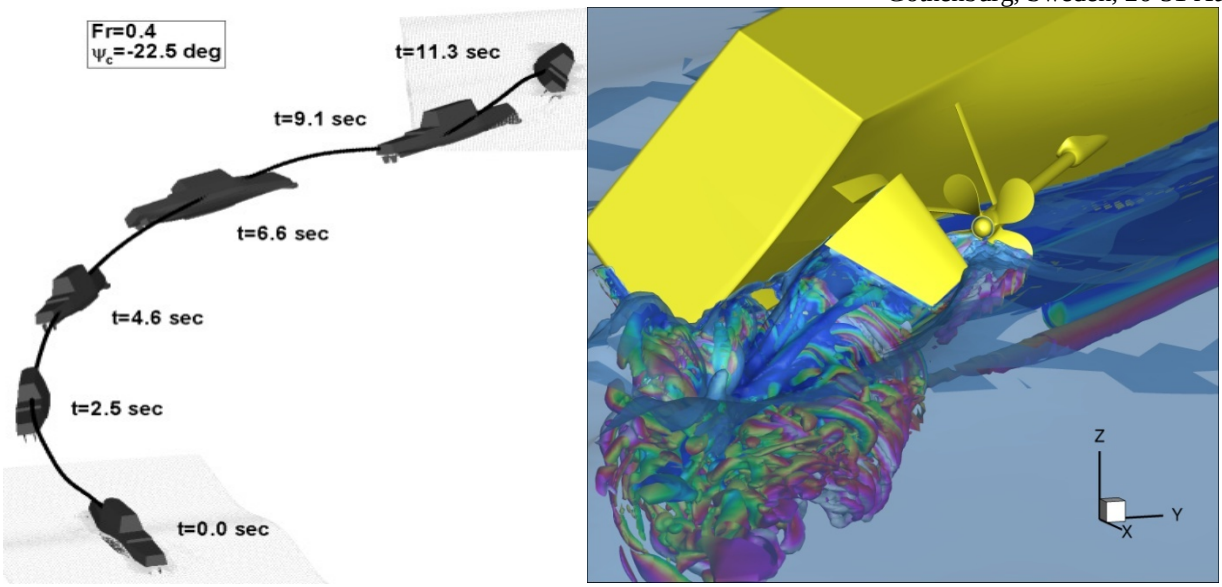

(a) (b)

Fig. 22. Broaching simulation of free running ONR Tumblehome in following waves using: (a) body force propeller model (Sadat-Hosseini et al., 2011); (b) actual propeller (Carrica et al., 2012b)

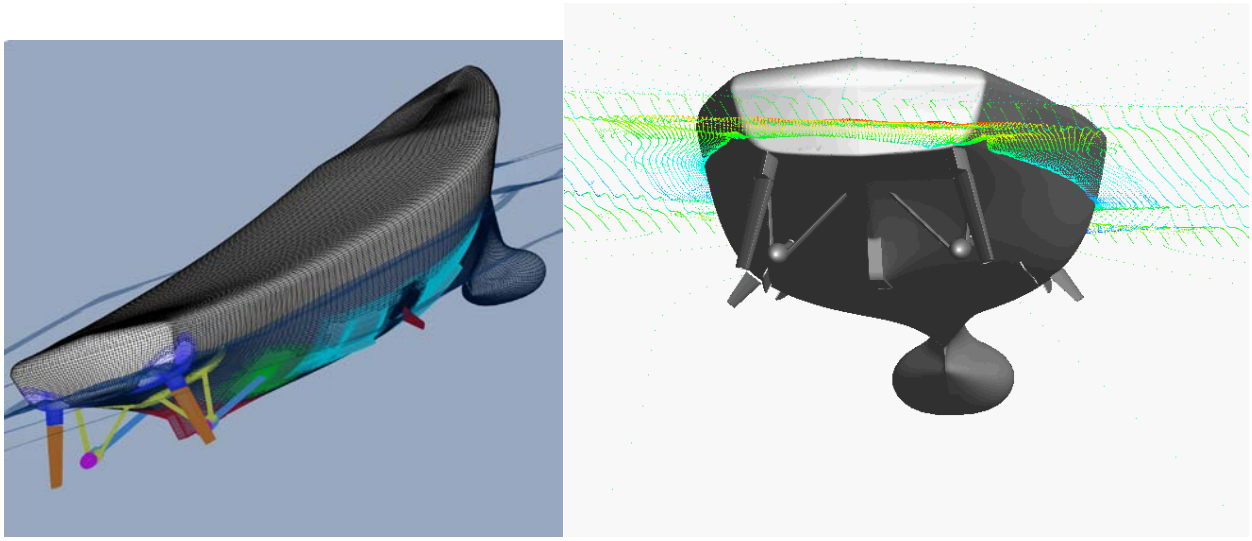

Fig. 23. The grid topology and the instant view of CFD solution during course keeping in beam waves for 5415M with active fins and body force propeller model (Sadat-Hosseini et al., 2012a).

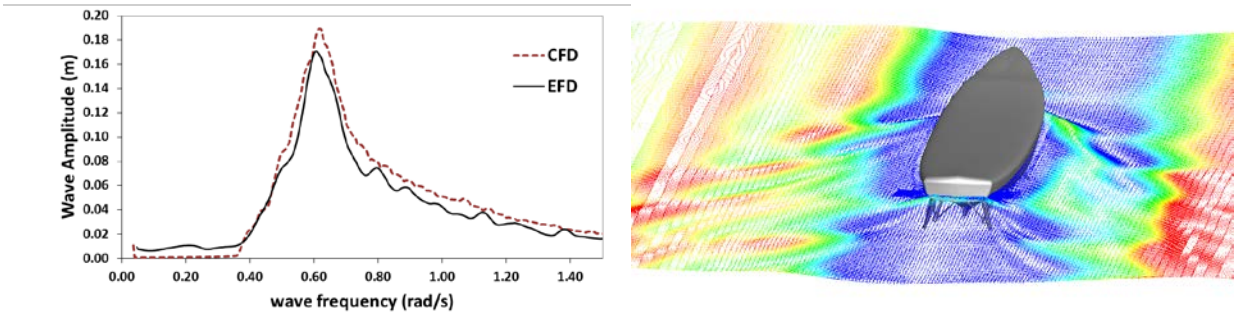

Fig. 24. CFD simulation of course keeping in irregular beam waves with JONSWAP spectrum for 5415M with active fins and body force propeller model (Sadat-Hosseini et al., 2012b).

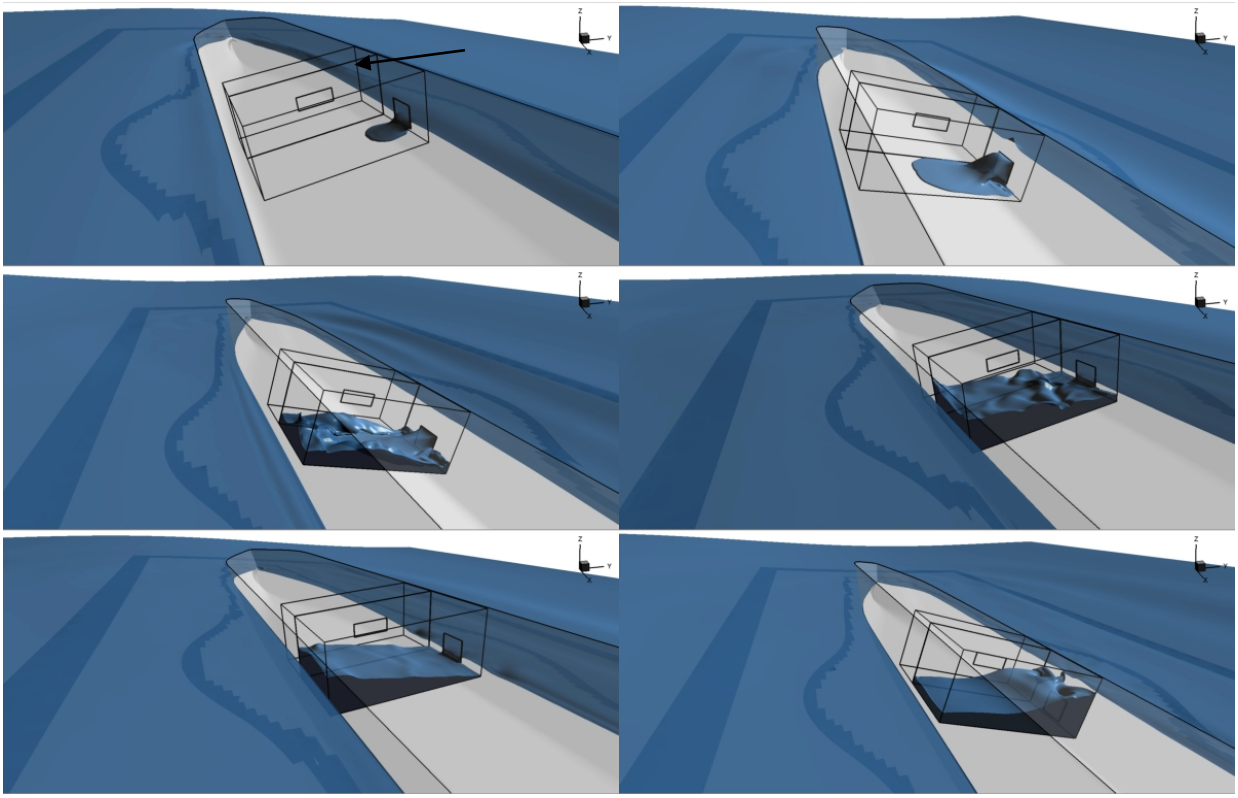

Fig. 25. CFD solution of flooding free SSRC cruiser with two-room compartment in beam waves at six instants (Sadat-Hosseini et al., 2012c).

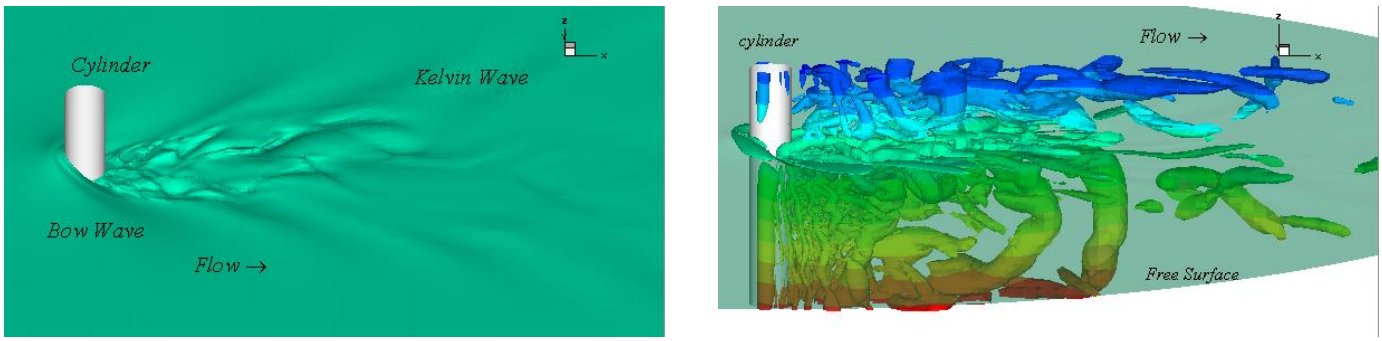

Fig. 26. Two-phase flow past a surface-piercing cylinder. Left: Instantaneous air-water interface; Right: instantaneous vortical structures colored by pressure, $Q = 0.25$.

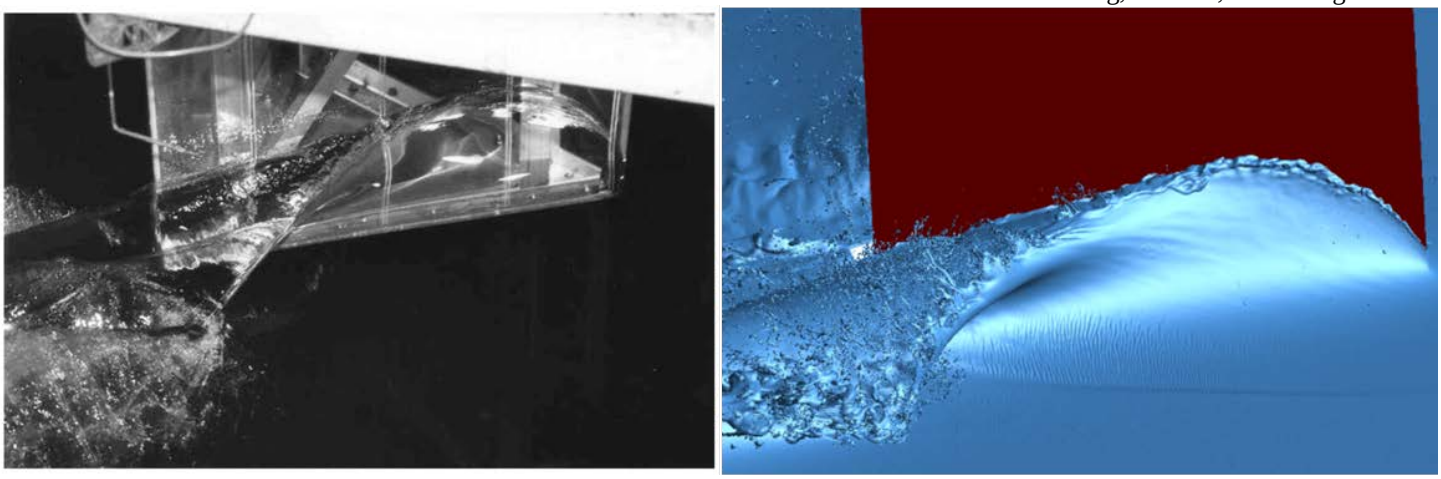

Fig. 27. Wave profiles for both experiment (Waniewski et. al, 2002) and simulation.

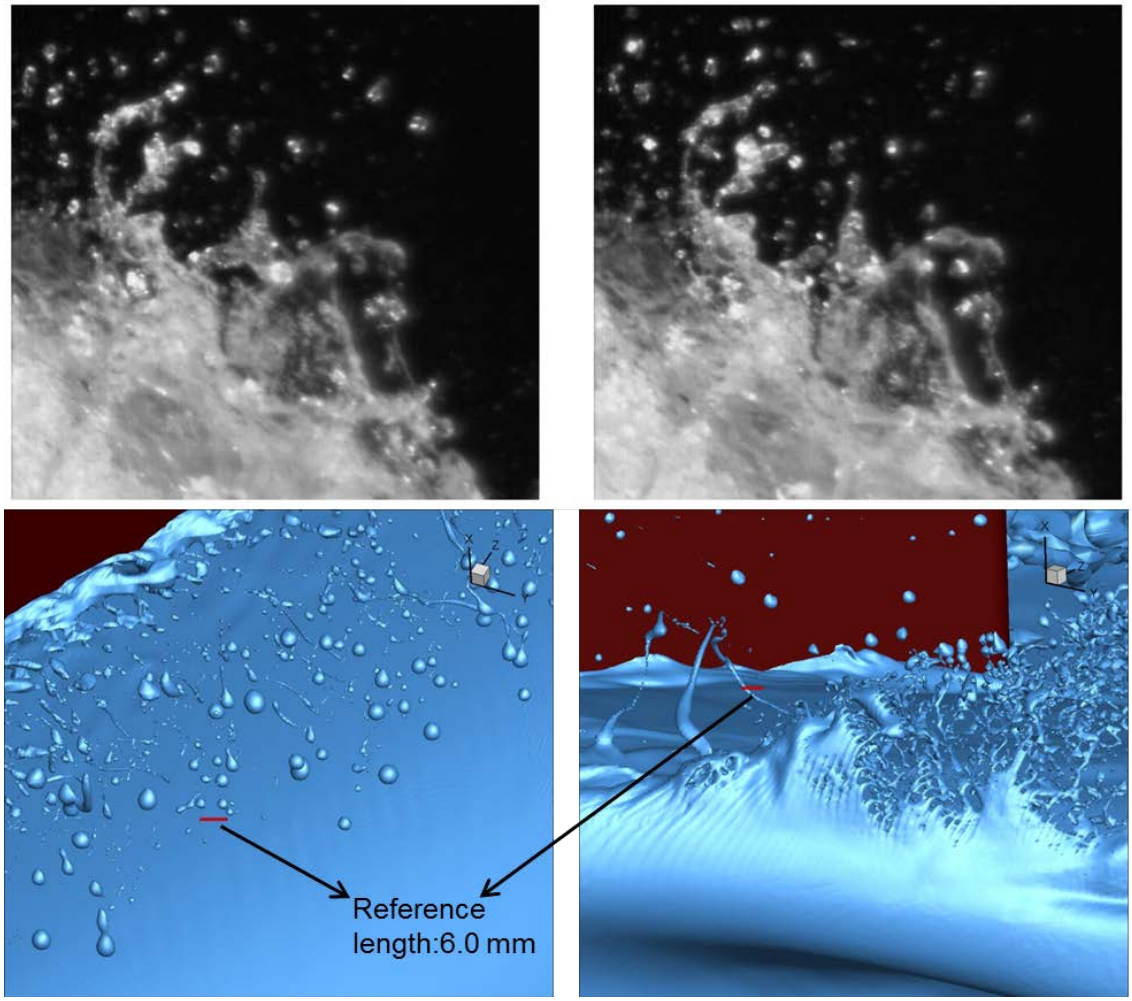

Fig. 28. Close-up view of the bow sheet breakup Top: Experiment (Karion et al., 2004); Bottom: Simulations.

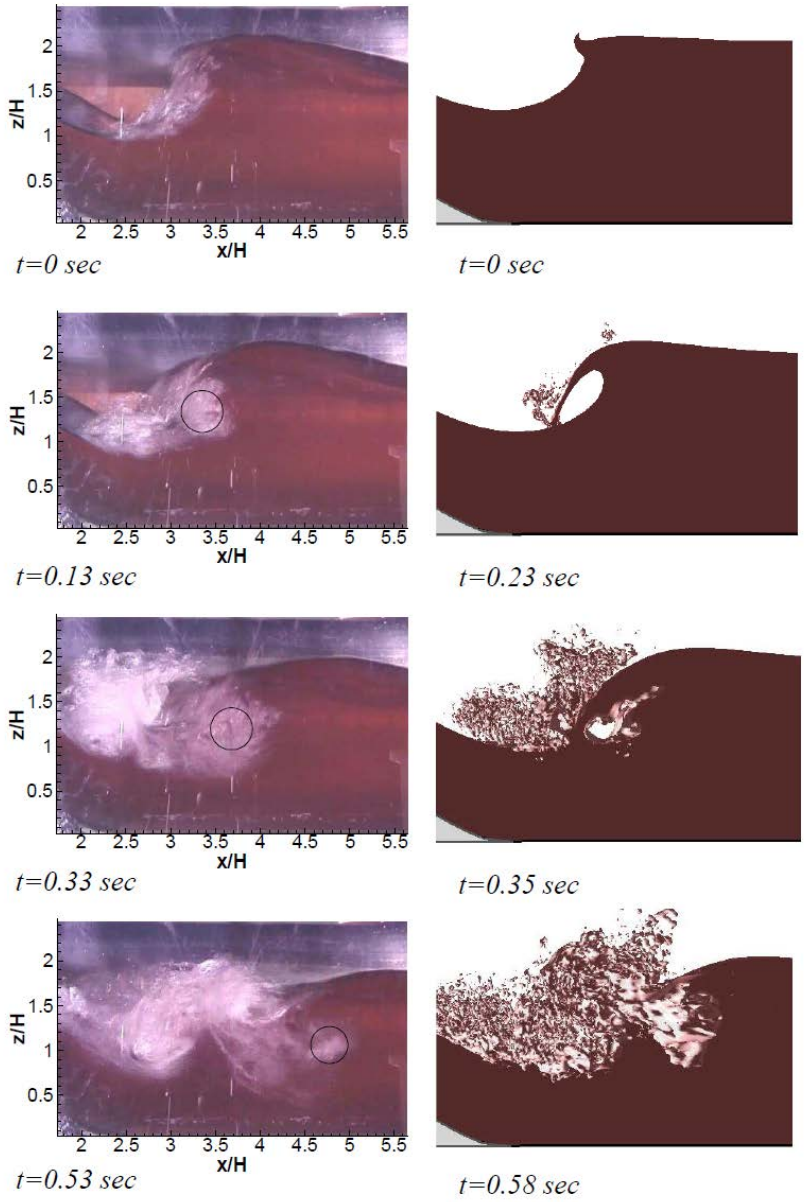

Fig. 29. Wave breaking process behind a submerged bump. Left: Experiment; right: Simulation.

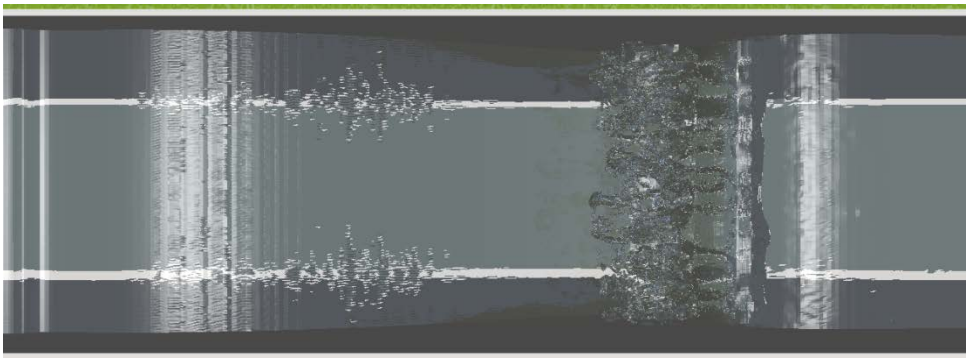

Fig. 30. Top view of the wave breaking behind a submerged bump, grid 768×256×64.

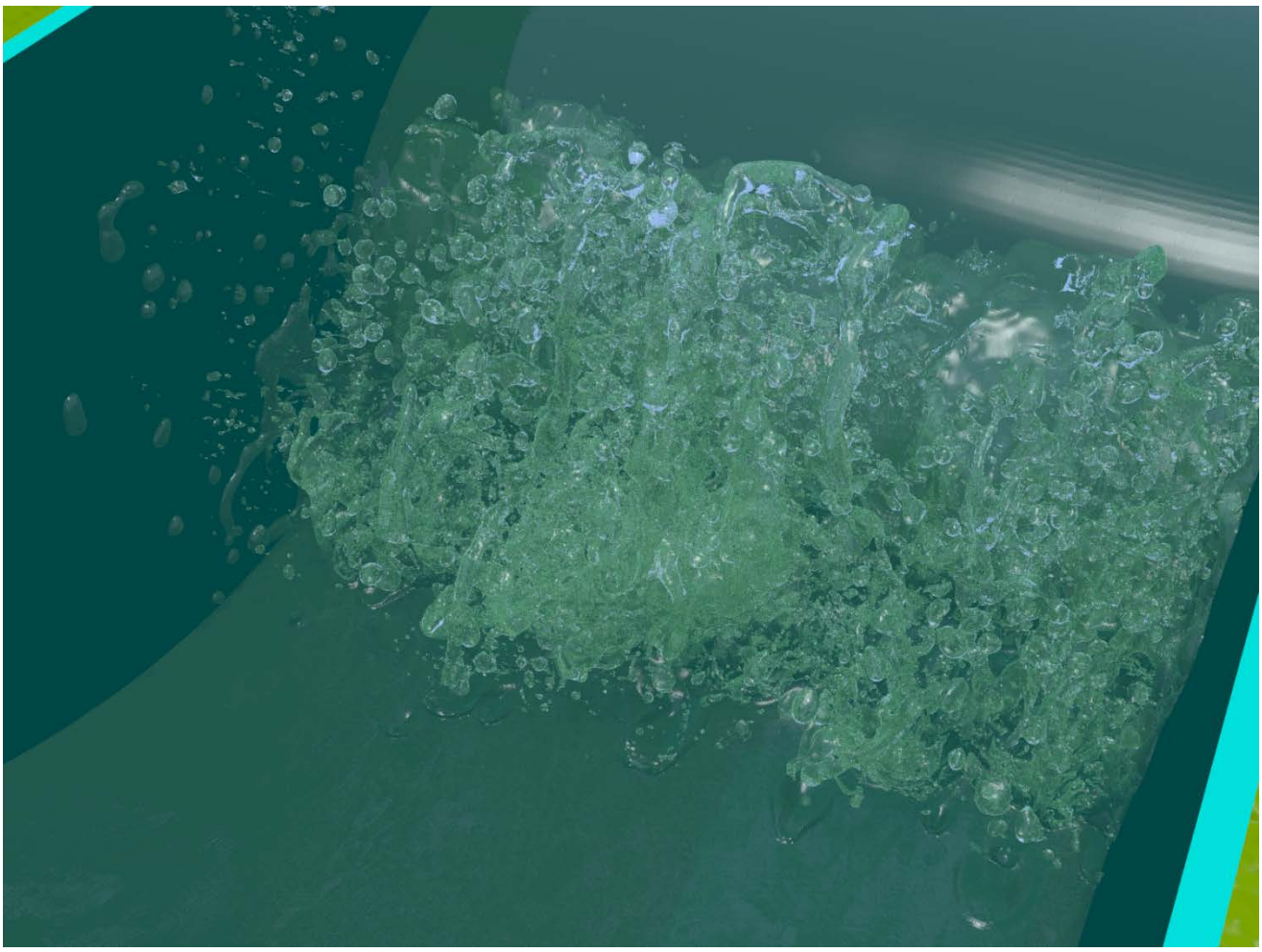

Fig. 31. Close-up view of the wave breaking region for the bump flow, grid 2.2 billion.